UNIVERSITY OF OKLAHOMA

GRADUATE COLLEGE

Stressed Out: Resistance-nodulation-division (RND) and Major Facilitator Superfamily (MFS) Efflux Pump Mediated Survival Strategies of *Acinetobacter baumannii*

A DISSERTATION

SUBMITTED TO THE GRADUATE FACULTY

In partial fulfillment of the requirements for the

Degree of

DOCTOR OF PHILOSOPHY

By

Marcela Olvera

Norman, Oklahoma

2024

Stressed Out: Resistance-nodulation-division (RND) and Major Facilitator Superfamily (MFS) Efflux Pump Mediated Survival Strategies of *Acinetobacter baumannii*

A DISSERTATION APPROVED FOR THE

DEPARTMENT OF CHEMISTRY AND BIOCHEMISTRY

BY THE COMMITTEE CONSISTING OF:

Dr. Helen Zgurskaya

Dr. Elizabeth Karr

Dr. Valentin Rybenkov

Dr. Christina Bourne

To my love

Acknowledgements

First and foremost I must thank my wonderful advisor Dr. Helen Zgurskaya. I could not have made it to this long-fought academic milestone without her guidance and support. Thank you for always believing in me. A huge thank you to all of the wonderful and helpful lab mates I have had the pleasure to work with over these seven years.

Thank you to my current and former committee members, especially Dr. Valentin Rybenkov and Dr. Christina Bourne, who helped me expand my understanding of their specific fields to complement my biochemical focus.

A colossal thank you to my favorite person in the world: (Dr.!) Jon Michael! Your love and support have been two sturdy pillars throughout this journey. I think it's pretty neat how brilliantly we work together. I can't wait to see what we do next. I wish I could lasso the stars to write you a thank you note! Looooooove you forever and ever.

Thank you to my parents who worked so hard to provide me with a strong academic foundation and love for science. I will always treasure our trips to the many wonderful museums of Chicago, especially the Natural History Museum and the Museum of Science and Industry. Thank you Vero for being the chilliest sister in the world! I am so happy we have found all our little ways to keep in touch over the years – it has been very grounding.

Thank you to all the amazing friends I have made during my time in Oklahoma (Partychem, Kriti + Neda, Biology folks, Tulsa folks). Y'all are my chosen family and you mean the world to me. XOXO

Thank you to all of our friends and family who hung out with us on discord. I can't wait to stream the new Nancy Drew game in May! Boooo to amazon, hulu, Disney+, hbo max, youtube, etc. who have recently started censoring movie streams. Long live the free internet!

Thank you to the incredible artists and creatives who helped get this dissertation done: Underscores, MUNA, Frost Children, Amaarae, Flo Milli, Tinashe, Slayyyter, Mon Laferte, Bomba Estéreo, Arca, NSQK, Remap Radio, A More Civilized Age, Stuff You Should Know, Hades, Animal Crossing, Baulder's Gate 3, Stardew Valley

Table of Contents

Dissertation Abstract

Originally discovered in soil microbial communities[1], reports of genus *Acinetobacter* associated infections started to increase around 1977[2] and continued to climb to frightening heights for the next 20 years[3] resulting in *Acinetobacter* becoming a high priority target for antibiotic resistance research, leading to the research detailed here. *A. baumannii*'s exceptional abilities to evade antimicrobials have long been known, but the details of those mechanisms have for the most part remained unclear. The better we can understand the pathogen's physiology, the more informed our efforts toward alternative treatments can be.

This dissertation is focused on the role RND and MFS efflux pumps play in *A. baumannii*'s survival strategies under various stress conditions. The first goal was to functionally characterize two putative EmrAB-like MFS pumps, identified as being overproduced in RND efflux deficient strains of *A. baumannii*, and to gain insight into their role in bacterial stress responses. The second goal was to better understand the substrate recognition of two RND pumps in *A. baumannii,* AdeG of AdeFGH and AdeJ of AdeIJK, and how specific binding pocket residues impact substrate specificity and export efficiency. I used biochemical methods such as cloning, mutagenesis, antibiotic susceptibility assays, inhibition studies, and fluorescence uptake assays to accomplish these goals. I coupled these biochemical results with genetic and structural analyses to compose a more refined picture of how multidrug efflux protects *A. baumannii* against extracellular stressors.

I found that while the two newly characterized MFS family efflux pumps, AmfAB and AmfCD, do not contribute to *A. baumannii*'s antibiotic non-susceptibility phenotypes, they are critical for *A. baumannii*'s survival under acidic conditions. These results also suggest that these two MFS transporters contribute to stress survival by modification of *A. baumannii*'s permeability barrier as a method of keeping stressors out of the cell. I also found several AdeG substrate binding pocket residues that are implicated in the export of nalidixic acid, norfloxacin, and the fluorescent probe NPN. Additionally, I used AdeG to characterize kinetic parameters of the putative efflux pump inhibitor, SLUPP_1377. And lastly, we found that the two AdeJ mutants (R701A and

F136A) improved the export efficiency of erythromycin, perhaps by better accommodating the antibiotic into the transporter binding pocket. This work provides new insight into the roles multidrug efflux pumps play in bacterial physiology, potential new drug targets which are vital for survival under acidic stress, and informed EPI development strategies from a more detailed model of the AdeG and AdeJ binding pockets.

Chapter 1: Introduction

The following literature review in part covers the escalating concern of Multidrug Resistance (MDR), particularly among the ESKAPE pathogen *Acinetobacter baumannii*. This pathogen is notorious for causing nosocomial infections, leading to increased mortality rates, longer hospital stays, and higher healthcare costs.[4] *A. baumannii* is of particular interest to this dissertation, and it is a Gram-negative pathogen responsible for a variety of infections. The chromosomes of drug resistant and drug susceptible *A. baumannii* strains encode efflux pumps, which aid in conferring antibiotic resistance. In addition to discussing the typical structure and mechanisms of Resistance-Nodulation-Division (RND) and Major Facilitator Superfamily (MFS) pumps, this review will also briefly examine Efflux Pump Inhibitors (EPIs) and their potential as alternative treatments for MDR bacterial infections. The review will also cover the various strategies bacterial pathogens have evolved to survive under stressful conditions posed by the host environments during infection. As this review will lay out, pathogenic bacteria like *A. baumannii* utilize a wide range of tools in their molecular arsenal to adapt to stressors like antimicrobial agents, heat shock, low pH, low iron, osmotic pressure, and bile stress. We lay this foundation in order to later go in depth into how substrate efflux and membrane permeability impact *A. baumannii*'s survival and fitness under stress.

1.1. Clinical multidrug resistance

Pathogenic bacteria have a variety of mechanisms to counteract antimicrobial compounds. These mechanisms can take place within the cell (target/drug modifications) and as part of the cell envelope (target modifications and influx/efflux alteration). Some bacteria can alter the molecular targets that antibiotics typically interact with or bind to. For instance, erythromycin is a macrolide antibiotic that works by binding to the bacterial ribosome, but some bacteria can modify the ribosome's structure via methylation, reducing the drug's ability to bind to it, and thus conferring resistance to erythromycin (**Figure 1.1**).

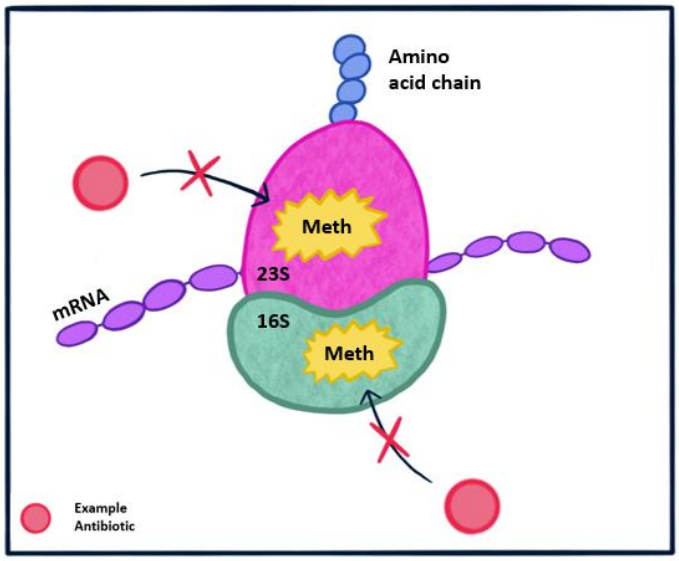

Figure 1.1 - Representation of methylation of 16S and 23S ribosomal RNA

An illustrated representation of an example of drug target modification: methylation of 16S and 23S prokaryotic ribosomal RNA. Antibiotic molecules that normally target the 16S and 23S subunits cannot bind due to the methylated RNA.[5]

Bacteria can also produce enzymes that modify the antibiotic's chemical structure, rendering it ineffective. For example, β-lactamases are enzymes produced by some bacteria that break down β-lactam antibiotics like penicillins and carbapenems (**Figure 1.2**). In carbapenem-resistant *A. baumannii* (CRAb), the most significant resistance mechanism appears to be the production of carbapenemases which can hydrolyze carbapenems and other β-lactams.[6] Another example is aminoglycoside-modifying enzymes which alter aminoglycoside antibiotics like gentamicin and streptomycin.

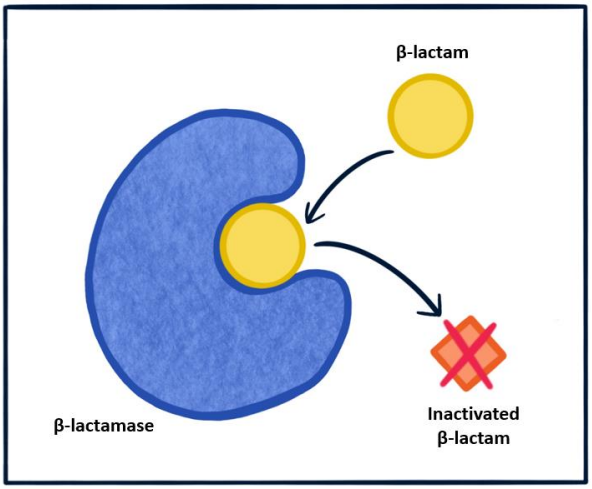

Figure 1.2 – Representation of β-lactam modification by β-lactamase

An illustrated representation of an example enzymatic modification of a drug molecule: β-lactam modification by β-lactamase. The β-lactam molecule (yellow circle) is enzymatically altered by the β-lactamase and is released in an inactivated state (orange diamond).[7]

Other examples of drug target modification can be found in the Gram-negative cell envelope (**Figure 1.3)**, like the addition of phosphoethanolamine (PEtN) to the 4'phosphate or 1-phosphate group of the lipid A segment of the LPS molecule, which leads to resistance against colistin.[8] Under colistin susceptible circumstances, the positively charged moiety of colistin interacts with the negatively charged phosphate groups of the lipid A segments of LPS. This initial interaction first displaces the calcium and magnesium divalent cations that are normally electrostatically bound to the LPS and are crucial for the integrity of the bacterial outer membrane.[9] Then the hydrophobic acyl fatty chain of the colistin molecule penetrates between the lipids of the outer membrane, leading to permeabilization and subsequent cell lysis. The addition of a PEtN moiety to lipid A of LPS has been seen as a result of mutations and overexpression of *pmrCAB*, *eptA,* or the presence of plasmid-mediated *mcr* genes. In *A, baumannii* cells with LPS that have this PEtN addition, the overall charge of the LPS region becomes positive, which then repulses the cationic colistin and thus conferring resistance to colistin.[8]

Also seen in **Figure 1.3** is the modification of penicillin-binding proteins (PBPs) leading to reduced susceptibility to β-lactams. PBPs are a family of enzymes that catalyze the synthesis of peptidoglycan, the polymer made up of repeating N-acetylglucosamine and N-acetylmuramic acid residues cross-linked by short peptide chains.[10] Peptidoglycan makes up the Gram-negative bacterial cell wall and provides major structural support for the cell. Properly functioning PBPs catalyze the polymerization of the glycan chain and the cross-linking the peptide stems to create the cell wall that gives the cell shape and support. β-lactam antibiotics have a molecular structure that is similar to the PBP's normal substrate – the D-Ala-D-Ala peptide stem ends. When a β-lactam molecule binds to the PBP's enzymatic active site, it inhibits the PBP enzyme from polymerizing the peptidoglycan, leaving the cell vulnerable to cytoplasmic leakage and cell rupture. There have been a few reports of *A. baumannii* strains containing PBP mutations that conferred resistance to β-lactams.[11]

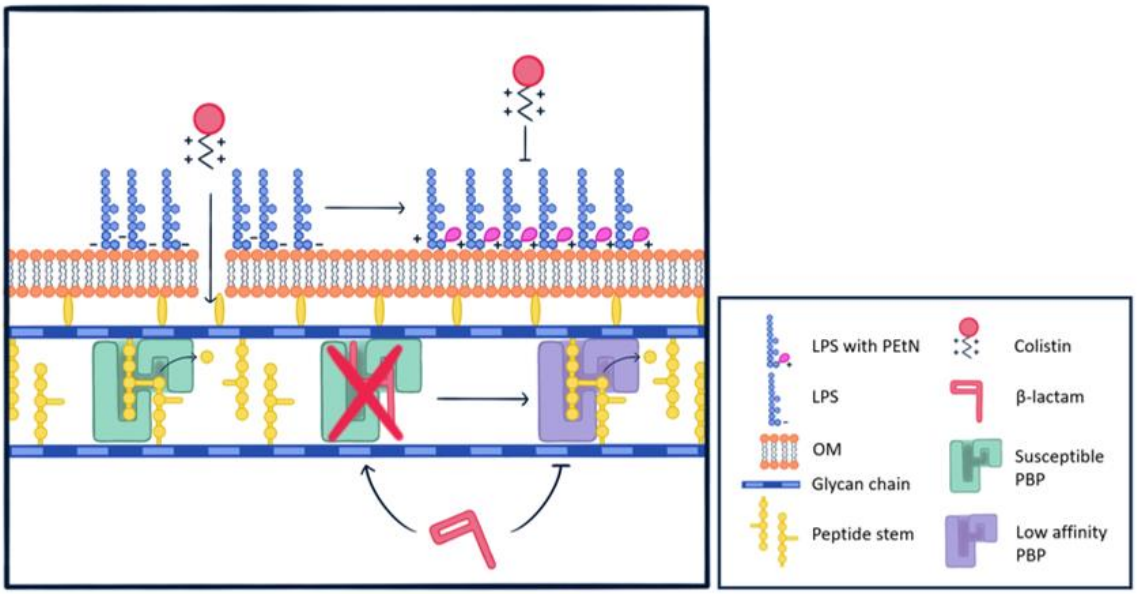

Figure 1.3 - Representation of antibiotic resistance mechanisms in the cell envelope

An illustrated representation of two bacterial mechanisms of antibiotic resistance within the Gram-negative cell envelope. The upper half of the figure shows lipopolysaccharide (LPS) attached to the outer leaflet of the outer membrane. Normal LPS is sensitive to cationic colistin molecules. LPS modified with phosphoethanolamine (PEtN) attached to lipid A neutralizes the negative charge of the LPS and repels colistin. The bottom half of the figure shows a drug-susceptible Penicillin Binding Protein (PBP) (in green), which

polymerizes the glycan chain and the peptide stems. The β-lactam molecule is shown binding to and inhibiting the susceptible PBP, but it is unable to inhibit the PBP with low affinity for β-lactams (in purple).[8,12]

The antibiotic resistance mechanisms most relevant to this work are those that reduce the intracellular accumulation of the antibiotic molecule (**Figure 1.4**). In terms of influx, antibiotic susceptibility can be decreased by structural modifications to porins, reduced expression of porins, or even complete loss of a porin.[13] For example, the inactivation of the outer membrane porin CarO confers resistance to carbapenems in some *A. baumannii* strains.[14] Bacteria can also reduce intracellular antibiotic concentrations via drug efflux. They can reduce drug accumulation by upregulating the expression of specific efflux pumps which expel antibiotics from the cell before the drugs can act on their target.[15]

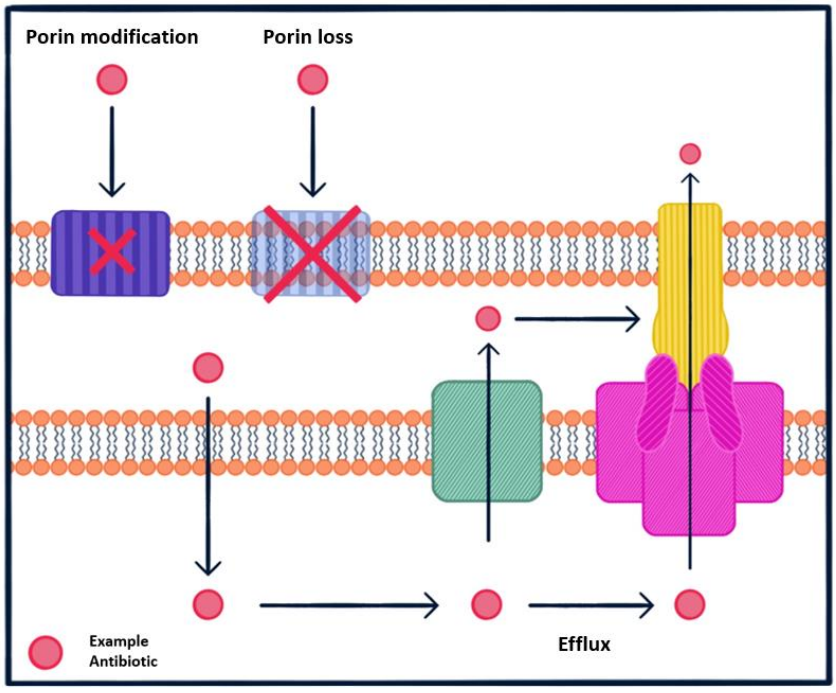

Figure 1.4 – Representation of mechanisms to reduce antibiotic accumulation

An illustrated representation of antibiotic resistance mechanisms that reduce intracellular accumulation of an antibiotic (red circle). The mechanisms shown are porin modification (purple striped rectangle), porin loss (translucent blue rectangle), efflux across the inner membrane (green rectangle), and efflux across both membranes (pink and yellow cartoon).[13] The black arrows represent the direction of antibiotic movement.

Multidrug resistance (MDR) has become an increasingly concerning issue in hospital settings, particularly among the ESKAPE pathogens. These highly virulent bacterial pathogens jeopardize patient safety with healthcare-associated infections. Patient outcomes for MDR infections can be quite serious depending on the type of infection, the overall health of the patient, and what specific MDR bacteria is involved. These patients face increased mortality rates compared to infections caused by drug susceptible bacteria, especially for critically ill patients and those with compromised immune systems.[16] They may also require longer hospital stays, leading to higher healthcare costs and a higher risk of complications during their hospitalization.[17]

Treatment regimens typically used in treating multidrug resistant infections often require substantial healthcare resources. A 2021 retrospective study of patients admitted for inpatient stays in the Department of Veterans Affairs healthcare showed that treatment of multidrug resistant bacterial infections (both community and hospital acquired) cost the United States government an estimated $1.9 billion in healthcare costs in 2017.[18]

As seen during the COVID-19 pandemic, living in such an interconnected world makes us vulnerable to the global health threat these infections pose.[19] Outbreaks of infectious diseases are public health eventualities we must prepare for. One of the primary challenges of MDR infections is the limited availability of effective antibiotics. With antimicrobial resistance on the rise, the scientific community must continue the push to discover new and more effective treatment options.

1.2. *Acinetobacter baumannii* – A concerning human pathogen

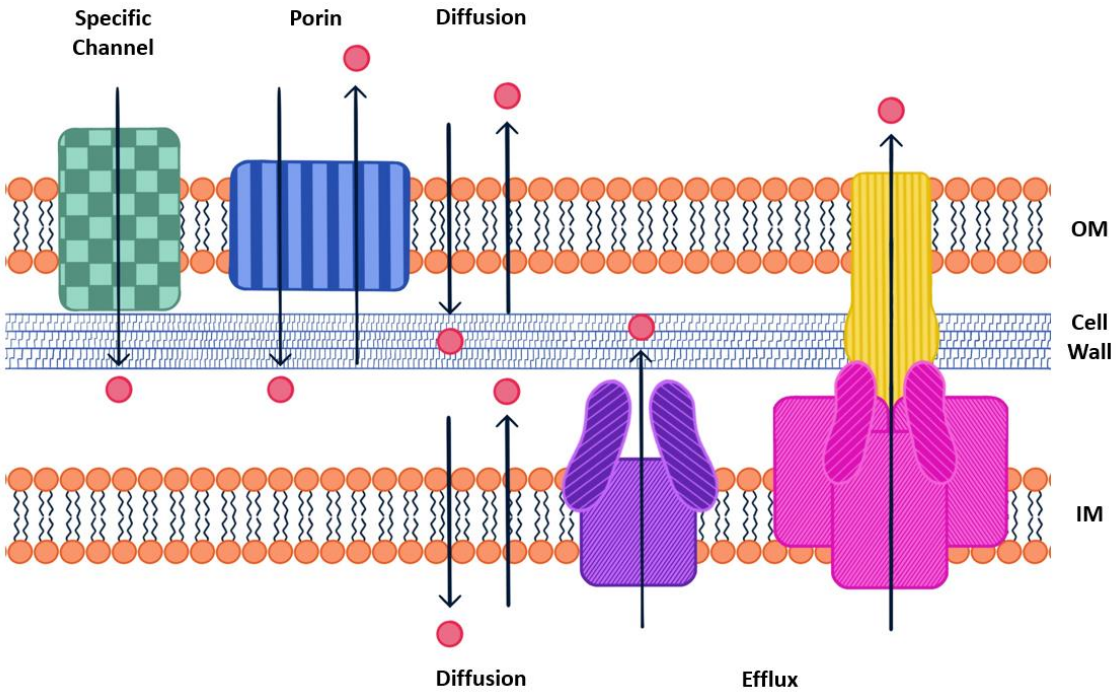

Figure 1.5 Gram-negative cell envelope of *A. baumannii*

An illustrated representation of the cell envelope of *A. baumannii* showing a small molecule (red circle) moving across the outer and inner membranes and being transported by membrane associated proteins. Small molecules can enter the cell through passive diffusion across the membranes, non-specific porin transport, and specific channel transport. Small molecules can exit the cell by passive diffusion across the membranes, non-specific porins, efflux across the inner membrane mediated by a Major Facilitator Superfamily (MFS) pump, and efflux across both membranes mediated by a Resistance-Nodulation-Division (RND) pump.[20]

The focus of this dissertation is the Gram-negative coccobacillus *A. baumannii*, known for its ability to rapidly develop multidrug resistance due to mechanisms like β-lactamase production, drug efflux, decreased membrane permeability, and altered drug target sites.[4] *A. baumannii* is responsible for a variety of infections, most notably ventilator-associated pneumonia and bloodstream infections. Rates of carbapenem-resistant *Acinetobacter* infections starting during hospitalization grew at least 78% during the first year of the COVID-19 pandemic (2019-2020)[19] for a number of reasons, including more hospitalized patients that required more frequent and longer use of catheters and ventilators, procedures which are known to increase risk of *A. baumannii* infections.[21]

The main focus of this dissertation is the antibiotic permeability barrier of *A. baumannii* and how the bacterium's efflux pumps work together with the outer membrane to protect the cell from antimicrobial agents. There are a few ways an antibiotic molecule can cross the outer membrane of an *A. baumannii* cell: it can (1) passively diffuse through the LPS and outer membrane, (2) passively diffuse through aqueous channel of a porin, or (3) transport via a specific channel protein. (**Figure 1.5**) Additionally, efflux pumps reduce intracellular accumulation of antimicrobial agents. Efflux pumps are transporter proteins and protein complexes that pump solutes out of the cell. They allow bacteria to regulate their internal environment by exporting small toxic molecules, including antimicrobial agents, metabolites, and quorum sensing signal molecules.[22] *A. baumannii*'s efflux pumps work in combination with the bacteria's decreased permeability of its outer membrane to further enhance its resistance to antimicrobial agents.[23]

1.3. Efflux pumps

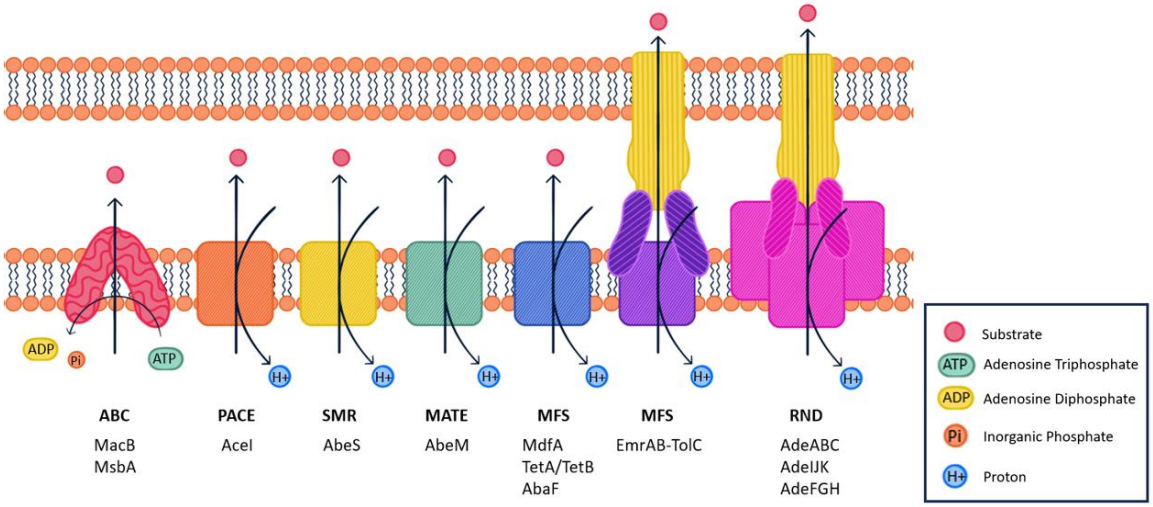

Figure 1.6 Efflux pump families

An illustrated representation of efflux pumps exporting a substrate molecule (red circle) and the associated energy cost. The names of *A. baumannii* transporters are listed below their corresponding family. From left to right: ATP-binding cassette (ABC) family, proteobacterial compound efflux (PACE) family, small multidrug resistance (SMR) family, multidrug and toxic compound extrusion (MATE) family, major facilitator

superfamily (MFS) (1- and 3-component), and resistance-nodulation-division (RND) family.[24]

The efflux pump families shown in **Figure 1.6** represent all known efflux pump families found within *A. baumannii* as of 2022.[24] The studies in the following research chapters of this dissertation focus on just the RND and MFS families of efflux pumps. Together, these two families cover a wide range of substrates exported by *A. baumannii*. In addition to exporting antibiotics, these kinds of efflux pumps have also been shown to contribute to physiological pathogenicity.[25] Delving into the details of how these families of pumps function can give us much needed insight into the survival strategies of *A. baumannii*.

1.3.1. Resistance-Nodulation-Division (RND) superfamily

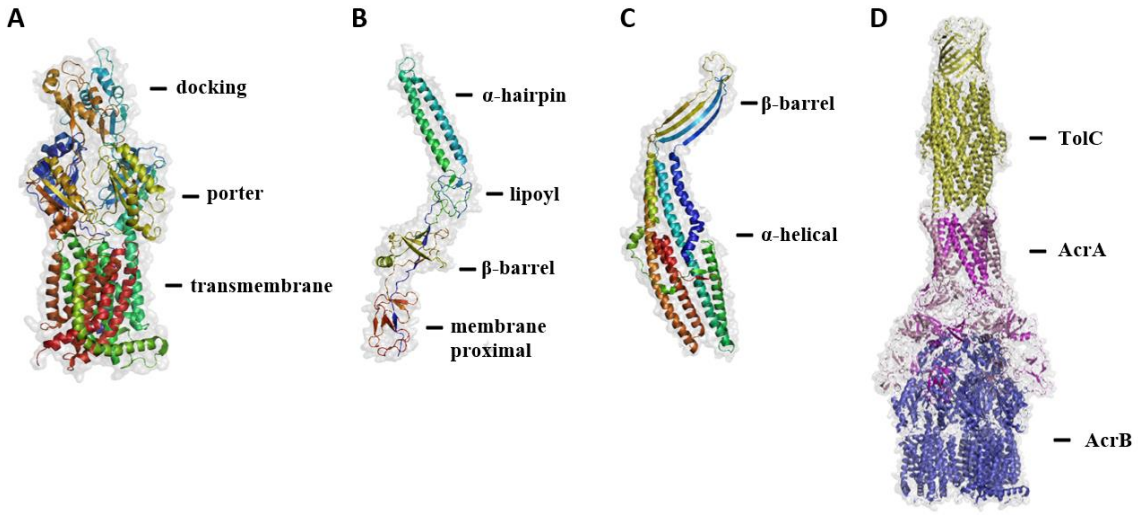

Figure 1.7 AcrAB-TolC protomers and tripartite complex

Structures of the AcrAB-TolC proteins (PDB code 5V5S)[26]. **A**) AcrB protomer showing N- to C- terminus as a blue to red rainbow gradient. The docking, porter, and transmembrane domains are labeled. **B**) AcrA protomer showing N- to C- terminus as a blue to red rainbow gradient. The alpha-hairpin, lipoyl, beta-barrel, and membrane proximal domains are labeled. **C**) TolC protomer showing N- to C- terminus as a blue to red rainbow gradient. The beta-barrel and alpha-helical domains are labeled. **D**) Assembled AcrAB-TolC complex with TolC (yellow), AcrA (magenta), and AcrB (blue).

The RND (Resistance-Nodulation-Division) Superfamily is a class of efflux pumps dependent on the proton motive force and act as proton/drug antiporters.[27] They are essential for exporting drugs and small toxic molecules located in the periplasmic

region of the cell envelope in Gram-negative bacteria. Pumping out these molecules reduces the intracellular concentration of an antibiotic and diminishes its efficacy. *A. baumannii* genomes contain at least three RND efflux pumps: AdeABC, AdeIJK, and AdeFGH.[15]

In *A. baumannii* and other Gram-negative bacteria, the RND pumps function as tri-partite complexes.[15] The best-studied is AcrAB-TolC of *E. coli* [28], as such, it is a good example to use for describing the structure of an RND pump (**Figure 1.7**) Typically, all three genes are encoded within the same operon, with the first gene encoded in the RND-type operon is a membrane fusion protein (MFP), like *E. coli*'s AcrA and AdeA of *A. baumannii*. The second encoded gene is typically the RND transporter located in the inner membrane, like AcrB and AdeB. Finally, the third encoded gene is usually the outer membrane protein (OMP), like TolC or AdeC. The periplasmic MFP connects the two membrane bound protein compounds to form the complete tripartite complex. Structural experts in the field have found evidence that AcrAB-TolC favors a stoichiometric ratio of 3:6:3 for AcrB:AcrA:TolC.[29] Once the complex is formed, the tripartite pump utilizes proton translocation to transport its substrates across both membranes.[29]

Membrane fusion proteins like AcrA are made up of four domains: the membrane proximal, β-barrel, lipoyl, and α-helical hairpin domains (**Figure 1.7-B**). AcrA assembles as a trimer of dimers and its overall structure is highly flexible. This flexibility is essential for translating the transport mechanism movement from AcrB to TolC and accommodating the transitional shapes of the complex.[30] While this protein mainly occupies space in the periplasm, it has been shown to be anchored to the inner membrane via palmitoylation of an N-terminal cysteine residue.[31] Mutational studies have found the amino acid residues located in AcrA's α-helical hairpin domain are important for interacting and interfacing with the TolC channel.[32–34] And it has been found that the unstructured, distal C-terminal region of AcrA is responsible for specific association with AcrB.[35] The residues within the β-barrel domain appear to be conserved: mutations in this area result in loss of function.[36]

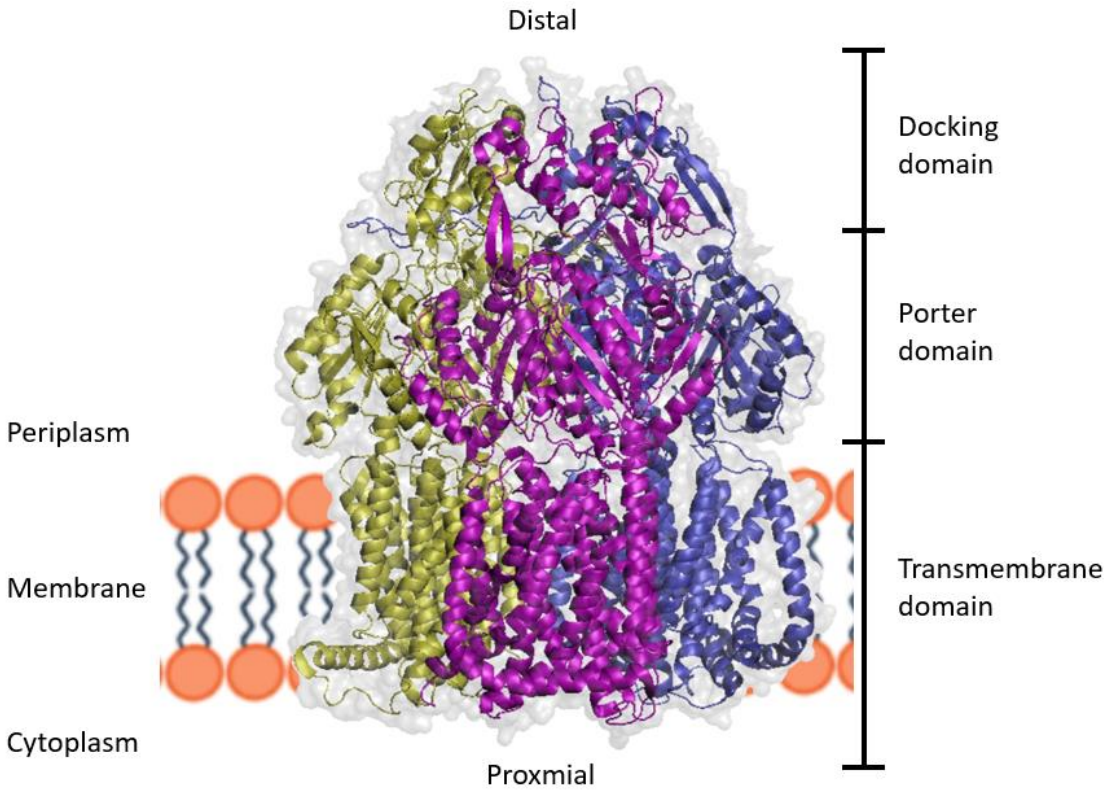

Figure 1.8 Diagram of AcrB trimer

A cartoon representation of the AcrB trimer (PDB code 5V5S)[26]. The three AcrB protomers are individually colored (yellow, magenta, and blue) and the protein surface is light grey.

The structure of RND transporter proteins is usually divided into the transmembrane domain, the porter domain, and the docking domain (**Figure 1.8**).[37] The transmembrane domain is made up of the transmembrane alpha-helices (12 per monomer) that embed the protein into the inner membrane and this region also contains the amino acid residues needed for proton translocation. There are highly conserved aspartic acid and lysine residues in this region that are needed to move protons from the periplasm to the cytoplasm.[38] The porter domain is the region of the transporter that contains the access and deep binding pockets. These binding pockets are made up of many phenylalanines and other hydrophobic residues that allow for non-specific and transient binding of a broad range of hydrophobic substrates. These two binding pockets are separated by an 11-residue long switch-loop, which is essential for substrate binding

and transport.[39] The docking domain forms a funnel shape that helps move the pump substrates further into the efflux pump complex.[40]

TolC is a promiscuous outer membrane channel that can form complexes with many proteins, including AcrAB, EmrAB, and MexAB.[36] TolC is assembled as a mono-barrel homotrimer, forming the final portion of the substrate transport channel within the periplasm (periplasmic α-helical barrel) and the outer membrane pore (transmembrane β-barrel) (**Figure 1.7-C**).[41] The region of mixed α/β-folds located in the periplasm, roughly in the middle of the periplasmic α-helical barrel, is known as the equatorial domain. The tube that TolC forms is an asymmetrical one. The end of TolC that faces the transporter end of the complex has an opening of about 20 Å in diameter. The pore at the end of TolC that faces the outside of the cell is only about 3.9 Å in diameter. This pore size is small enough to keep the transport substrates from passing through. This is how TolC appears in its closed conformation. This closed shape is made in part by the pairs of coiled-coiled helices in the interior of the channel that angle towards each other. These helix pairs meet at a point near the outside facing end of TolC and are stabilized by salt bridges near this point.[31] Six conserved aspartate residues (D^{371} and D^{374}, two per monomer) near this point form a narrow pore that even ions cannot easily diffuse through.[42,43]

The RND complex transport mechanism involves the transporter protein trimer cycling through three transport states. Each of the three transporter protomers are in one of three asymmetrical structure states: access (or loose) state , binding (or tight) state, or extrusion (open) state.[37,38,44] The protomers cycle through these three states to (1) allow pump substrates to enter the transporter in the access state, (2) move substrates further into the drug-binding pocket during the binding state, and (3) funnel substrates into the channel created by the periplasmic AcrA and outer membrane channel TolC in the extrusion state. The transition transporter protomers make between conformational states is driven by changes in the protonation of specific amino acid side chains located in the transmembrane domain.[45] Pump substrates can enter the transporter trimer via the periplasm or from the intermembrane region of the inner membrane. Du et al. and other researchers have been able to determine drug pathways and drug binding sites in AcrB through X-ray crystallography and cryo-electron microscopy studies.[26,37,46] These studies

have shown that AcrB's periplasmic entrance includes the proximal binding pocket in the loose protomer. Further past the proximal binding pocket is the distal binding pocket, containing the so-called hydrophobic trap. The hydrophobic trap location within each AcrB protomer can be seen in **Figure 1.9-B,C**, where the pyranopyridine inhibitor MBX3132 was found to bind when co-crystalized with the AcrABZ-TolC complex. There are several different binding sites within these channels and binding pockets. How specific substrates interact with these binding sites depends on the chemical and physical properties of the substrate as well as those of the amino acid side chains found in the binding site residues – this is characterized as a pump's substrate specificity.

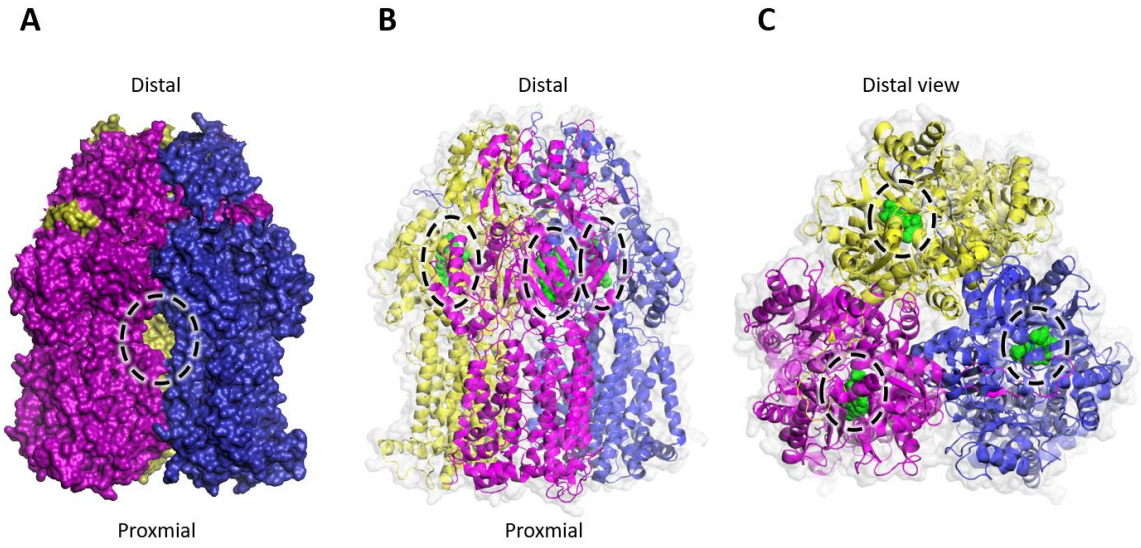

Figure 1.9 AcrB trimer bound to three MBX3132 molecules

Diagram of AcrB trimer bound with pyranopyridine inhibitor MBX3132 (PDB code 5NG5).[26] The three AcrB protomers are individually colored (yellow, magenta, and blue). **A**) A surface view of the AcrB trimer with the vestibule pathway circled in a dashed line.[47] **B**) A cartoon representation of the AcrB trimer with bound MBX3132 molecules shown as green spheres and circled in a dashed line. **C**) A cartoon representation of the AcrB trimer viewed from the distal side with bound MBX3132 molecules shown as green spheres and circled in a dashed line.

When the AcrB protomers bind a substrate and switch their conformational sstates, this causes a reconfiguration of the AcrA structure, a conformational shift that translates to TolC transitioning into its open state.[26,48] The structure state change of AcrA is also crucial for the sealing of the efflux pump complex channel so that substrates do

not leak out into the periplasm while being shuttled from the transporter to TolC. When there is no substrate bound to the AcrAB-TolC complex, the TolC channel is in a closed state. But when there is a substrate bound, followed by the structure state changes, TolC opens its channel in an aperture-like manner and releases the transported substrates into the extracellular space.[45]

In 2001, Sulavik et al. demonstrated that *E. coli* strains with *acrAB* or *tolC* deleted had overlapping substrate susceptibility profiles, which lines up with them forming a tripartite complex together. Additionally, their *tolC* deletion strain also showed higher susceptibility to seven of the tested compounds compared to the *acrAB* deletion strain. This finding supported the concept that TolC contributes to *E. coli*'s intrinsic resistance when complexed with AcrAB as well as separately from AcrAB. This additional substrate susceptibility linked to *tolC* is likely due to TolC interacting with other efflux pumps, like the EmrAB-TolC complex.[49] *E. coli* strains with a deletion in *acrAB* resulted in an increase in susceptibility to 25 of the 35 tested compounds. When all five RND class genes were deleted in a single strain, the resulting strain was even more susceptible to eight compounds than that of strains with *acrAB* deleted. The strain's susceptibility to these eight compounds is dependent on multiple RND efflux systems, meaning there is overlap in RND substrate ranges. Deleting *tolC* from *E. coli* resulted in a strain with increased susceptibility to 29 of the 35 compounds. Genes other than *tolC* that contribute to *E. coli*'s intrinsic resistance were found to be *acrAB, yicP, yohG, mdfA,* and *emrE*.[50]

The RND efflux pumps of *A. baumannii* are thought to be structurally similar to *E. coli*'s AcrAB-TolC, but they have different substrate specificities. Of the three main RND pumps in *A. baumannii*, the amino acid sequence for AdeJ is the most similar to *E. coli*'s AcrB with 57.68% identity, followed by AdeB with 49.51% and AdeG with 40.08%. AdeJ has a wide substrate range that includes β-lactams, chloramphenicol, trimethoprim, fluoroquinolones, and tetracyclines as well as erythromycin, lincosamides, fusidic acid, novobiocin, and rifampicin.[51,52] AdeB also exhibits polyspecificity in its substrate range, but to a narrower extent compared to AdeJ, with its ability to export β-lactams, fluoroquinolones, tetracyclines, tigecycline, macrolides, lincosamides, chloramphenicol, and aminoglycosides.[53] Lastly, AdeG exports mainly trimethoprim,

chloramphenicol, and fluoroquinolones, but also tetracycline, tigecycline and clindamycin.[54] This dissertation will identify specific amino acid residues located within the hydrophobic binding pocket of RND transporters AdeG and AdeJ that are involved with the export of specific pump substrates.

1.3.2. Major Facilitator Superfamily (MFS)

The Major Facilitator Superfamily (MFS) represents one of the largest and most diverse groups of transporters.[55,56] Members of this family include uniporters (transporters that do not require coupling ions), symporters (transporters that couple substrate transport with ion transport in the same direction as the substrate), and antiporters (transporters that facilitate substrate and ion transport in opposite directions). Most MFS transporters function as single, monomeric units that usually have 12 transmembrane helices, but sometimes have been found to have 14 (like EmrB of *E. coli*). These pumps have a transport mechanism called an alternate access – the two halves of the pump structure switch between the inward-open state and the outward-open state.[56] The transport cycling of MFS pumps appears to be coordinated by the ordered binding and release of proton and substrate, which drives the conformational shift between inward and outward states.[45]

Similar to RND pumps, MFS pump activity is dependent on the electrochemical gradient across the inner membrane rather than ATP hydrolysis.[57] MFS pumps usually consume one proton for every one substrate molecule transported across the inner membrane. This is a significantly more energy efficient method of substrate transport compared to ABC transporters, which require two ATP molecules (the equivalent of six protons). This suggests that MFS pumps are especially useful for cells under various stress conditions, like starvation and in the presence of antibiotics.[58]

MFS efflux pumps contribute to a bacterium's resistance to antimicrobial agents by actively pumping out these small molecules from the cell.[59] The substrates of MFS efflux pumps can vary wildly, including ions, sugars, lipids, and drugs. Even so, MFS pumps have not been seen to be overproduced in clinical isolates of multidrug resistant bacterial strains. This dissertation aims to shed light on the role MFS pumps play in *A. baumannii* physiology.

Like RND pumps, MFS pumps also form tripartite complexes with outer membrane channels like *E. coli*'s EmrAB. Yousefian et al. found that the periplasmic membrane fusion protein EmrA links to the outer membrane channel TolC, forming the EmrAB-TolC complex which can then facilitate the export of substrates all the way across the outer membrane.[49] We anticipate the mechanism of transport of other MFS pumps to be similar to the EmrAB-TolC tripartite complex.

The first Gram-negative multidrug efflux pump reported on in the literature was the MFS pump EmrAB.[60] The transporter EmrB was found to be homologous to QacA, a multidrug-resistant pump from *Staphylococcus aureus*. Reports on QacA describe it as appearing to be a membrane translocase that could extrude ethidium bromide and other drugs from the cell in a proton motive force (PMF) dependent manner.[61] Lomovskaya and Lewis found that the chromosomal locus, *emr* (*E. coli* mdr) protects the cell from damage caused by carbonylcyanide *m*-chlorophenylhydrazone (CCCP) and from a number of structurally unrelated compounds like nalidixic acid and thiolactomycin. From the compounds they tested, they found that EmrAB seems to confer resistance only to the more hydrophobic compounds. An example of this was seen when *emr* carrying cells were protected from nalidixic acid, but not from more hydrophilic nalidixic acid analogues.[60] Expression of plasmid encoded EmrKY in a drug-susceptible strain of *E. coli* significantly increased MICs for the following: doxorubicin (32-fold), rhodamine 6G (16-fold), benzalkonium (8-fold), erythromycin (4-fold), crystal violet (4-fold), TPP (tetraphenylphosphonium bromide) (4-fold), deoxycholate (4-fold).[62]

Again, referring back to Sulavik et al.'s 2001 publication, in the case of MFS pumps, strains with single deletions in *emrD, emrAB,* and *emrKY* showed no differences in susceptibility to the 35 tested compounds compared to the drug-susceptible *E. coli* W3110 strain. The *E. coli* strain with deletions for *emrAB* and *emrKY* showed a susceptibility profile similar to WT W3110. Although previously published studies showed that *E. coli* strains overexpressing *emrAB* were resistant to nalidixic acid and CCCP [60], deletion of *emrAB* did not increase the strains' susceptibility to these two compounds. A 2004 study showed that deletion of *emrKY* genes from a K-12 derived *E. coli* strain with *acrAB* deleted did not change drug susceptibility levels, suggesting that

EmrKY is not expressed under normal conditions.[63] The MFS pump with the highest difference in susceptibility when deleted was *mdfA*, as its deletion resulted in increased susceptibility to ethidium bromide and benzalkonium chloride. Even deleting all four MFS loci resulted in MICs similar to those for the *E. coli* strain with a deletion of *mdfA* alone. This result suggests that among these four specific MFS pumps, there is no additive or synergistic effect of multiple deletions.

Based on EmrAB's nucleotide sequence, amino acid sequence, and related protein homologies, the researchers noted that that it was likely that EmrAB worked with some other mechanism to extrude compounds across both membranes, as "such a mechanism would take advantage of the low permeability of the outer membrane to hydrophobic substances".[60] These findings laid the foundation for decades of MDR efflux research that continues today.

RND efflux deficient strains of *A. baumannii* have been found to overexpress some MFS efflux pumps, including EmrAB-like homologs.[64] However, their role in *A. baumannii*'s bacterial physiology is still unknown. Through genetic context analysis and functional characterization, this dissertation begins to identify some of the cellular processes the MFS pumps are involved in.

1.4. Pathogen strategies to survive during infections

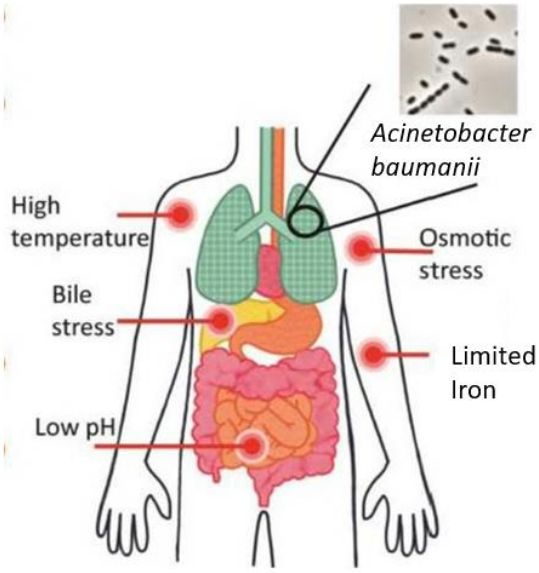

Figure 1.10 Human host infection stress conditions

An illustrated representation of five human host associated stress conditions that *A. baumannii* encounters during infection, including high temperature (41°C), bile stress (0.5% bile salts/DOC), low pH (pH 4.6), osmotic stress (0.5 M NaCl), and limited iron (125 μM 2-2'-dipyridyl).

Immediately upon entering the human host, pathogenic bacteria must adapt to various stress conditions in order to survive. Some of these conditions include low pH, high temperature, and nutrient scarcity.[65] Bacteria have general and specific stress response systems they use to respond to detrimental growth environments.[66] Avican et al. identified species-specific "universal stress responders" that were seen to have altered expression under multiple stress conditions, including some transporters.[67] In addition to conferring multidrug resistance, efflux pumps have been implicated in bacterial virulence and stress responses.[68] Targeting these bacterial stress responses could be a potential alternative treatment strategy, and therefore it is beneficial to better understand these stress responses systems.

1.4.1. Heat shock

Environmental temperatures higher than a bacteria's optimum temperature can cause defects in the formation and stability of macromolecules. This leads to loss of protein function and misfolded proteins, which can accumulate within the cell and lead to

more disruption of regular cellular processes.[69] Protein aggregates damage membranes[70] and heat shock can induce changes to the membrane's fluidity through membrane lipid remodeling.[71] High heat can also denature nucleic acids, leading to unfolded ribosomes and stalled protein synthesis. Further cell disruption would be caused by the loss of the many functions of small RNAs as well.

Bacterial pathogens possess intricate mechanisms to survive and adapt to heat shock. These mechanisms ensure a balanced physiological state, enabling the bacteria to withstand thermal stress while maintaining vital cellular functions. One of the primary responses to heat shock is the increased production of heat shock proteins (HSPs).[69] These proteins are molecular chaperones that play a critical role in maintaining cellular homeostasis by assisting in proper protein folding, preventing aggregation of denatured proteins, and aiding in their refolding or degradation. Some HSP proteins perform essential functions under normal physiological conditions, like assisting in correct protein folding.[72]

Production of proteins associated with DNA repair machinery is also needed to repair heat-induced mutations.[73] As the repair process gets underway, it is advantageous for the cell to alter its metabolic pathways to conserve resources. Some bacteria respond to heat stress by enhancing biofilm formation. This complex communal formation offers increased resistance to environmental stressors, including heat.[74] This adaptation includes shifts in energy production and consumption patterns, ensuring that recourses are optimally managed and utilized for survival under heat stress.[75]

In pathogenic bacteria, heat shock can trigger changes in the expression of virulence factors. This adaptive response can influence the pathogen's ability to infect and survive within the host. These mechanisms collectively enhance the bacterial cell's ability to endure heat stress, ensuring survival and continued pathogenicity in hostile environmental conditions.

1.4.2. Low pH

Acid damage in bacterial cells can have several significant effects including pH homeostasis disruption, membrane damage, and DNA damage. Bacterial pathogens

employ various strategies to survive in acidic environments, including "maintenance of pH homeostasis, cell membrane integrity and fluidity, metabolic regulation, and macromolecule repair".[76] Bacteria maintain their internal pH within a viable range despite external acidity. This involves mechanisms that expel excess protons from the cell or neutralize internal protons, thus preventing acidification of the cytoplasm.[76] Some bacteria may modify their membrane structures as a response to acidic stress. Acidophiles, for example, may have a positively charged membrane surface and a high internal buffer capacity, helping to protect against acid damage.[77] Bacteria also adapt to acidic environments through the expression of acid shock proteins and alterations in metabolic pathways to reduce the production of acidic by-products.

Some of the less energy intensive acid resistance systems (ARs) utilized by *E. coli* are amino acid dependent: AR2 and AR3.[78,79] These two systems function by the decarboxylation of glutamate and arginine by GadA or GadB (for glutamate) or AdiA (for arginine), a reaction which consumes one cytoplasmic proton and produces either γ-amino butyric acid (GABA) or agmatine. The decarboxylation products are then exported from the cell in exchange for new amino acid substrates.[80] An additional acid response mechanism *E. coli* has been found to employ the deamination of amino acids to raise intracellular pH. Researchers Wiebe et al. found that the deletion of L-serine deaminases SdaA and SdaB from uropathogenic *E. coli* strain UTI89 resulted in acid stress susceptibility, similar to other *E. coli* acid stress deletion mutants.[81] The deamination of L-serine produces pyruvate and ammonia, and the researchers postulate that the produced ammonia functions as a base which increases intracellular pH of *E. coli* when under acidic stress conditions.[81]

1.4.3. Low iron

Iron is critical for various physiological functions in bacteria, including DNA replication, transcription, metabolism, and energy generation via respiration.[82] Iron is similarly critical for eukaryotic cells and is one of the most restricted micronutrients in the human host.[83] In order to protect host cells from iron toxicity, intracellular iron is either incorporated into metalloproteins or stored by associating with ferritin.[84] This iron sequestration system used by the host cells doubles as pathogen protection by limiting the

amount of free iron. In order for bacteria to obtain this vital metal, they have developed various mechanisms to sequester or scavenge iron from their environment. One key strategy involves the production of siderophores, which are small, high affinity iron-chelating compounds secreted by bacteria.[85] These siderophores scavenge iron from the host environment and transport it back to the bacterial cells. The siderophores solubilize the iron and then are taken up back into the cell via specific outer membrane receptors involved in a process driven by the proton motive force and mediated by the energy-transducing TonB-ExbB-ExbD system.[86] Once back within the cell, the ferri-siderophore complex dissociates to free the complexed iron for use in cellular metabolism. Besides using bacterial siderophores to acquire iron from the host, pathogenic bacteria can acquire iron directly from iron-binding proteins from the host by using receptor-mediated transport systems specific for those host-iron protein complexes. Under low iron stress, bacteria are likely to upregulate the production of siderophores and iron transport systems.

Bacteria will also mobilize their intracellular iron storage proteins to provide a source of iron when external iron availability is limited. Additionally, in response to low levels of freely available iron, bacteria reduce the activity of non-essential iron-utilizing enzymes, activate iron-independent pathways, and express specific genes that are regulated by the availability of iron.[87]

1.4.4. Osmotic pressure

Changes in external osmotic pressure have direct effects on the integrity and hydration of bacterial cells. A decrease causes water influx and swelling or even cell lysis. An increase in external osmotic pressure causes water efflux and dehydration.[88] Both of these changes can perturb many cellular properties including cell volume, turgor pressure, cell wall strain, and cytoplasmic membrane tension. Bacterial cells exposed to high osmotic pressure must maintain correspondingly high intracellular solute concentrations.

Bacteria possess osmoregulatory machinery that senses changes in osmotic pressure. This machinery helps in maintaining cell integrity by balancing the internal and external osmotic pressure. Much of this machinery is made up of enzymes, transporters,

and channels that mediate solute accumulation and release. The structural integrity of the cell wall allows bacteria to withstand the mechanical stress exerted by osmotic pressure changes, thus protecting the cell from lysis or collapse.[89] Bacteria often respond to high salinity by using compatible solutes. For example, the halophile *Halobacillus halophilus* responds to high salinity by upregulating proline production.[90] These small organic molecules help in balancing the intracellular osmotic pressure without interfering with normal cellular processes.[91] When these low molecular weight compounds accumulate within the cell it causes an increase in free water, which then alleviates the osmotic stress.[91,92] Bacteria can accumulate these osmolytes through biosynthesis or via uptake from the environment, with the latter being more energetically favorable. For example, marine bacteria belonging to the family *Vibrionaceae* were found to use a variety of transporters to facilitate the uptake of osmolytes in response to high osmotic pressure. These transporters include members of the betaine-carnitine-choline transporter (BCCT) family and the ATP-binding cassette (ABC) family. Other bacteria have been known to utilize transporters from the MFS to facilitate osmolyte uptake as well. Bacteria may also use transporters to uptake substrates for osmolyte metabolism.[91]

ABC type efflux pump MacAB-TolC has been found to be involved in osmotic protection and is likely to be involved in the maintenance of iron homeostasis in *A. baumannii*. This pump has also been found to play an essential role in biofilm formation and has been found to be involved in cell envelope stress responses that help maintain membrane rigidity.[93]

Porins like OmpF and OmpC play an important role in regulating cellular permeability as they allow the passive diffusion of small molecules, including osmolytes. Under osmotic stress, such as high salt concentrations, porins can alter their conformation or expression levels to regulate the influx and efflux of solutes, thereby helping the bacteria maintain the balance of solutes and water across the bacterial membrane.[94] High osmotic pressure conditions in *Enterobacteriaceae*, the expression of OmpC is favored, whereas OmpF is more expressed under lower osmotic conditions. This differential expression helps the bacteria adapt to osmotic stress by altering the permeability of their outer membrane to different solutes.[95]

1.4.5. Bile salts

Bacterial pathogens have evolved various strategies to survive under the harsh conditions caused by bile salts in the host gastrointestinal tract. Bile salts, primarily acting as detergents, are critical for the digestion and absorption of fats but can also impose oxidative stress on bacterial cells due to the production of reactive oxygen and nitrogen species. Bile's main role in digestion is to emulsify and solubilize lipids, so it can disrupt cell membrane integrity by interacting with membrane phospholipids. This disruption could alter important membrane characteristics like permeability, fluidity or charge. An additional stressor comes from the deconjugation of bile salts that release protons, which results in intracellular acidification and exhibits toxicity similar to organic acids. This causes bacteria to have to respond to both bile and acid stresses.

To counteract the complicated nature of bile-based stresses, bacteria have developed a wide variety of resistance mechanisms. Bacteria like *Lactobacillus* activate specific genes in response to bile salts.[96] These genes play a role in halting cell division and to repair any damage to DNA caused by the bile salts. Some bacterial species, like *L. acidophilus*, have been seen to decrease production of oxidant molecules as a way to enhance bile tolerance.[97] And similar to how bacteria respond to heat shock, cells responding to the negative effects of bile overexpress chaperones and proteases to recycle damaged proteins and facilitate proper folding of nascent proteins.[98] *E. coli* is known to use the RND efflux pump AcrAB and MFS pump EmrAB to extrude bile salts (chenodeoxycholic acid) out of the cell.[99] The Gram-positive *Listeria monocytogenes* uses a bile salt hydrolase (BSH) enzyme to degrade bile acids, potentially as a detoxification mechanism.[100]

Gram-negative bacteria like *Klebsiella pneumoniae* remodel their outer membrane in response to bile stress.[101] The remodeling is essential to maintain the integrity of the cell envelope and it involves alterations in the lipid composition, porin expression, and surface structures of the outer membrane to reduce permeability and prevent bile salt uptake.[101] It is also possible that low levels of bile molecules intercalate with membrane lipids, resulting in mixed membranes that are more resistant to further detergent effects.[98]

1.5. Efflux pump inhibitors (EPIs)

Efflux pump inhibitors (EPIs) targeting RND pumps have the potential to become alternative treatment options when dealing with multidrug resistant bacterial infections. By inhibiting RND efflux pumps, EPIs can restore efficacy of antibiotics which are substrates of the inhibited pump. Reducing the export of antibiotics allows intracellular concentrations to accumulate to an effective level.[102] EPIs work by disrupting the normal function of these pumps and they can do so in various ways - preventing the energy supply from the PMF from reaching the efflux system, physically blocking substrates from binding to efflux pump active sites, as well as downregulation of efflux pump gene expression.[103] EPIs could also be anti-bacterial on their own because efflux pumps are required for survival in the host.[104] Currently there have only been EPIs identified that act against RND pumps. No EPIs have been identified to act against MFS pumps.

The first EPI discovered was first known as MC-207,100, and now known as PAβN (Phenylalanine-Arginine-β-Naphthylamide).[105] PAβN is an inhibitor and substate of RND efflux pumps in Gram-negative bacteria, including the AdeFGH pump of *A. baumannii*.[106] This inhibitor has been found to be a potentiator of antibiotics from various antibiotic classes, like fluoroquinolones, macrolides, oxazolidinones, chloramphenicol, and rifampin. When used alone, without an accompanying antibiotic, it did not demonstrate antibacterial activity. Researchers later found PAβN to be toxic in mice and found it to accumulate in several organs and resulted in nephrotoxicity due to accumulation in the kidneys.[107] While there have been numerous EPIs, like PAβN and its analogs, described in the literature, none have made it to clinical trials.

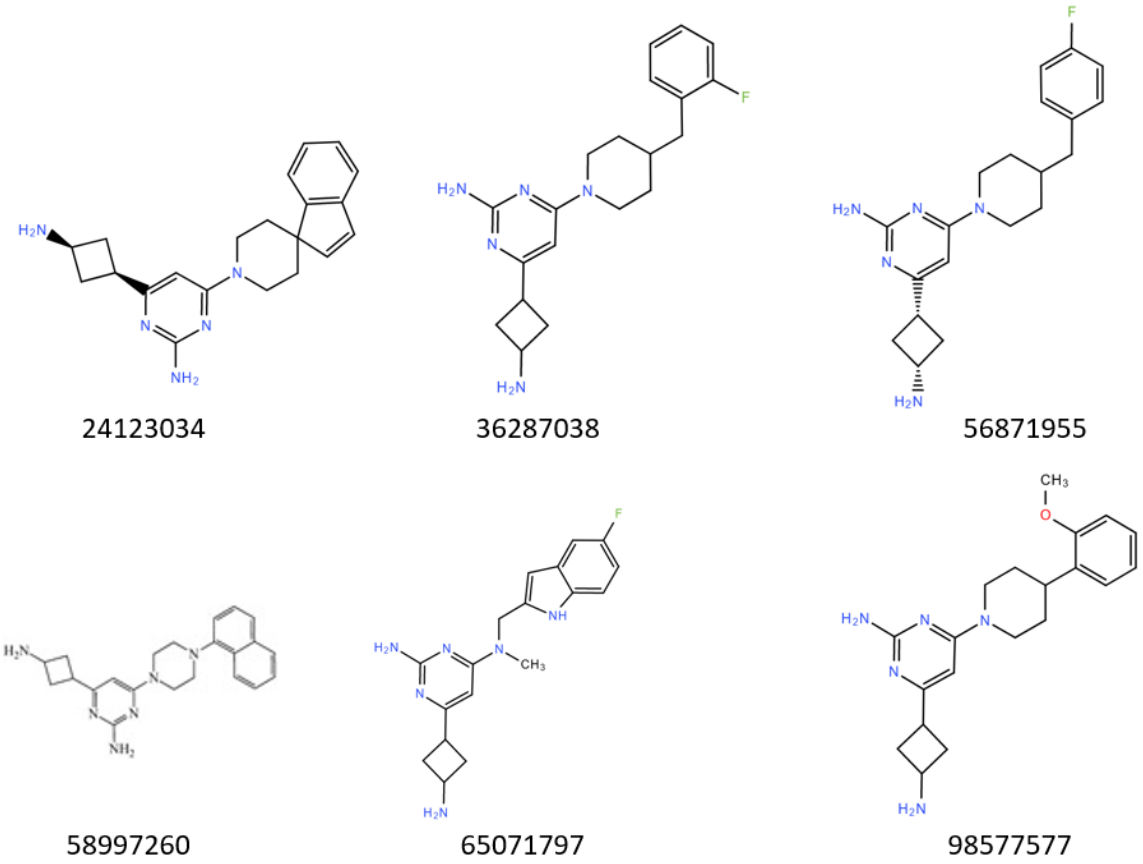

Figure 1.11 Structures of six Chembridge efflux pump inhibitors

Chembridge ID numbers listed under each structure.[108]

There have been several EPIs discovered in the Zgurskaya lab. They have a broad spectrum of activity and act against both *E. coli* and *A. baumannii.* These EPIs include six molecules with a shared scaffold that potentiate the activity of erythromycin and novobiocin in hyperporinated *E. coli* cells (**Figure 1.11**), and they also potentiate erythromycin and novobiocin up to 8-fold in WT *A. baumannii*.[108] There are also four small molecules that were found to inhibit AcrA of *E. coli*'s AcrAB-TolC and potentiate the activity of novobiocin: NSC227186, NSC60339, NSC33353, and NSC305798 (**Figure 1.12**).[109] Our lab has been able to determine the mechanism of action for some of these EPIs. For example, the AcrA inhibitor NSC 60339 was found to wedge itself into the cleft between the lipoyl and β-barrel domains of AcrA.[30]

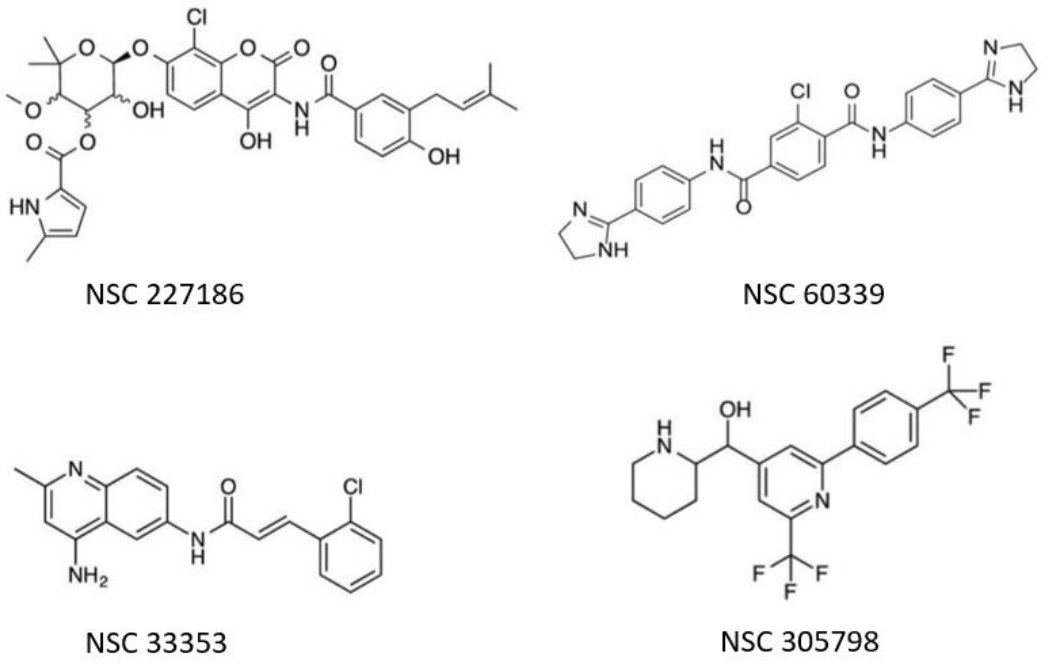

Figure 1.12 Structures of four NSC efflux pump inhibitors

NSC ID number listed below each structure. [109]

1.6. Critical assessment of the literature

While there are many published studies on *E. coli*, as it is the model Gram-negative organism, there is still much to uncover about the specifics of how *A. baumannii* responds to host-associated stress conditions. The research chapters of this dissertation aim to identify some of the missing pieces in these adaptive processes. For instance, how do multidrug efflux pumps work with the outer membrane to keep stressors out while maintaining normal cellular functions? The literature presents the hypothesis that MFS pumps likely facilitate osmolyte uptake and are involved in cell envelope stress responses that help maintain membrane integrity, but it is still unclear what specific cellular processes are dependent on these pumps. And while no additive or synergistic effects were seen in antibiotic susceptibility resulting from multiple deletions of MFS transporters, perhaps MFS pumps do work additively or synergistically with other multidrug transporters under different stress conditions besides antibiotic pressure. Secondary transporters like MFS and RND pumps provide the cell with energy efficient

substrate transport, compared to active transporters, so they are likely to be relied on by the cell when under stress from limited nutrients and/or exogenous stressors.

More research into *A. baumannii* active EPIs is also needed. Previous studies have mainly focused on EPIs targeting RND pumps in *E. coli* and *P. aeruginosa*, but none so far have focused on targeting *A. baumannii* RND transporters like AdeG. This work aims to provide insight into where substrates and EPIs bind in the AdeG transporter. It would also be beneficial to better understand what amino acid residues are important for substrate recognition and selectivity and how a single amino acid mutation may impact substrate specificity and EPI activity.

Chapter 2: Methods

2.1. Tables

Table 2.1 - List of bacterial strains used in these studies

Escherichia coli		
Strains	**Relevant Genotype**	**Source**
BW 25113	Wild-type strain Δ(*araD-araB*)567 Δ(*rhaD-rhaB*)568 Δ*lacZ*4787 (::rrnB-3) hsdR514 rph-1	[110]
DH5a	*fhuA2 lac(del)U169 phoA glnV44 Φ80' lacZ(del)M15 gyrA96 recA1 relA1 endA1 thi-1 hsdR17*	[111]
Sm10(λpir)	*thi thr leu tonA lacY supE recA*::RP4-2-TcR::Mu KmR λpir	[112]
Acinetobacter baumannii		
Strains	**Relevant Genotype**	**Source**
ATCC17978	Drug-susceptible wild type	ATCC
JWW30 (17978 WT)	*A. Baumannii* ATCC17978 resistant to streptomycin	[20]
IL188 (WTΔAmfAB)	JWW30 Δ*A1S_1772-73*	[113]

IL189 (WTΔAmfCD)	JWW30 Δ*A1S_1799-1800*	[113]
IL190 (WTΔ2)	IL189 Δ*A1S_1772-73::Gm*^{r}	[113]
IL119 (AbΔ3)	JWW30 Δ*adeIJK* Δ*adeAB* Δ*adeFGH*	[20]
IL139 (AbΔ3-Pore)	JWW30 Δ*adeAB*Δ*adeFGH*Δ*adeIJK att*Tn*7*::mini-Tn*7*T-Km^r -*araC*-P$_{BAD}$-FhuA	[52]
IL141 (AbΔ3 pAdeFGH)	JWW30 Δ*adeAB*Δ*adeFGH*Δ*adeIJK att*Tn*7*::mini-Tn*7*T-Tp^r -*araC*-P$_{BAD}$-*adeFGH* carrying pTJ1-*adeFGH*	[52]
IL 142 (AbΔ3 pAdeIJK)	JWW30 Δ*adeAB*Δ*adeFGH*Δ*adeIJK att*Tn*7*::mini-Tn*7*T-Tp^r -*araC*-P$_{BAD}$-*adeFGH* carrying pTJ1-*adeIJK*	[52]
IL 147 (AbΔ3-Pore pAdeFGH)	JWW30 Δ*adeAB*Δ*adeFGH*Δa*deIJK att*Tn*7*::mini-Tn*7*T-Km^r-*araC*-P$_{BAD}$-FhuA carrying pTJ1-*adeFGH*	[52]
IL198 (Δ3 ΔAmfAB)	IL119 Δ*A1S_1772-73*	[113]
IL199 (Δ3 ΔAmfCD)	IL119 Δ*A1S_1799-1800*	[113]
IL200 (Δ5)	IL199 Δ*A1S_1772-73::Gm*^{r}	[113]
IL186 (WT pAmfAB)	JWW30 *att*Tn*7*::mini-Tn*7*T-Tp^r-*araC*-P$_{BAD}$-*ABUW_1949-50* carrying pMOM101	[113]
IL187 (WT pAmfCD)	JWW30 *att*Tn*7*::mini-Tn*7*T-Tp^r-*araC*-P$_{BAD}$-*ABUW_1930-31* carrying pMOM102	[113]
MOM101 (Δ2 pAmfAB)	IL190 *att*Tn*7*::mini-Tn*7*T-Tp^r-*araC*-P$_{BAD}$-*ABUW_1949-50* carrying pMOM101	[113]
MOM102 (Δ2 pAmfCD)	IL190 *att*Tn*7*::mini-Tn*7*T-Tp^r-*araC*-P$_{BAD}$-*ABUW_1930-31* carrying pMOM102	[113]
IL194 (Δ3 pAmfAB)	IL119 *att*Tn*7*::mini-Tn*7*T-Tp^r-*araC*-P$_{BAD}$-*ABUW_1949-50* carrying pMOM101	[113]

IL195 (Δ3 pAmfCD)	IL119 *att*Tn*7*::mini-Tn*7*T-Tp^r-*araC*-P$_{BAD}$-*ABUW_1930-31* carrying pMOM102	113
MOM103 (Δ5 pAmfAB)	IL200 *att*Tn*7*::mini-Tn*7*T-Tp^r-*araC*-P$_{BAD}$-*ABUW_1949-50* carrying pMOM101	113
MOM104 (Δ5 pAmfCD)	IL200 *att*Tn*7*::mini-Tn*7*T-Tp^r-*araC*-P$_{BAD}$-*ABUW_1930-31* carrying pMOM102	113

Table 2.2 - List of plasmids used in these studies

Plasmid	**Relevant Genotype**	**Source**
pTNS3	Amp^r; Helper plasmid encoding Tn*7* transposase proteins TnsABCD from P1 and P$_{lac}$ promoter	114
pTJ1	pUC18T-mini-Tn*7*T-Tp-*araC*-P$_{BAD}$-MCS, Amp^r, Tp^r	115
pMOM101 (pTJ1-AmfAB)	pUC18T-mini-Tn*7*T-Tp-*araC*-P$_{BAD}$-*ABUW_1949-50*, Amp^r, Tp^r	113
pMOM102 (pTJ1-AmfCD)	pUC18T-mini-Tn*7*T-Tp-*araC*-P$_{BAD}$-*ABUW_1930-31*, Amp^r, Tp^r	113
pTJ1-adeFGH	pUC18T-mini-Tn*7*T-Tp-*araC*-P$_{BAD}$-*adeFGH*, Amp^r, Tp^r	52
pTJ1-adeIJK	pUC18T-mini-Tn*7*T-Tp-*araC*-P$_{BAD}$-*adeIJK*, Amp^r, Tp^r	52
pTJ1-adeG S620A	pUC18T-mini-Tn*7*T-Tp-*araC*-P$_{BAD}$-*adeG S620A*, Amp^r, Tp^r	This work
pTJ1-adeG A705I	pUC18T-mini-Tn*7*T-Tp-*araC*-P$_{BAD}$-*adeG A705I*, Amp^r, Tp^r	This work
pTJ1-adeG Q83A Y79S	pUC18T-mini-Tn*7*T-Tp-*araC*-P$_{BAD}$-*adeG Q83A Y79S*, Amp^r, Tp^r	This work
pTJ1-adeG I621A	pUC18T-mini-Tn*7*T-Tp-*araC*-P$_{BAD}$-*adeG I621A*, Amp^r, Tp^r	This work

pTJ1-adeG Q83A	pUC18T-mini-Tn*7*T-Tp-*araC*-P$_{BAD}$-*adeG Q83A*, Amp^r, Tp^r	This work
pTJ1-adeG G679I	pUC18T-mini-Tn*7*T-Tp-*araC*-P$_{BAD}$-*adeG G679I*, Amp^r, Tp^r	This work
pTJ1-adeG Y725A	pUC18T-mini-Tn*7*T-Tp-*araC*-P$_{BAD}$-*adeG Y725A*, Amp^r, Tp^r	This work
pTJ1-adeG L138A	pUC18T-mini-Tn*7*T-Tp-*araC*-P$_{BAD}$-*adeG L138A*, Amp^r, Tp^r	This work
pTJ1-adeJ G721A	pUC18T-mini-Tn*7*T-Tp-*araC*-P$_{BAD}$-*adeJ G721A*, Amp^r, Tp^r	This work
pTJ1-adeJ R701A	pUC18T-mini-Tn*7*T-Tp-*araC*-P$_{BAD}$-*adeJ R701A*, Amp^r, Tp^r	This work
pTJ1-adeJ N81A	pUC18T-mini-Tn*7*T-Tp-*araC*-P$_{BAD}$-*adeJ N81A*, Amp^r, Tp^r	This work
pTJ1-adeJ E675A	pUC18T-mini-Tn*7*T-Tp-*araC*-P$_{BAD}$-*adeJ E675A*, Amp^r, Tp^r	This work
pTJ1-adeJ F618A	pUC18T-mini-Tn*7*T-Tp-*araC*-P$_{BAD}$-*adeJ F618A*, Amp^r, Tp^r	This work
pTJ1-adeJ F136A	pUC18T-mini-Tn*7*T-Tp-*araC*-P$_{BAD}$-*adeJ F136A*, Amp^r, Tp^r	This work
pTJ1-adeJ A134I	pUC18T-mini-Tn*7*T-Tp-*araC*-P$_{BAD}$-*adeJ A134I*, Amp^r, Tp^r	This work

Table 2.3 - List of primers used in these studies

Primer Name	Sequence 5' → 3'
Ab (17978) glmS FWD	TTCGCTGATGAAAATAGTGG
Ab (17978) glmS REV	ATTCACCTCAAACCGTACAACG
PTn7R	CACAGCATAACTGAAACTTGTCACTATTCGGACTGATTTC
AmfAB_NcoI_FWD	CGCTCCATGGATAACGTAGCTCAGCTAGA
AmfAB_HindIII_REV	CGCAAGCTTCTAGTGGTGGTGGTGGTGCATATTCATTTTCTT
AmfCD_NcoI_FWD	CCTTCCATGGCAAATATACGACCACTCATCGGTTTG

AmfCD_EcoRI_REV	CTTGAATTCTTAGTGGTGGTGGTGGTGGTGTTTGGTCGTAT CCACAGAAAC
AdeG I621A FWD	TGGCCTCTCAgcTAATGGTTTCACCAATAG
AdeG I621A REV	GGGAAGGCAACAGCAC
AdeG Q83A FWD	TATGCAATCTgcAGCAAACAGC
AdeG Q83A REV	TACAGCATGTCTTCGAC

2.2. Strains and growth conditions

E. coli, A. baumannii AB5075, *A. baumannii* ATCC 17978 cells were grown at 37 °C with shaking in Luria-Bertani (LB) broth (10 g Bacto tryptone, 5 g yeast extract, and 5 g NaCl per liter; Research Products International, Mt. Prospect, USA). *A. baumannii* AB5075 was isolated from a diabetes patient's osteomyelitis of the tibia.[116]

When indicated, cultures were incubated with 1% L-arabinose (Sigma-Aldrich, St. Louis, USA) to induce expression of efflux pump proteins. For selection, ampicillin (100 µg/ml; Research Products International, Mt. Prospect, USA), 2,6-Diaminopimelic acid (0.3 mM; Sigma-Aldrich, St. Louis, USA), gentamicin (30 µg/ml; Sigma-Aldrich, St. Louis, USA), trimethoprim (100 µg/ml; Tokyo Chemical Industry, Portland, OR, USA), and streptomycin (100 µg/ml; Sigma-Aldrich, St. Louis, USA) were used.

2.3. Plasmid construction

Sequences of all primers can be found in **Table 2.3**. All primers were obtained from Sigma-Alrich (St. Louis, USA). Plasmids for the overexpression of EmrAB-like efflux pumps AB50751949-1950 and AB50751930-1931 were constructed using the vector pTJ1, an L-arabinose inducible overproduction plasmid that works well in *Acinetobacter* (plasmid genotypes can be found in **Table 2.2**). The genes of interest were PCR amplified from *A. baumannii* AB5075 genomic DNA, purified using the GenElute Bacterial Genomic DNA Kit (Sigma-Alrich. St. Louis, USA), and amplified using the primers "AmfAB_NcoI_FWD" and "AmfAB_HindIII_REV" for AmfAB, or "AmfCD_NcoI_FWD" and "AmfCD_EcoRI_REV" for AmfCD. Amplification condition was performed in a 50 ml reaction volume and consisting of 10 µl GC buffer, 2.5 µl forward primer, 2.5 µl reverse primer, 1 µl 10 mM dNTPs, 0.5 µl template DNA, 31.5 µl nuclease free water, 1.5 µl DMSO, and 0.5 µl Phusion DNA polymerase (New England Biolabs, Ipswich, USA). The mixture was amplified by an Eppendorf (Hamburg,

Germany) Mastercycler nexus gradient thermocycler. The thermocycler was programed for an initial denaturation at 98 °C for 30 seconds, followed by 25 cycles of denaturation at 98 °C for 30 seconds, annealing at 72 °C for 30 seconds, extension at 72 °C for 80 seconds, and a final extension at 72 °C for 10 minutes. The PCR products were examined by electrophoresis at 160 V for 25 minutes in a 1% (w/v) agarose gel containing 0.001 mg/ml of ethidium bromide (Sigma-Aldrich, St. Louis, USA) in 1X TAE buffer (4.84 g Tris, 1.14 mL acetic acid, 0.74g $Na_2EDTAx2H_2O$). The marker 1 Kb Plus DNA Ladder (Invitrogen, Carlsbad, USA) was used as a reference ladder. The electrophoresis gel was visualized in UV light.

PCR amplified fragments and the vector pTJ1 were digested with NcoI-HF and HindIII-HF for AB1949-1950, or NcoI-HF and EcoRI-HF for AB1930-1931 using the reaction conditions recommended by the manufacturer of the restriction enzymes (New England Biolabs, Ipswich, USA). The digested gene insert and vector were ligated together using T4-Ligase (Invitrogen, Carlsbad, USA) according to the manufacturer's recommended protocol. The constructs were confirmed by restriction analysis and DNA sequencing (as described below). Constructed plasmids pTJ1_AB1949-1950 or pTJ1_AB1930-1931 were electroporated into *A. baumannii* strains ATCC 17978 and its derivatives.

2.4. Chromosomal DNA insertion

Insertion of the efflux pump operons was carried out using previously described methods.[20] Overexpression vectors pTJ1_AB1949-1950 or pTJ1_AB1930-1931 and helper plasmid pTNS3 were electroporated into *A. baumannii* strains JWW30 (AbWT), AbΔ2, AbΔ3, and AbΔ5, and then plated onto LB agar plates supplemented with 100 μg/ml trimethoprim. Colonies were picked individually, and insertion was confirmed by PCR using 2 sets of primers: Set A as "Ab (17978) glmS FWD" and "Ab (17978) glmS REV" and Set B as "Ab (17978) glmS FWD" and "PTn7R".

2.5. Site-directed mutagenesis

All single and one double substitution mutations were introduced using either Agilent (Santa Clara, USA) QuikChange II XL Site-Directed Mutagenesis Kit or New England Biolabs' (Ipswich, USA) Q5 Site-Directed Mutagenesis Kit, as recommended by the manufacturer. The starting plasmid is pTJ1 containing the wild type operon of

AdeFGH. The resulting PCR products were treated with DpnI, transformed into DH5α competent cells and plated on Luria Bertani (LB) agar containing trimethoprim (100 μg/mL). For each mutant, at least two plasmids were purified and sequenced to assess the presence of the desired mutation and absence of any non-desired mutations. All mutations were verified by whole plasmid DNA sequencing at Plasmidsaurus (Eugene, USA) DNA Sequencing Facilities.

2.6. Minimum inhibitory concentration (MIC) determination

The MIC determinations were carried out as previously described[117] using the 2-fold broth dilution method. Briefly, the cells were grown in LB broth with appropriate antibiotics wherever necessary at 37 °C with shaking at 200 rpm. MICs of different classes of antimicrobial agents were measured in 96-well micro-titer plates. For this purpose, exponentially growing cells were inoculated at a density of 10^5 cells per mL into wells containing just LB or LB medium supplemented with 1% L-arabinose in the presence of two-fold-increasing concentrations of the following antibiotics (ten concentrations in total): chloramphenicol (Sigma-Alrich, St. Louis, USA), norfloxacin (Sigma-Alrich, St. Louis, USA), novobiocin (Sigma-Alrich, St. Louis, USA), erythromycin (Sigma-Alrich, St. Louis, USA), ciprofloxacin (Sigma-Alrich, St. Louis, USA), tetracycline (Sigma-Alrich, St. Louis, USA), nalidixic acid (Sigma-Alrich, St. Louis, USA), azithromycin (Tokyo Chemical Industry, Portland, OR, USA), zeocin (Alfa Aesar, Ward Hill, USA), and sodium dodecyl sulfate (Sigma-Alrich, St. Louis, USA). The first concentration in the experiment was drug-specific and is usually 2–4 fold higher than the MIC of AbWT, if it is possible to determine. There were two control wells per plate with no antibiotics +/− cells for quality control. Cell growth was determined visually after incubation of the micro-titer plates at 37 °C for 16–20 h. All measurements were performed in duplicates and repeated at least two times independently.

2.7. MPC4 determination

The minimal potentiating concentration (MPC) was defined as a concentration of a compound that decreases the MIC of an antibiotic by four (MPC4) or more fold.[105] A checkerboard titration assay was used to measure the MPC4 of a compound, in which an antibiotic was dispensed alone in the first row of the plate and was combined with a test

compound in the remaining rows. The test compound was also dispensed alone in the first column. The antibiotic was tested at 11 concentrations and the test compound was tested at 7 concentrations. The plate was then inoculated with $5x10^4$ cells per well, placed in the incubator at 37 °C with shaking for 18 hours, and the MIC values were read by visual inspection of the wells.

2.8. Growth curve determination

Cells from frozen stocks were inoculated into LB medium containing appropriate antibiotics if needed and incubated for 16 h at 37 °C. Exponentially growing cells were inoculated at a density of 10^5 cells per mL into wells containing LB or LB + 1% L-arabinose medium with and without stress condition. The strength of the stress with the different agents was designed to be as similar and relevant as possible for *A. baumannii* (**Table 3.2**).[67] Bacterial growth assay was performed in a temperature-controlled micro-plate reader (Tecan Spark 10M, Männedorf, Switzerland). The optical density of cells was measured every 30 min in clear 96-well micro-titer plates over 24 h. All measurements were performed in triplicate and repeated at least three times independently. After averaging, area under the curves (AUC)[118,119] were calculated for each strain under different exposures using the formula:

$$AUC = (OD_{n+1} + OD_n)/2 \times (T_{n+1} - T_n).$$

To test the effect of iron deficiency on the bacterial growth in the absence of 2,2'-dipyridyl, we followed the same protocol, but instead of using LB broth, the deletion strains were grown in the M9 citrate minimal medium [120] with and without a ferric iron supplement (3.1 μM).

2.9. Membrane fraction purification

The preparation of bacterial cell membranes was performed as described in Koronakis et al., with minor alterations.[121] Cells were grown overnight in LB medium containing appropriate selection antibiotic if applicable. Overnight cells were inoculated into fresh LB at a 1:50 ratio and grown for 1 hour at 37 °C with shaking at 200 rpm to OD_{600} ~0.3. Cells were induced with 1% L-arabinose and grown for another 3 hours. Cells were pelleted at 4 °C, 4,000 rpm (Eppendorf Centrifuge 5804, rotor S-4-72), for 15

minutes. Cell pellets were resuspended in Lysis buffer (50 mM Tris, 5 mM EDTA, 100 µg/mL Lysozyme, 1 mM PMSF) and kept on ice for 30 minutes. Lysed cells were sonicated 2-3 times in 30 second rounds. Unbroken cells were pelleted at 4 °C, 4,000 rpm (Eppendorf Centrifuge 5804, rotor S-4-72), for 15 min. The supernatant containing lysed cell content was pelleted in a Beckman Coulter Optima TLX Ultracentrifuge at 4 °C, 45,000 rpm (Beckman Coulter Optima TLX Ultracentrifuge, rotor TLA 55), for 1 hour. The pellet containing the membrane fraction was resuspended in Resuspension buffer (100 mM Tris, 300 mM NaCl, 2 mM PMSF) using water sonication.

2.10. Protein concentration determination

Dye reagent was prepared by diluting 1 part Dye Reagent Concentrate (Bio-Rad, Hercules, USA) with 4 parts deionized water and filter sterilized. Bovine Serum Albumin (BSA; Research Products International, Mt. Prospect, USA) standards were prepared in the following concentrations: 0.2 mg/ml, 0.4 mg/ml, 0.6 mg/ml, 0.8 mg/ml, and 1.0 mg/ml. For each standard, 20 µL of standard solution was added to a clean, dry microfuge tube. For each sample, 18 µL of Resuspension buffer and 2 µL of sample were added to a microfuge tube. The blank was prepared with 20 µL Resuspension buffer. To each prepared microfuge tube, 1 mL of diluted dye reagent was added and mixed. The tubes were incubated at room temperature for ~5 minutes. Absorbance was measured at 595 nm. Sample protein concentration was calculated based on BSA standard curve equation.

2.11. Inner and outer membrane fraction separation

For each set of membrane fractions the total protein concentration was determined using a standard curve and a Bradford assay as described above. Resuspension buffer and 0.4% Triton were used to adjust all samples to the lowest protein concentration and a final concentration of 0.2% Triton. The samples were then rotated at 4 °C overnight to solubilize membrane proteins. The samples were then pelleted at 4 °C, 50,000 rpm (Beckman Coulter Optima TLX Ultracentrifuge, rotor TLA 55) for 1 hour. The supernatant containing the inner membrane protein fraction was separated from the pellet. The pellet containing the outer membrane protein fraction was resuspended in resuspension buffer.

2.12. NPN fluorescent probe uptake assay

These experiments were carried out as described before.[20] Cells were grown overnight in LB medium containing appropriate selection antibiotic if applicable. An aliquot of 0.5 mL overnight cell culture was inoculated into fresh 20 mL LB medium and grown at 37 °C with shaking at 200 rpm to OD_{600} 0.3. Cells reach this approximate OD_{600} after an hour of growth, at which point the cell cultures were induced with 1% L-arabinose and grown for three more hours. The cells were then pelleted at room temperature by centrifugations for 20 minutes. The pellet was resuspended and washed in 10 mL HMG buffer (50 mM HEPES-KOH buffer (pH 7.0) containing 1 mM $MgSO_4$ and 0.4 mM glucose). The pellet was resuspended again in HMG buffer with a variable volume that resulted in a final OD_{600} of 1.0 +/- 0.05 for each cell strain. The cells were kept at room temperature during the course of the experiment. Uptake assays were performed in a multimode microplate reader (Tecan Spark 10M, Männedorf, Switzerland). The fluorescence of NPN (1-N-phenylnaphthylamine; Sigma-Alrich. St. Louis, USA) was monitored at λex = 350 nm and λem = 405 nm at a gain of 75 for 10 min. All measurements were collected in duplicates and performed with at least two biological and two technical repeats.

2.13. Analysis of fluorescence uptake data

The data was first plotted in Microsoft Excel, with replicates averaged and standard deviation or standard error also calculated for each curve. Fluorescence was normalized to the first reading of the wells without cells and the data was inspected for outliers. To calculate initial rates and steady states of fluorophore uptake, the time courses were imported into MATLAB (MathWorks, Natick, USA) and analyzed using the home written program STEADYSTATE_PREPROCESS.[122]

2.14. Clustering

Clustering analysis was performed by Dr. Justyna Adamiak. Multivariate statistical techniques (principal component analysis, PCA) were applied to investigate the association between strains depending on their physiological properties (growth under stress conditions, NPN uptake, MICs). Data for conducting PCA were normalized by

centering to the mean and dividing by the standard deviation. All code, unless indicated, was written in house using RStudio 1.4 and R version 4.04.

2.15. Antigen preparation for antibody production

E. coli C43 cells containing pTJ1_AdeB or pTJ1_AdeJ were grown overnight in LB media containing 100 µg/ml Ampicillin at 37 °C with shaking. The cells were then subcultured into 1 L of fresh LB media containing 100 µg/mL Ampicillin and grown at 37 °C with shaking. After 2 hours the cultures were induced with [0.2 mM] Isopropyl β-d-1-thiogalactopyranoside (IPTG; Inalco SAS, Milano, Italy) then grown for another 5 hours. To collect the cells, the cultures were centrifuged at 4,000 rpm (Eppendorf Centrifuge 5804, rotor S-4-72) in 4 °C for 30 minutes. The pellets were resuspended in 40 mL resuspension buffer (100 mM NaCl, 10 mM Tris-HCl pH 7.5, 1 mM PMSF). The cells were once again centrifuged at 4,000 rpm (Eppendorf Centrifuge 5804, rotor S-4-72) in 4 °C for 20 minutes, then the pellets were frozen at -20 °C. To prepare cells for lysis, the pellets were defrosted at room temperature and resuspended in 40 mL lysis buffer (20 mM Tris-HCl pH 7.5, 5 mM EDTA, 0.05 mg/mL DNAse, 1 mM PMSF).

The cells were lysed using a FRENCH Pressure Cell Press (SLM Instruments Inc.). The samples were centrifuged at 4,000 rpm (Eppendorf Centrifuge 5804, rotor S-4-72) in 4 °C for 20 minutes to pellet the unbroken cells. The supernatant was collected and centrifuged at 35,000 rpm (Beckman Coulter Optima TLX Ultracentrifuge rotor TLA 55) at 4 °C for 1 hour. The pellets containing the membrane fraction were washed with 40 mL resuspension buffer then centrifuged again at 35,000 rpm (Beckman Coulter Optima TLX Ultracentrifuge rotor TLA 55) in 4 °C for 30 minutes. The pellets were resuspended in 10 mL of solubilization solution (25 mM HEPES, 150 mM NaCl, 2% DDM, 1 mM PMSF) and set up to rotate overnight at 4 °C. The samples were then centrifuged at 40,000 rpm (Beckman Coulter Optima TLX Ultracentrifuge rotor TLA 55) in 4 °C for 1 hour. The supernatant was collected as the soluble fraction and purified using a nickel-affinity column. The resulting fractions were visualized on a 12% SDS-PAGE gel followed by Coomassie staining and western blot to identify the fractions with the highest concentration of the protein. The selected fractions were combined and visualized on another 12% SDS-PAGE gel along with bovine serum albumin (BSA) standards (0.2 µg,

0.5 µg, 1.0 µg, 1.5 µg, 2.0 µg). Quantity One (Bio Rad) was used to quantify the samples' protein concentrations.

The remaining samples were run on 8% SDS-PAGE gels and stained with Coomassie dye. Our protein bands were cut out of the gels and placed in conical tubes containing PBS (Phosphate-buffered saline) buffer (10 mM Phosphate, 2.7 mM Potassium Chloride, 137 mM Sodium Chloride, pH 7.4). These protein samples serve as our supplied antigens for rabbit immunization.

2.16. Protein structure modeling

The newly named AmfA, AmfB, AmfC, and AmfD efflux pump protomer structures were predicted by the I-TASSER (Iterative Threading ASSembly Refinement) online platform, made and maintained by the Yang Zhang lab[123,124,125], which uses I-TASSER based algorithms for protein structure and function predictions. For each protomer, the protein's amino acid sequence was submitted to the I-TASSER server. The server first attempts to retrieve template proteins of similar folds from a locally stored copy of the PDB library, by LOMETS (Local Meta-Threading Server, version 3. A meta-server approach to template-based protein structure prediction and structure-based function annotation). Then the snippets of template folds are reassembled into full-length models by replica-exchange Monte Carlo simulations. Any unaligned regions (mainly flexible loop regions) are built by ab initio modeling and incorporated into the full-length model. Clustering the simulation decoys via SPICKLER (a clustering algorithm to identify the near-native models from a pool of protein structure decoys) was done to find the low free-energy states of the protein models. Next, the structure is re-assembled starting from the SPICKLER cluster centroid. This second assembly is guided by the spatial restraints collected from the LOMETS templates and the PDB structures by TM-align (an algorithm for sequence independent protein structure comparisons). The aim of the second assembly is to remove steric clash and to refine the previously identified lowest free-energy structures. The final models are obtained by REMO (an algorithm for constructing protein atomic structures from C-alpha traces by optimizing the backbone hydrogen bonding networks), which finishes the atomic detail of the assembled model through the optimization of the hydrogen-binding network. Part of the I-TASSER server

output includes up to five full-length atomic models (ranked based on cluster density). The models with the highest cluster density were chosen for this work. The models, downloaded as PDB files, were visualized, colored, and labeled on Pymol (a molecular visualization system).

Results

Chapter 3: Characterization of Two MFS Efflux Pumps, AmfAB and AmfCD, from Multidrug Resistant Strain *A. baumannii* 5075

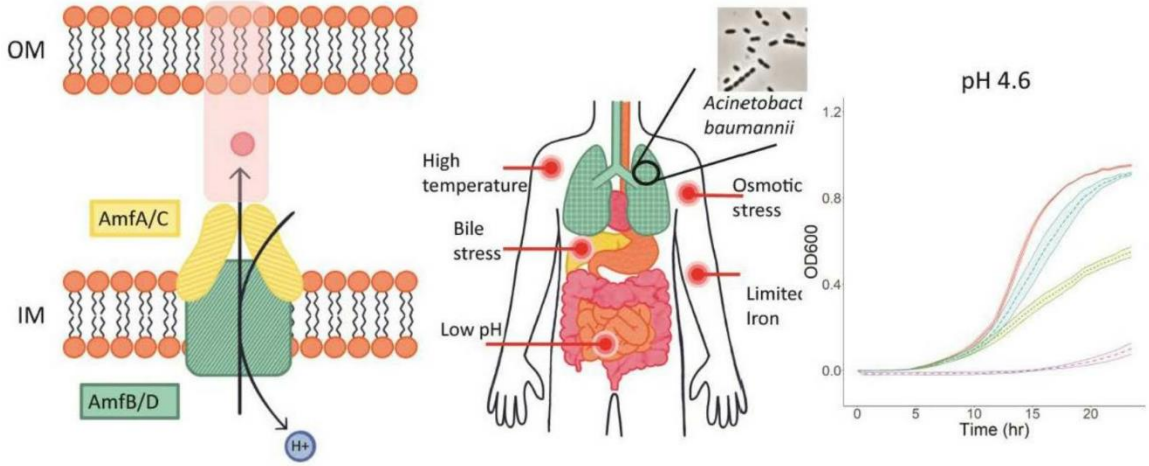

3.1. Abstract

Multidrug efflux transporters are major contributors to the antibiotic resistance of *A. baumannii* in clinical settings. Previous studies showed that these transporters are tightly integrated into the physiology of *A. baumannii* and have diverse functions. However, for many of the efflux pumps, such functions remain poorly defined. In this study, we characterized two putative drug efflux pumps, AmfAB and AmfCD (Acinetobacter Major Facilitator), that are homologous to EmrAB-like transporters from *Escherichia coli* and other Gram-negative bacteria. These pumps comprise the Major Facilitator Superfamily (MFS) transporters AmfB and AmfD and the periplasmic membrane fusion proteins AmfA and AmfC, respectively. I overproduced these pumps in the wild-type ATCC 17978 strain and its derivative strains lacking the major efflux pumps from the Resistance–Nodulation–Division (RND) superfamily in order to functionally characterize the pumps under various stress conditions, including several classes of antibiotics and stress conditions typically encountered during human infections. I found that neither AmfAB nor AmfCD significantly contribute to *A.*

baumannii's antibiotic susceptibility profile, meaning that they do not confer resistance to any antibiotic. However, I did find that the two pumps are crucial for *A. baumannii* survival under acidic conditions. This suggests that these pumps play a role in maintaining intracellular pH homeostasis in *A. baumannii*. I also found that inactivation of either AmfAB or AmfCD makes cells less permeable to the fluorescent probe NPN. On the other hand, over expression of either pump impairs cell growth and is toxic to cells. These results suggest that MFS transporters assist in stress adaptation by modifying the permeability barrier of *A. baumannii* and perhaps also by helping maintain normal metabolic processes.

3.2. Introduction

A. baumannii is a Gram-negative ESKAPE pathogen that can cause a broad range of severe infections in humans.[126,114] This microorganism is well known for its environmental persistence—its ability to grow across a range of temperatures, osmotic conditions, and pHs.[115] Extensive antibiotic use in the hospital environment has allowed this pathogen to develop resistance to all classes of antibiotics and become better suited to out-competing other bacteria that are drug-susceptible.[127] As a result, multidrug-resistant *A. baumannii* infections commonly occur in hospital settings and can spread quickly among patients within those environments.[128] These adaptations make *A. baumannii* a worrisome pathogen, especially for vulnerable and critically ill patients.

A. baumannii utilizes a variety of antibiotic resistance mechanisms, among which the active efflux of antibiotics and biocides is the major contributor of antimicrobial resistance in clinical settings.[129] As in other Gram-negative bacteria, the efflux pumps of *A. baumannii* belong to several families of transporters. The most clinically important are transporters from the RND superfamily of proteins.[114,130,131] We previously found that the inactivation of major RND efflux pumps AdeABC and AdeIJK in MDR *A. baumannii* AB5075 strain leads to changes in antibiotic susceptibilities and to pump-specific changes in transcriptomes and growth phenotypes.[52,64] Among others, the putative efflux pumps from the MFS superfamily ABUW_1930/ABUW_1931 (now named AmfCD) and ABUW_1949/ABUW_1950 (now named AmfAB) were significantly overproduced in RND-deficient cells.[64] Based on the previous study's results, we anticipated that, similar

to RND pumps, these putative EmrAB-like pumps would have substrate specificities and some involvement in *A. baumannii*'s antimicrobial non-susceptibility, perhaps as alternative exporters to make up for the loss of RND efflux.

A study published by Lin et al. in 2017 demonstrated that A1S_1772 and A1S_1773 (AmfAB) were *A. baumannii* homologues of EmrA and EmrB, respectively, by in silico analysis, expression analysis, and efflux assay.[132] The study identified a link between this efflux pump system and *A. baumannii*'s response to osmotic stress and the bacterium's ability to resist several compounds. Going into our study we anticipated AmfAB to have a noticeable impact on *A. baumannii*'s ability to survive under antibiotic stress and/or under osmotic stress.

Like RND efflux pumps, these MFS transporters function as tripartite complexes. The first genes in the ABUW_1930/ABUW_1931 (AmfCD) and ABUW_1949/ABUW_1950 (AmfAB) operons encode the periplasmic membrane fusion proteins followed by the MFS transporters. However, genes encoding the OMP components are not present in the operons and are likely encoded somewhere else on the chromosome. EmrAB is known to confer resistance to hydrophobic compounds like nalidixic acid and thiolactomycin in *E. coli* [60], but the substrate specificities of MFS efflux pumps and their potential functions in the drug resistance and physiology of *A. baumannii* remain unknown.

In this study, Dr. Inga Leus generated deletions of genes encoding the putative EmrAB-like multidrug efflux pumps of *A. baumannii* and I constructed strains overproducing these transporters in the cells with the wild-type repertoire of RND efflux pumps (derivatives of *A. baumannii* ATCC17978), cells lacking the EmrAB-like transporters, and cells lacking the RND pumps.[20] The constructed strains were characterized for their susceptibilities to representative antibiotics and their abilities to grow under stress conditions associated with human infections. We found that EmrAB homologs have non-complementary functions, but both contribute to the survival of *A. baumannii* under acidic stress.

3.3. Results

3.3.1. Genomic Context

Analyzing the genomic context of a gene of interest provides insights into the gene's function and its interactions with other genes. In bacterial chromosomes, genes that are physiologically linked are often closely clustered together and adjacent to their regulatory elements. This arrangement facilitates coordinated gene regulation and function. In most bacteria, genes within the same operon are usually separated by 20 nucleotides bases or fewer.[133]

3.3.1.1 Genomic Context of AmfAB

First, looking at ABUW_1949/1950 within the AB5075 chromosome we can see that the two genes follow the efflux pump naming convention where the first gene in the two gene operon is the membrane fusion protein *amfA* followed by the inner membrane protein transporter *amfB*. There is a 23 nucleotide intergenic region between *amfA* and *amfB*. This region was conserved during the cloning process.

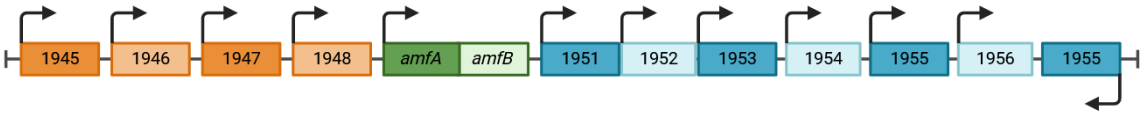

Figure 3.1 Genomic locus of *amfAB*

Schematic of the *amfAB* gene locus within the Ab5075 chromosome. The *amfAB* genes are shown in green. ABUW genes upstream of *amfAB* are shown in orange. ABUW genes downstream of *amfAB* are shown in blue. The black arrows indicate the direction of transcription. Created in BioRender.com.

Upstream of *amfAB* the next closest annotated gene in the ABUW genome is 683 nucleotides away (**Figure 3.1**). The upstream genes are annotated to be an indoleacetamide hydrolase (ABUW_1948), a LuxR family transcriptional regulator (ABUW_1947), a hypothetical protein (ABUW_1946), and a methlenetetrahydrofolate reductase domain (ABUW_1945). It is possible that AmfAB is involved in quorum sensing due to its proximity to the LuxR gene, but the genes in this area are unlikely to interact with *amfAB* due to its distance away from the *amfAB* operon.

Downstream of *amfAB* the next closest annotated gene is 154 nucleotides away. The downstream genes are annotated to be a hypothetical protein (ABUW_1951), an auxin-responsive GH3-related protein (ABUW_1952), an outer membrane efflux protein (ABUW_1953), a putative acid phosphatase (ABUW_1955), another hypothetical protein

(ABUW_1956), and a guanosine 3',5'-bis(diphosphate) 3'-pyrophosphohydrolase (ppGppase) (ABUW_1957). From this group of genes, it is possible that AmfAB interacts with ABUW_1953, the outer membrane efflux protein. The amino acid sequence of ABUW_1953 aligns with A1S_1769 (99% ID, 93% coverage), which is annotated as a putative RND transporter in the *A. baumannii* ATTC 17978 genome.

An alignment of the amino acid sequence of ABUW_1953 showed it is likely to be an outer membrane channel. When aligned with the ABUW genes *adeABC, adeFGH,* and *adeIJK,* ABUW_1953 only had significant alignment with the outer membrane proteins (**Table 3.1**). ABUW_1953 also showed some similarity to the promiscuous outer membrane channel TolC from *E. coli* K-12.[134] It is possible, due to its proximity to the *amfAB/CD* operons, that ABUW_1953 could be the outer membrane protein the Amf efflux pumps form complexes with to extrude substrates outside the cell.

3.3.1.2. Genomic Context of AmfCD

Next, looking at the ABUW_1930/1931 I found that in this operon the first gene is for the transporter AmfD followed by the membrane fusion protein AmfC. This arrangement is unusual because typical efflux pump operons have the membrane fusion protein as the first gene, followed by the transporter gene.[135,136] There is no gap between *amfC* and *amfD* as the stop codon for *amfD* overlaps with the start codon of *amfC*.

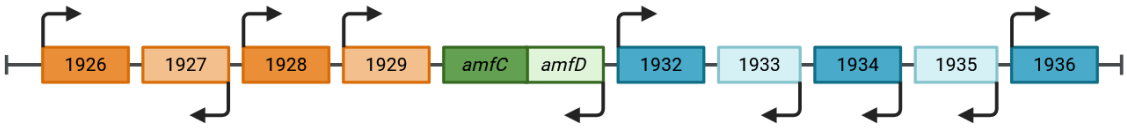

Figure 3.2 Genomic locus of *amfCD*

Schematic of the *amfCD* gene locus within the Ab5075 chromosome. The *amfCD* genes are shown in green. ABUW genes upstream of *amfCD* are shown in orange. ABUW genes downstream of *amfCD* are shown in blue. The black arrows indicate the direction of transcription. Created in BioRender.com

Upstream of ABUW_1930/1931, the next closest annotated gene is 100 nucleotides away (**Figure 3.2**). The upstream genes are annotated to be an MFS transporter (ABUW_1926), a LysR family transcriptional regulator similar to adeL (ABUW_1927), and two hypothetical proteins (ABUW_1928 and ABUW_1929). The MFS transporter

ABUW_1926 appears to have a homologue in *A. baumannii* 17978 in A1S_1805 with a 100% identity and 92% coverage when aligning their protein sequences. The gene A1S_1805 is annotated as a general substrate transporter.

After BLASTing the amino acid sequence for ABUW_1928, the top alignment result with 28% identity and 84% coverage was LMOf2365_1219 from *Listeria monoctyogenes str.* 4bF2365. This *L. monocytogenes* gene is annotated as a putative membrane protein. Chakravarty, et al. found the gene LMOf2365_1219 to be upregulated in response to bile stress at acidic pH under anaerobic conditions. BLASTing the amino acid sequence for ABUW_1929 revealed a somewhat similar alignment to gene G8E09_17135 from *Acinetobacter pittii* with 31% identity and 88% coverage. The gene G8E09_17135 is annotated as the putative inner membrane exporter YdcZ of the drug/metabolite transporter (DMT) family.

Downstream of *amfCD* the next closest gene is 166 nucleotides away. The downstream genes are annotated as a TetR family transcriptional regulator (ABUW_1932), an NADP-dependent fatty acid dehydrogenase (ABUW_1933), a dihydroxy-acid dehydratase (ABUW_1934), a fumarylacetoacetate hydrolase (ABUW_1935), a LysR family transcriptional regulator (ABUW_1936), a nucleoside-diphosphate-sugar epimerase (ABUW_1937), and a transporter from the anion/cation symporter family (ABUW_1938). The dihydroxy-acid dehydratase ABUW_1934 appears to have a homologue in *A. baumannii* 17978: A1S_1795 with 99% identity and 100% coverage.

The transporter ABUW_1938 has a homologue in *A. baumannii* 17978: A1S_1791 with 99% identity and 93% coverage in their amino acid sequences, which is annotated as a putative tartrate symporter protein from the MFS superfamily. A protein BLAST of ABUW_1938 results in many MFS proteins, including the quinolone resistance transporter AbaQ with 39% identity and 88% coverage.

The closest RND operon to the *amf* genes is *adeABC,* which is located about 23.6 kbp away from *amfAB*. Unlike in *A. baumannii* 17978, AB5075 has only one copy of *adeA* plus a copy of *adeC*, which AB17978 does not have. It is possible that one or both of the Amf pumps utilize AdeC to complete their efflux complex, and because the drug susceptible strain *A. baumannii* 17978 does not encode a copy of *adeC* this could be why

overexpression of the Amf pumps did not show a significant difference in antibiotic susceptibility.

Table 3.1 Aligning ABUW_1953 against outer membrane proteins

	(N/P %ID)
AdeC	- / 23%
AdeH	- / 19%
AdeK	- / 30%
TolC	- / 24%

Table shows values of nucleotide % identity / protein % identity as determined by NBCI's nucleotide and protein BLAST. (-) symbolizes no significant alignment.

Table 3.2 Aligning ABUW *amf* genes against *A. baumannii* ATCC 17978 MFS pumps

	AmfA	AmfB	AmfC	AmfD
AmfB (1772)	- / -	96% / 100%	- / -	- / 27%
AmfA (1773)	97% / 99%	- / -	- / 35%	- / -
AmfD (1799)	- / -	- / 27%	- / -	99% / 100%
AmfC (1800)	- / 31%	- / -	98% / 97%	- / -
AbaF	- / -	- / 26%	- / -	- / -
AbaQ	- / -	- / 22%	- / -	- / -
AmvA	- / -	- / 21%	- / -	- / 22%
CraA	- / -	- / 27%	- / -	- / 31%
TetA	- / -	- / 26%	- / -	- / -
AedD	- / -	- / 22%	- / -	- / 25%

Table shows values of nucleotide % identity / protein % identity as determined by NBCI's nucleotide and protein BLAST. (-) symbolizes no significant alignment.

Table 3.3 Aligning ABUW and A1S MFS genes

MFS GENE	(N/P % ID)
AbaF	98% / 100%
AbaQ	96% / 99%
AmvA	98% / 99%
CraA	99% / 100%
TetA	95% / 95%
AedD	99% / 100%

Table shows values of nucleotide % identity / protein % identity as determined by NBCI's nucleotide and protein BLAST

3.3.1.3. MFS transporters of *A. baumannii* homologous to AmfAB and AmfCD

In another effort to help decipher the function of AmfAB and AmfCD, their nucleotide and protein sequences were aligned against other *A.baumannii* MFS pumps

(**Table 3.2**). As expected, the membrane fusion proteins AmfA and AmfC had no significant similarity with the MFS transporters. The transporter AmfB had the highest protein ID similarity to AmfD (27%), followed by CraA (27%), AbaF (26%) and TetA (26%). These similarity scores are not very high and indicate marginal similarity between protein sequences. AmfB showed similar protein identities with all MFS transporters it was aligned against, but AmfD only showed significant similarity when aligned against CraA (31%), AmfB (27%), AedD (25%), and AmvA (22%).

No other close homologues were identified. A putative outer membrane efflux protein ABUW_1953 and A1S_1763 identified here could function in complex with AmfAB and/or AmfCD. The genomic context revealed three possible transcriptional regulators of these pumps: a LuxR family (ABUW_1947) regulator involved in quorum sensing upstream of *amfAB* and two LysR family regulators near *amfCD.* The LysR gene upstream of *amfCD* (ABUW_1927) was found to be similar to *adeL*, a gene encoding a regulator of *adeFGH*. The other LysR gene (ABUW_1936) was found downstream of *amfCD.* More genetic work is needed to further investigate the regulation of the MFS pumps.

3.3.2 Structure predictions of MFS transporters

To get a better idea about the structures of these newly characterized MFS pumps, their amino acid sequences were submitted to the I-TASSER server for structure prediction because no solved structures exist for these pumps. AmfAB and AmfCD are homologues of the MFS pump EmrAB from *E. coli* , so the Amf models are shown with their EmrAB counterparts (**Figures 3.3** and **3.4**) for comparison. Due to crystallization complications, an engineered version of EmrA lacking the transmembrane helix domain was used and the final model includes EmrA residues 27-321 and 343-373. The structure of the engineered EmrA was obtained by X-ray diffraction to a resolution of 2.85 Å (**Figure 3.4-A**).[137] There is currently no solved structure for EmrB, but a model was predicted using AlphaFold available for use on the AlphaFoldDB with the UniProt accession code P0AEJ0 (**Figure 3.3-A**).[138–140]

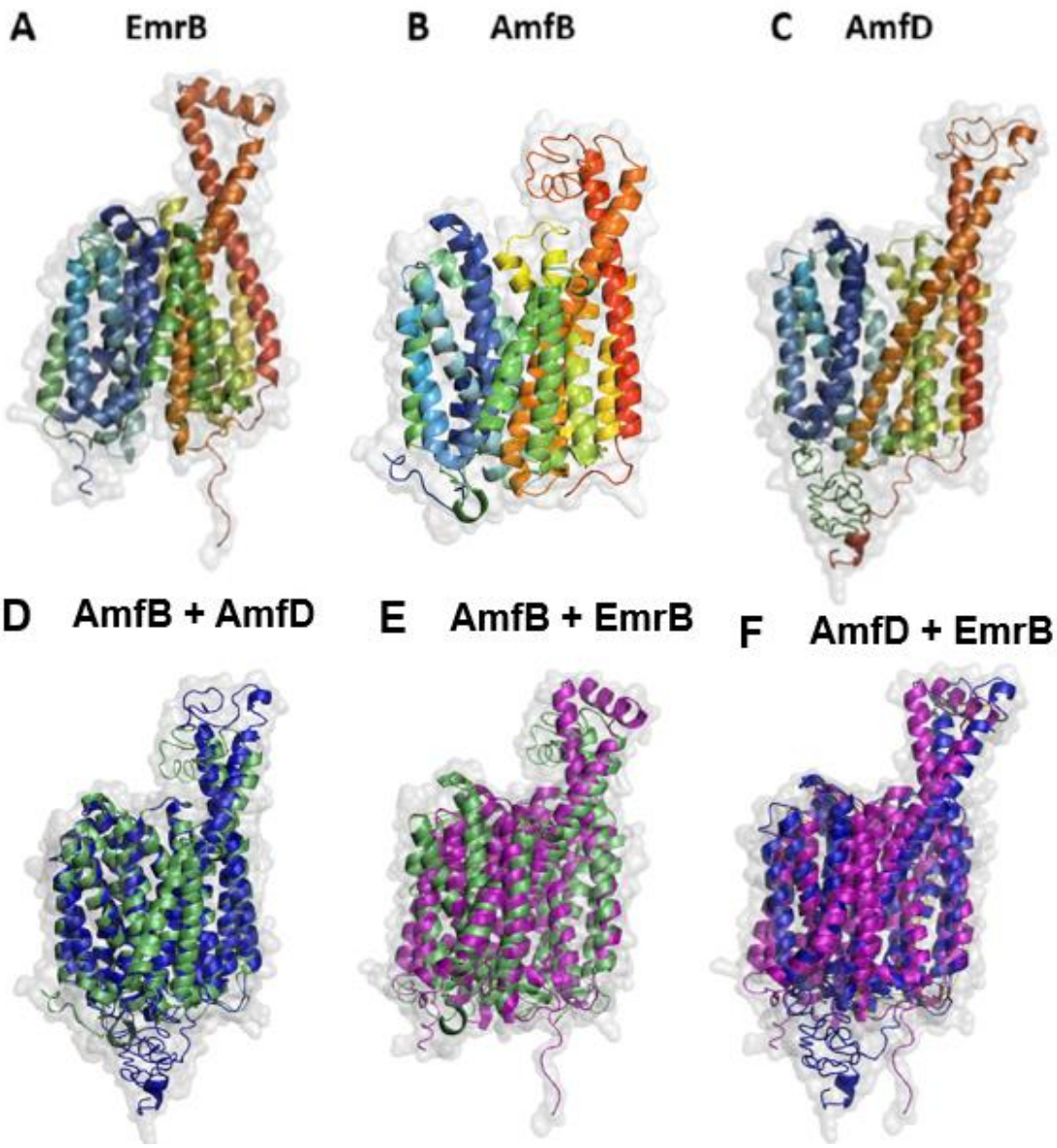

Figure 3.3 Transporter protomer structure models
3D Structure Models of the inner membrane transporter protomers EmrB (**A**), AmfB (eTM=0.76) (**B**), and AmfD (eTM=0.60) (**C**), and aligned models of AmfB (green) + AmfD (blue) (RMSD=1.78) (**D**) AmfB (green) + EmrB (magenta) (RMSD=3.00) (**E**) and AmfD (blue) + EmrB (magenta) (RMSD=5.44) (**F**). The EmrB model was predicted with AlphaFold[138,140] and the PDB file can be found in the AlphaFoldDB with UniProt Accession code: P0AEJ0. The AmfB and AmfD models were predicted with I-TASSER[123–125] by inputting their AB5075 protein sequences (see appendix). The models were arranged and aligned in Pymol[141], showing the amino acid chain as a rainbow cartoon within the surface model shown in 80% transparency light grey.

The I-TASSER output results gave the top 5 final models in a PDB file format, along with an estimated TM-score, an indicator of model confidence calculated based on significance of threading template alignments, contact map satisfaction rate, mean absolute error between distance of model and distance of AttentionPotential and convergence of I-TASSER simulations. Estimated TM scores are usually in the range of 0 to 1, with higher eTM scores signifying a higher confidence in model quality. The predicted Amf transporter models had the following eTM scores: AmfB eTM = 0.76, AmfD eTM = 0.60.

To compare how well the two Amf transporters overlapped with EmrB, they were each aligned to the EmrB model using the align function in Pymol (**Figure 3.3-D,E,F**). AmfB and AmfD share the same general shape as EmrB (**Figure 3.3-A,B,C**), although alignment of these transporter monomers shows that the Amf transporters are more similar to each other (RMSD = 1.78) than they are to EmrB (AmfB + EmrB RMSD = 2.99, AmfD + EmrB RMSD = 5.44). The alignment differences can be in part attributed to unstructured regions within the predicted Amf transporter models. The two longer helices in EmrB are bridged at the top by a short alpha helix while AmfB and AmfD instead have its two longer helices linked by an unstructured region. Additionally, AmfD also has an unstructured region at the proximal end of the transporter. This difference in alignment is also in part due to the difference in number of transmembrane helices: The I-TASSER predicted models of AmfB and AmfD both have 12 transmembrane helices, unlike the AlphaFold predicted model EmrB which has 14. In MFS transporters, the transmembrane domain plays an important role in proton translocation[142], which provides the transporter with energy to drive substrate efflux. Perhaps the difference in number of transmembrane helices suggests that AmfB and AmfD have different export kinetics compared to EmrB. Between the two I-TASSER predicted Amf transporter proteins, AmfD had the lowest eTM score at 0.60, which signifies a medium level of model quality confidence. This lower confidence score may account for some of the differences seen between the two predicted Amf transporter models.

3.3.3 Structure predictions of periplasmic MFPs

Similar to the transporters, the predicted models of AmfA (eTM = 0.75) and AmfC (eTM = 0.73) share a similar shape with EmrA, since they are all MFS membrane fusion proteins, but there are also notable differences (**Figure 3.4-A,B,C**). To facilitate protein crystallization, an engineered version of EmrA lacking the N-terminus TM helix was used for structural studies, the final model includes EmrA residues 27-321 and 343-373. This region of the protein is not conserved and is what anchors the adaptor protein in the inner membrane.[137] Differences between the predicted AmfA and AmfC structures and the EmrA structure can in part be attributed to this lacking TM domain. AmfA shows an additional α-helix in between what appears to be the lipoyl domain and the β-barrel domain, which may be that TM helix missing from the EmrA model. The AmfA model shows two short beta sheets in the lipoyl domain and one short beta sheet in what could be the lipoyl domain and the membrane proximal domain, respectively. It is difficult to identify specific regions besides the α-hairpin domain due to the low number of notable secondary structures in the predicted AmfA and AmfC models. The AmfC model has more notable secondary structures, but it is still not fully clear what regions match up to the lipoyl domain, the β-barrel domain, and the membrane proximal domain. Perhaps these predicted models are not close enough to the actual protein structures to show these regions clearly.

To compare how well the two Amf MFPs overlapped with EmrA and each other, their models were aligned using the align function in Pymol (**Figure 3.4-D,E,F**). The two Amf membrane fusion protein models aligned more closely to EmrA than they did to each other: AmfA + AmfC RMSD = 5.44, EmrA + AmfA RMSD = 4.69, EmrA + AmfC RMSD = 4.26. These apparent differences are at least partially attributed to limitations of the predicted models. The unstructured amino acids in the predicted AmfA and AmfC lipoyl/β-barrel/TM helix regions make it difficult to speculate on their predicted functions compared to EmrA. Crystal structures of AmfA and AmfC would illuminate these dissimilarities.

The α-helical hairpin domains of the predicted Amf MFPs were visually the most well aligned regions and both AmfA and AmfC appear to be a bit shorter than EmrA. The tip of AmfC's α-helical hairpin does not extend out as far as the tip of EmrA's α-helical

hairpin (**Figure 3.4-F**). This is the same for AmfA (**Figure 3.4-E**). This could suggest that the periplasm may be narrower in *A. baumannii* than in *E.coli*.

In conclusion, the predicted Amf MFP regions besides the α-hairpin are too unstructured to be able to compare with the truncated EmrA crystal structure. The α-hairpin of both AmfA and AmfC is shorter than the corresponding α-hairpin of EmrA, which suggests that *A. baumannii* may have a more narrow periplasm compared to *E. coli*.

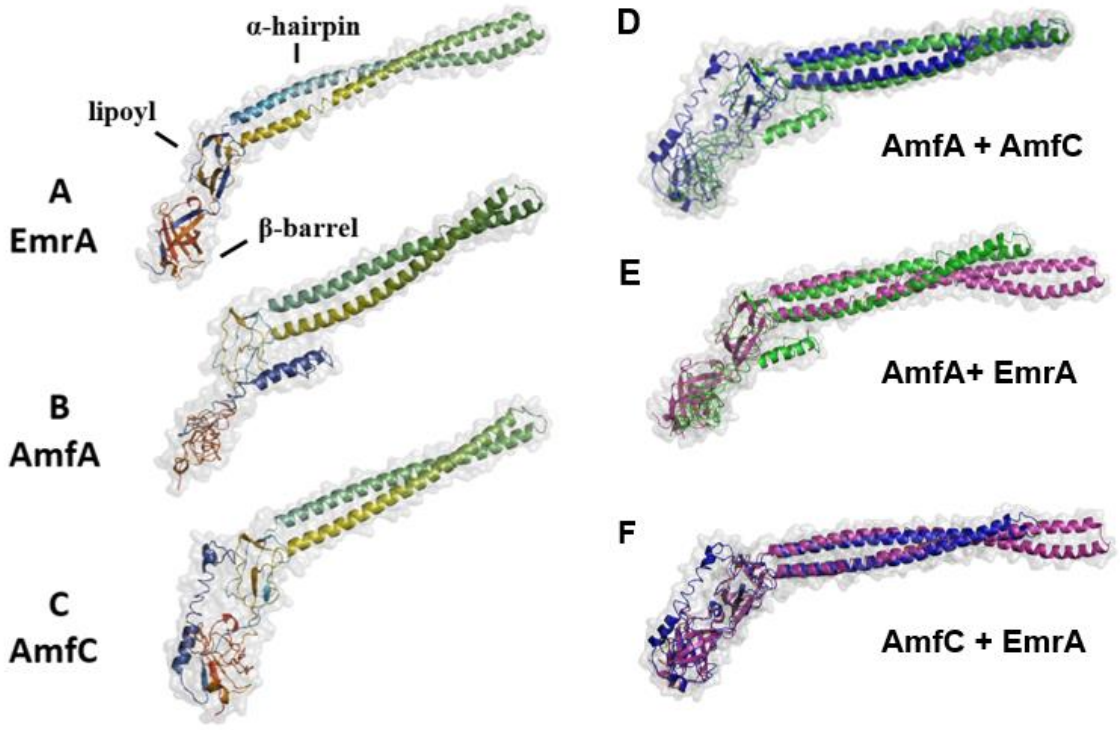

Figure 3.4 – MFP protomer structure models
3D Structure Models of the inner membrane transporter protomers EmrA, with labeled α-hairpin, lipoyl, and β-barrel domains (**A**), AmfA (eTM=0.75) (**B**), and AmfC (eTM=0.73) (**C**), and aligned models of AmfA (green) + AmfC (blue) (RMSD=5.44) (**D**), AmfA (green) + EmrA (magenta) (RMSD=4.70) (**E**), and AmfC (green) + EmrA (magenta) (4.26) (**F**). An engineered version of EmrA lacking the TM helix was used to facilitate crystallization (final model includes EmrA residues 27-321 and 343-373). The EmrA structure was solved using X-ray crystallography by Hinchliffe et al.[137] and the PDB file can be found in the Protein Data Base (PDB) with PDB code: 4TKO. The AmfA and AmfC models were predicted with I-TASSER[123–125] by inputting their AB5075 protein sequences (see appendix). The models were arranged and aligned in Pymol[141], showing

the amino acid chain as a rainbow cartoon within the surface model shown in 80% transparency light grey.

3.3.4. MFS pumps do not contribute to antibiotic efflux

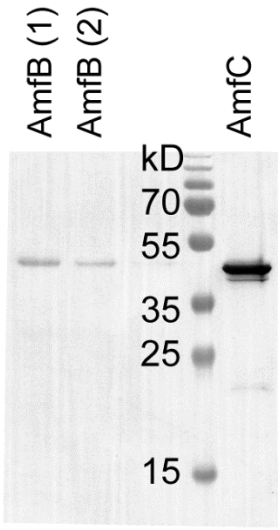

Figure 3.5 Expression of AmfB and AmfC proteins in AbWT(pAmfAB) and AbWT(pAmfCD) cells

Proteins were purified from the isolated membrane fractions, resolved on 12% SDS-PAGE and visualized by immunoblotting with monoclonal anti-6xHis antibody (Sigma). This experiment was done by Dr. Inga Leus.

The genome of ATCC17978 (AbWT) cells encodes A1S_1772/1773 and A1S_1799/1800 operons corresponding to the ABUW_1949/1950 (98/99% identity) and ABUW_1930/1931 (99/99% identity) operons in AB5075, respectively. We renamed A1S_1772/1773 and A1S_1799/1800 as AmfAB and AmfCD (*Acinetobacter* Major Facilitator), respectively. To determine the role of these EmrAB-like pumps in A. baumannii physiology, Dr. Inga Leus deleted genes encoding these pumps one by one and together in the AbWT and Δ3 (ΔadeIJK ΔadeAB ΔadeFGH) genetic backgrounds (**Table 2.1**). We then characterized the susceptibility to antibiotics of the constructed strains.

To complement the constructed deletion strains, *amfAB* and *amfCD* genes were cloned into the pTJ1 vector enabling the expression of the plasmid-borne genes under an arabinose-inducible promoter as well as the integration of the expression cassette into the Tn7 site on the chromosome. After transformation into the AbWT strain and its

derivatives, the corresponding proteins tagged with six histidine residues at the C-termini were produced from both the plasmid and the Tn7 chromosomal site. Based on immunoblotting with anti-His tag antibodies, both proteins were expressed, albeit to different levels (**Figure 3.5**). The expression of AmfC was the strongest, whereas the amounts of AmfB were very low.

The overproduction of Amf pumps in different genetic backgrounds did not increase the MICs of antibiotics (**Table 3.4**). Thus, in agreement with the gene deletion analyses, neither of the pumps contribute to the efflux of antibiotics. Furthermore, the AbWT cells carrying either AmfAB or AmfCD plasmids became 2–4-fold more susceptible to erythromycin and zeocin (**Table 3.4**), suggesting that the overproduction of these pumps compromises the intrinsic protection of *A. baumannii* cells against these antibiotics.

3.3.5. Both AmfAB and AmfCD pumps are important for growth under acidic conditions, but AmfCD also contributes to survival under other stresses

We next compared the growth of AbWT and the constructed overproduction strains under the typical laboratory conditions of 37 °C and pH 7.2 and the virulence-induced stresses such as growth at a high temperature of 41 °C, at acidic pH 4.6, in the presence of 0.5 M NaCl (osmotic shock), 125 μM, and 250 μM 2,2′-dipyridyl (a ferrous iron chelator generating low iron stress) and 0.5% bile salts (**Table 3.6**). These conditions were used previously to mimic in vitro the stress conditions that are experienced by various pathogens during infections.[67] To compare bacterial growth under different conditions, we calculated the area under the curve for each growth curve collected during a 24 h period (**Table 3.7**). We found that AbWT cells grow equally well at 37 °C and 41 °C (**Table 3.7** and **Figure 3.6**). At acidic pH, there is a notable lag, but once cells resume growth, it is even faster than that at pH 7.2. All other conditions reduce the growth of AbWT by 3–4-fold.

TABLE 3.4 Antibiotic susceptibilities of *A. baumannii* strains to different classes of antibiotics

Strain	ERY (μM)	NOV (μM)	CIP (μM)	TET (μM)	AZI (μM)	CHL (μM)	SDS (μM)	GEN (μM)	ZEO (μM)
Ab WT	10	10 – 20	0.125 – 0.25	0.25 – 0.5	0.63 – 1.25	64	>1024	4 – 8	8
WT ΔAmfAB	5	10	0.125 – 0.25	0.5	0.63 – 1.25	64	>1024	8	8
WT ΔAmfCD	5 – 10	5 – 10	0.125	0.25 – 0.5	1.25	64	>1024	8	8
Δ2::Gm	10	10	0.125	0.25	1.25	32	≥1024	R	8
WT (pAmfAB)	**2 - 4**	4 – 8	0.125	0.5 – 1	0.31 – 0.63	64	>1024	4	**2**
WT (pAmfCD)	**2**	8 – 16	0.125	0.5	0.63	64	>1024	4	4
Δ2 (pAmfAB)	8	4 – 8	0.0625 – 0.125	0.5	0.63 – 1.25	32	>1024	R	4 -8
Δ2 (pAmfCD)	4	4 – 8	0.0625 – 0.125	0.25	1.25	32	>1024	R	16
Ab Δ3	1.25	0.08	0.016 – 0.031	0.031 – 0.063	0.31 – 0.63	16 – 32	16	8	1
Δ3 ΔAmfAB	1.25	0.08	0.008 – 0.016	0.031	0.63	8 – 16	16	8	1
Δ3 ΔAmfCD	1.25	0.08	0.016	0.031	0.63	8 – 16	16	8	1 – 2
Δ5::Gm	2.5	0.08	0.016	0.031	0.31 – 0.63	8	16	R	1 – 2
Δ3 (pAmfAB)	**4**	0.03	0.016	0.016 – 0.03	0.31	8	16	8	1 – 2
Δ3 (pAmfCD)	**2 – 4**	0.03	0.016	0.016	0.31 – 0.63	8	16	8	0.5 – 1
Δ5 (pAmfAB)	4	0.03	0.016	0.016 – 0.031	0.63	8	16	R	**0.25 – 0.5**
Δ5 (pAmfCD)	2 - 4	0.03	0.016	0.016 – 0.031	0.63	8	16	R	0.5 - 1

ERY – Erythromycin, NOV – Novobiocin, CIP – Ciprofloxacin, TET – Tetracycline, AZI – Azithromycin, CHL – Chloramphenicol, SDS – Sodium dodecyl sulfate, GEN – Gentamicin, ZEO – Zeocin, R - Resistant

Minimal inhibitory concentrations [μg/mL] of strains lacking or overproducing AmfAB and AmfCD efflux pumps. MIC values that differ by four-fold are shown in underlined bold.

Table 3.5 – Details of growth and stress conditions for *A. baumannii* mutants

Type of Stress	Stress Exposure Agent in LB Broth or LB Broth + 1% L-Arabinose
No stress control	LB broth, pH 7.2; 37 °C
Acidic stress	LB broth adjusted to pH 4.6 with HCl
Osmotic stress	LB broth supplemented with 0.5 M NaCl
Bile stress	LB broth supplemented with 0.5% bile salts (Millipore (Darmstadt, Germany), ~50% sodium cholate and ~50% sodium deoxycholate)
Low iron	LB broth supplemented with 125 µM or 250 µM 2,2-dipyridyl
Temperature	LB broth, pH 7.2; 41 °C

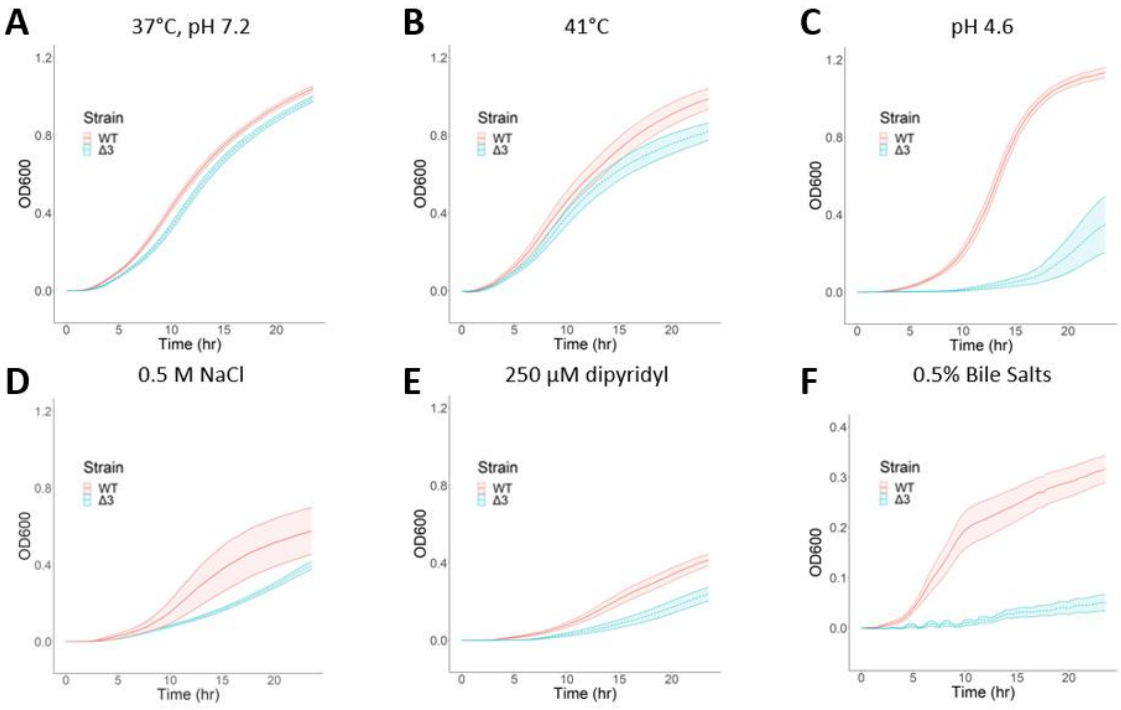

Figure 3.6 - Growth curves of AbWT and AbΔ3 strains under different stresses

Growth curves of AbWT and AbΔ3 strains under indicated conditions. Error bars are SD (n = 3). (**A**) No stress control; (**B**) high temperature; (**C**) acidic stress; (**D**) osmotic stress; (**E**) low iron; (**F**) bile stress.

We next characterized the stress phenotypes of the complemented cells and calculated the corresponding AUCs values (**Table 3.7**). For these experiments, all cell cultures were grown in the presence of 1% L-arabinose needed to induce the expression of both plasmid-borne and chromosomally integrated efflux pump genes. Since 250 μM 2,2′-dipyridyl was notably toxic to complemented strains, the iron depletion experiments were carried out at 125 μM 2,2′-dipyridyl.

In the AbWT and Δ2 cells, the overproduction of AmfAB but not AmfCD was toxic to the cells, as seen from the significant growth reduction in AbWT(pAmfAB) and Δ2(pAmfAB), even under the normal conditions (**Table 3.7** and **Figure 3.7**). The toxicity of AmfAB overproduction in the AbWT strain can also be seen when cells are grown in the pH 4.6 medium (**Figure 3.7-C**). In contrast, the overproduction of either AmfAB or AmfCD rescued the growth deficiency of Δ2 cells grown in pH 4.6 (**Figure 3.8-C**). Thus, both AmfAB and AmfCD contribute to the growth of *A. baumannii* under acidic conditions.

3.3.6. Overproduction of MFS pumps do not complement loss of RND pumps under virulence related stress conditions

Neither AmfAB nor AmfCD overproduction was able to complement the growth deficiencies of Δ3 and Δ5 cells and their derivatives. Hence, the activities of AmfAB and AmfCD depend on the presence of functional RND pumps. Furthermore, at pH 4.6, the overproduction of either AmfAB or AmfCD was toxic to Δ3 and Δ5 cells and led to the lack of growth (**Figures 3.9** and **3.10**). In contrast, the toxicity of AmfAB overproduction seen in AbWT and Δ2 cells under standard conditions, pH 4.6, high temperature and in the presence of 2,2′-dipyridyl and bile salts (**Figure 3.8** and **Figure 3.7**) was also alleviated in Δ3 cells lacking RND pumps (**Figure 3.9**). This result suggests that the overproduction of AmfAB in AbWT cells might interfere with the functions of RND pumps.

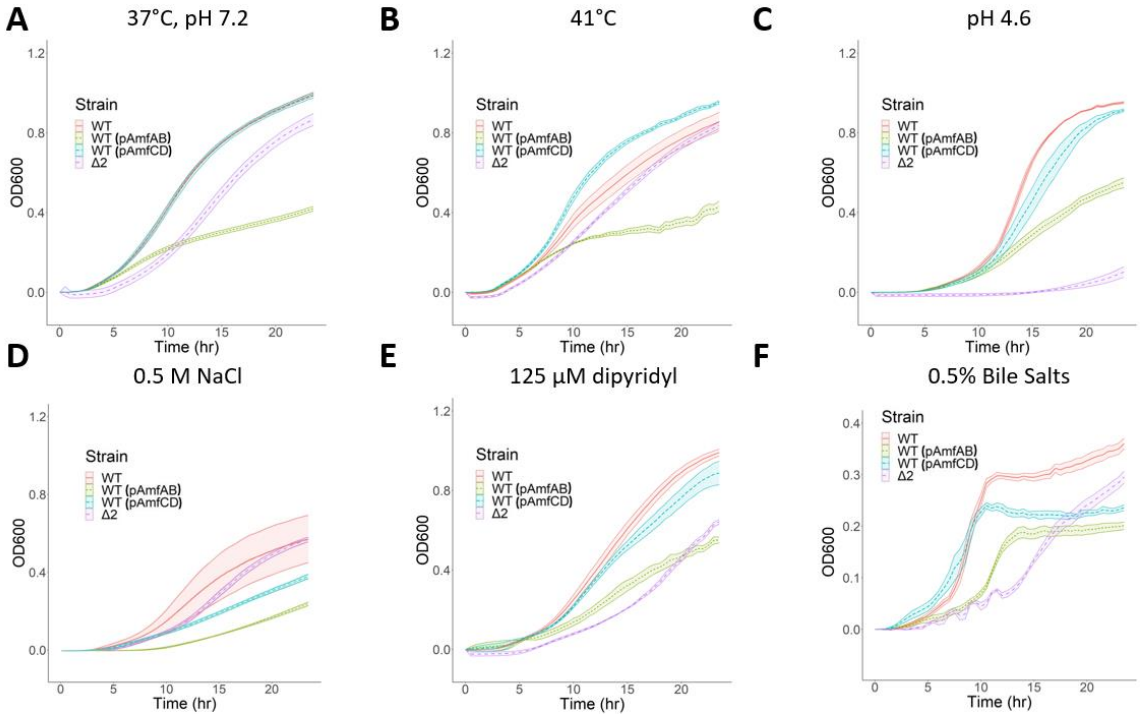

Figure 3.7 - Growth curves of AbWT (pAmfAB) and AbWT (pAmfCD) overexpression strains under different stresses

Growth curves of AbWT (pAmfAB) and AbWT (pAmfCD) strains under indicated conditions. Error bars are SD (n = 3). (**A**) No stress control; (**B**) high temperature; (**C**) acidic stress; (**D**) osmotic stress; (**E**) low iron; (**F**) bile stress.

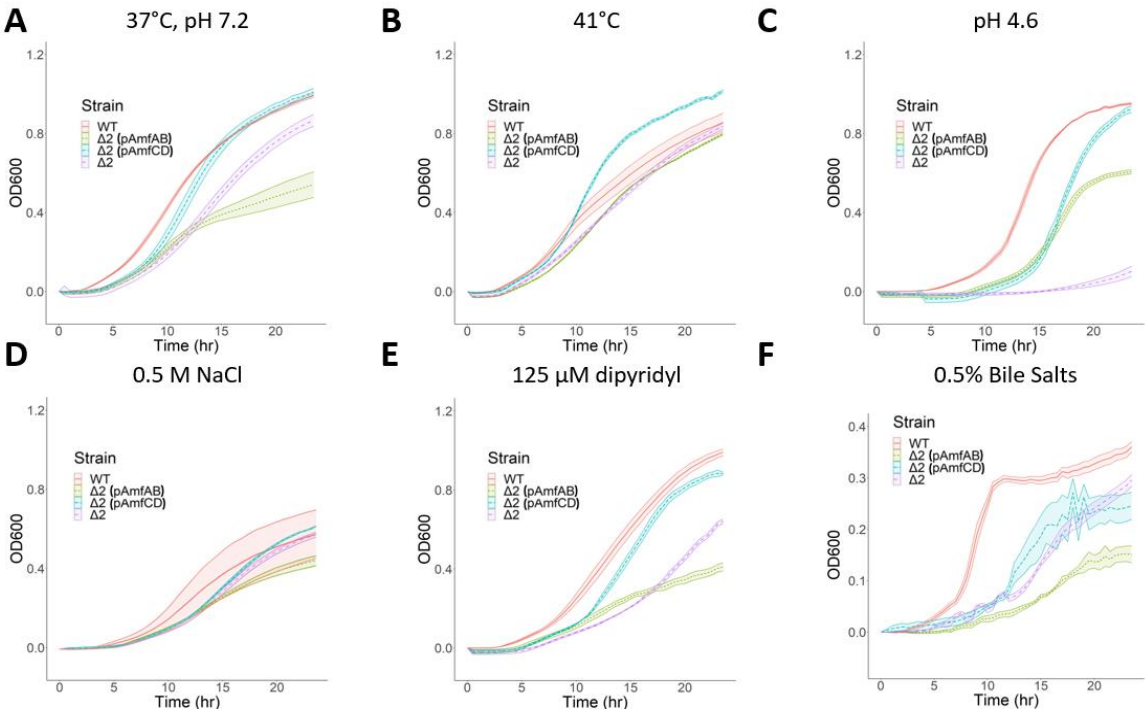

Figure 3.8 - Growth curves of AbΔ2 (pAmfAB) and AbΔ2 (pAmfCD) overexpression strains under different stresses

Growth curves of AbΔ2 (pAmfAB) and Ab Δ2 (pAmfCD) strains under indicated conditions. Error bars are SD (*n* = 3). (**A**) No stress control; (**B**) high temperature; (**C**) acidic stress; (**D**) osmotic stress; (**E**) low iron; (**F**) bile stress.

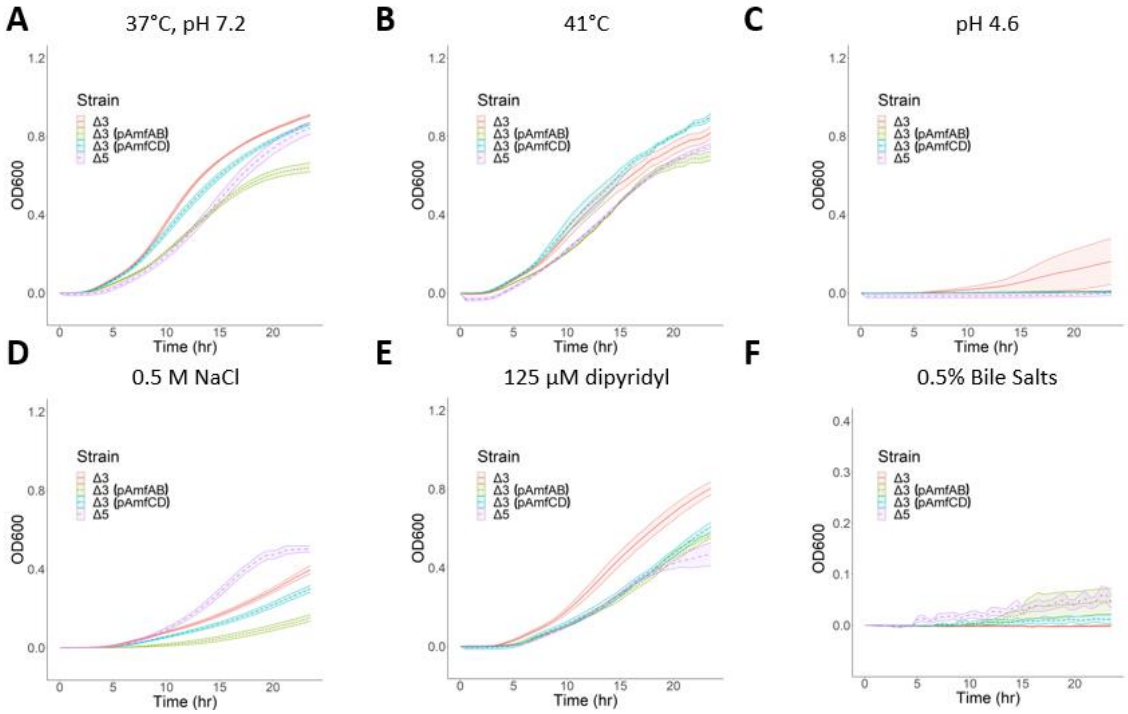

Figure 3.9 - Growth curves of AbΔ3 (pAmfAB) and AbΔ3 (pAmfCD) overexpression strains under different stresses

Growth curves of AbΔ3 (pAmfAB) and Ab Δ3 (pAmfCD) strains under indicated conditions. Error bars are SD (n = 3). (**A**) No stress control; (**B**) high temperature; (**C**) acidic stress; (**D**) osmotic stress; (**E**) low iron; (**F**) bile stress.

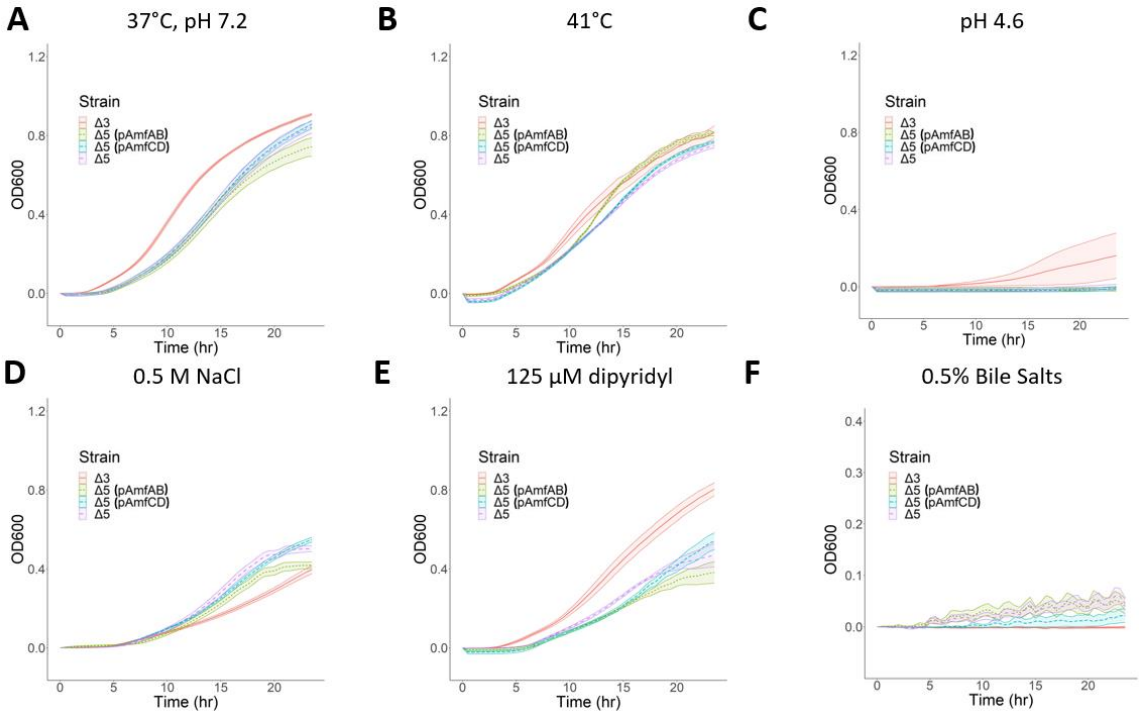

Figure 3.10 - Growth curves of AbΔ5 (pAmfAB) and AbΔ5 (pAmfCD) overexpression strains under different stresses

Growth curves of AbΔ5 (pAmfAB) and Ab Δ5 (pAmfCD) strains under indicated conditions. Error bars are SD (n = 3). (**A**) No stress control; (**B**) high temperature; (**C**) acidic stress; (**D**) osmotic stress; (**E**) low iron; (**F**) bile stress.

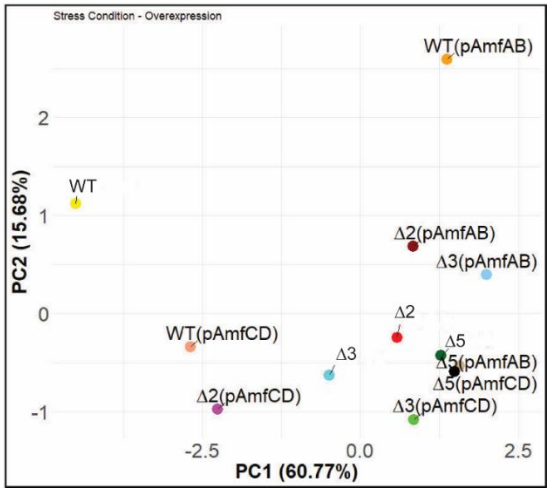

Figure 3.11 PCA analyses of *A. baumannii* growth

The areas under curves (AUCs) were calculated for the complemented strains and analyzed using hierarchical clustering. The principal component decomposition in the first and second principal components (PC1 and PC2) coordinates is shown.

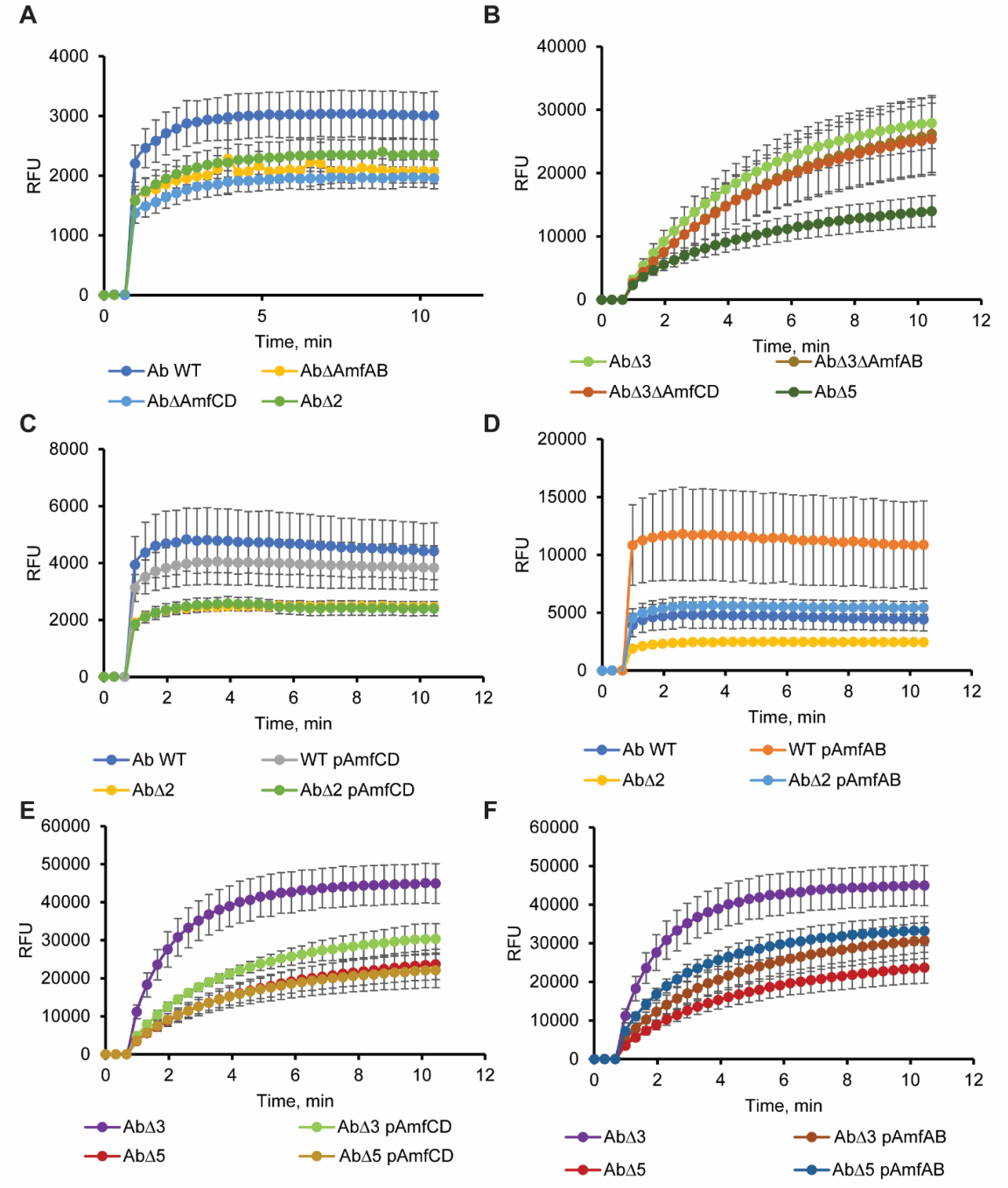

Figure 3.12 - Fluorescence Uptake Analysis of NPN

Intracellular accumulation of fluorescent membrane probe NPN. Indicated strains were grown in LB broth and induced with 1% L-arabinose when appropriate. Washed cells were injected into HMG buffer containing 4 µM NPN and the resulting fluorescence was monitored continuously for 10 minutes. The plots are changes in fluorescence intensity as a function of time. Error bars are SD (n = 3). (**A**) Single and double deletions of AmfAB

and AmfCD in the AbWT genetic background. (**B**) Single and double AmfAB and AmfCD deletions in AbΔ3 genetic background. (**C**) Overproduction of AmfCD in AbWT and AbΔ2 backgrounds. (**D**) Overproduction of AmfAB in AbWT and AbΔ2 backgrounds.(**E**) Overproduction of AmfCD in AbΔ3 and AbΔ5 backgrounds. (**F**) Overproduction of AmfAB in AbΔ3 and AbΔ5 backgrounds.

3.3.7 Principal component analysis reveals differences between the strains

To compare the growth phenotypes of the constructed strains, Dr. Justyna Adamiak carried out the principal component analysis (PCA) of the AUC values calculated for the averaged growth curves of all strains under the analyzed growth conditions (**Table 3.7**). The relationships between overproducers are complex, reflecting the dependence of the phenotypes on specific plasmid-borne pumps and genetic backgrounds (**Figure 3.11**). The PC1 and PC2 explain ~76% of the total variance and separated AbWT from the rest of the strains, demonstrating that overproduction of either AmfAB or AmfCD does not fully complement their deletion phenotypes. In addition, AbWT(pAmfAB) and AbWT(pAmfCD) are distant from each other and other strains. This separation is likely due to the finding that the overproduction of AmfAB was the most toxic to the cells.

3.3.8 Efflux pump overproducers modify the permeability barrier of *A. baumannii*

The involvement of efflux pumps in acid tolerance suggests that their functions are important for the adaptation to this stress. Previous studies implicated the RND pumps of *A. baumannii* in the maintenance of lipid composition of the cellular membranes.[52,143] Since membrane modification is one of the established mechanisms of acid tolerance in bacteria, we next analyzed whether the plasmid-borne overproductions of Amf pumps affect the permeability barrier of *A. baumannii*. For this purpose, we analyzed the intracellular accumulation of a membrane fluorescent probe N-phenyl-1-naphthylamide (NPN). NPN is a hydrophobic probe, which penetrates slowly across the outer membrane and is a known substrate of AdeIJK pump.[20] Therefore, the fluorescence of NPN is dramatically enhanced when AdeIJK is inactivated and/or when the outer membrane is permeabilized.

Neither inactivation of AmfAB nor AmfCD increased the intracellular accumulation of NPN in AbWT cells, suggesting that the permeability barriers of these

cells are not compromised and even if NPN is the substrate of these pumps they are not the major contributors to its efflux in AbWT (**Figure 3.11-A**). Furthermore, all three deletion mutants ΔAmfAB, ΔAmfCD and the double knockout Δ2 were less fluorescent than AbWT. Hence, the inactivation of these pumps makes *A. baumannii* cells less permeable to NPN. As expected, Δ3 cells lacking the RND pumps accumulated at least ten times higher amounts of NPN than AbWT (**Figure 3.11-B**). Although single knockouts Δ3ΔAmfAB and Δ3ΔAmfCD were indistinguishable from the parental Δ3 cells, in the double knockout Δ5 cells the levels of NPN fluorescence were at least three times lower. We conclude that deletions of AmfAB and AmfCD pumps either promote the efflux of NPN from cells by other transporters or reduce the permeation of NPN across the outer membrane in both RND plus and minus backgrounds.

The effect of overproduction on the permeability barrier was both the pump- and genetic background-specific (**Figure 3.11-C-F**). The increased fluorescence of NPN in AbWT(pAmfAB), AbΔ2(pAmfAB) and AbΔ5(pAmfAB) suggests that these cells are leaky to NPN, and this result is consistent with the toxicity of the overproduction of AmfAB pump seen in the growth curves (**Table 3.7**). In contrast, AmfCD overproduction has no effect on the NPN accumulation and on the growth of AbWT(pAmfCD), AbΔ2(pAmfCD) and AbΔ5(pAmfCD) cells. Surprisingly, the overproduction of either of the two pumps in Δ3 cells lead to decreased NPN accumulation and, hence, a stronger permeability barrier, highlighting the physiological difference between Δ3 and Δ5 cells in how they respond to the overproduction of the Amf pumps.

Table 3.6 – Area under the curve values for overproduction strains

Strains	No Stress	Acid	Osmotic	Bile	Iron Depletion	High Temperature
	37 °C, pH 7.2	pH 4.6	0.5 M NaCl	0.5% DOC	2,2′-Dipyridyl (125 mM)	41 °C
WT	11.89 ± 1.47	9.39 ± 0.61	5.94 ± 2.36	4.78 ± 0.58	9.93 ± 5.7	9.78 ± 3.03
WT(pAmfAB)	5.21 ± 1.23	4.85 ± 1.04	1.61 ± 0.12	2.62 ± 0.24	5.41 ± 0.08	5.33 ± 0.57
WT(pAmfCD)	11.83 ± 0.69	7.91 ± 1.9	3.47 ± 0.39	3.77 ± 0.27	8.67 ± 0.13	11.95 ± 0.57
D2	8.19 ± 0.53	0.16 ± 0.21	5.04 ± 0.49	2.47 ± 0.17	4.28 ± 0.17	8.48 ± 0.59
D2(pAmfAB)	6.12 ± 0.7	4.3 ± 0.7	4.33 ± 0.44	1.3 ± 0.32	4 ± 0.67	8.15 ± 0.12
D2(pAmfCD)	10.95 ± 0.7	5.49 ± 0.96	5.43 ± 0.11	2.71 ± 1.1	7.96 ± 0.4	11.88 ± 0.21
D3	10.62 ± 1.27	1.13 ± 0.13	3.19 ± 0.78	NG	7.52 ± 4.82	9.1 ± 2.14
D3(pAmfAB)	7.2 ± 1.78	0.08 ± 0.08	0.98 ± 0.62	0.39 ± 0.7	4.69 ± 0.01	7.58 ± 0.4
D3(pAmfCD)	9.65 ± 1.17	0.04 ± 0.07	2.32 ± 0.44	0.12 ± 0.31	4.96 ± 0.19	9.95 ± 0.91
D5	8.01 ± 1.01	NG	4.81 ± 0.59	0.57 ± 0.42	4.45 ± 0.32	7.61 ± 0.4
D5(pAmfAB)	7.3 ± 1.08	NG	3.96 ± 0.59	0.62 ± 0.6	3.49 ± 0.69	8.73 ± 0.37
D5(pAmfCD)	8.07 ± 0.75	NG	4.65 ± 0.31	0.14 ± 0.35	4.04 ± 0.74	7.73 ± 0.29

3.4. Discussion

All bacterial genomes encode multiple efflux transporters, but the functions of many of these transporters are unknown or undefined. The commonly used approach to the characterization of such transporters is to delete the genes and/or overproduce them in RND-deficient genetic backgrounds and to analyze their possible contribution to drug

efflux.[50,62] In this study, I first analyzed the genomic context and putative structure of *A. baumannii* transporters AmfAB and AmfCD, the abundances of which increased in cells lacking the two major multidrug efflux pumps AdeIJK and AdeABC.[64] Next, I cloned and overproduced these pumps in plus or minus efflux deficient *A. baumannii* strains and characterized their functions. The results show that the overproduction of AmfAB and AmfCD in the RND and Amf plus and minus genetic backgrounds did not lead to pump-specific decreases in antibiotic susceptibilities (**Table 3.4**). Thus, in *A. baumannii*, these pumps do not contribute to antibiotic non-susceptibility. In contrast, AbWT(pAmfAB) cells became more susceptible to erythromycin and zeocin, the result consistent with the finding that the overproduction of AmfAB is toxic to AbWT and make the cells leaky to NPN (**Figure 3.12-D**). The lack of contribution to antibiotic non-susceptibility is unexpected because the EmrAB-TolC pump from E. coli, the best characterized homolog of Amf pumps, was the first multidrug efflux pump identified in bacteria[60] and is able to expel select antibiotics, dyes and detergents from cells.[62]

Unlike the susceptibility to antibiotics, bacterial growth and survival under various stresses depend on Amf pumps. Both AmfAB and AmfCD contribute to *A. baumannii* growth in the pH 4.6 medium, with AmfCD playing a larger role (**Figure 3.8** and **Table 3.7**). Efflux appears to be a common adaptation to acidic stress among various bacterial species.[76,144] In *E. coli*, the inactivation of the RND pump MdtEF-TolC reduces the bacterial fitness in acidic pH and survival in macrophages.[145] Similarly, the MFS pump EmrKY-TolC of *Shigella flexneri* was reported to be important for survival in macrophages and is activated in response to acidic pH.[146] However, it remains unclear how efflux pumps contribute to acid adaptation.

One possibility is that efflux pumps play a role in the consumption of protons needed to sustain pH homeostasis in the cytoplasm. The production of ammonia by *A. baumannii* has been reported to be important for the survival and replication in macrophages.[147] However, ammonia and CO_2 released during amino acid transformations can rapidly diffuse across membranes, whereas uptake and efflux of amino acids are carried out by specific amino acid exchangers such as ArcD for arginine/ornithine or CadB for lysine/cadaverine.[76]

Alternatively, efflux pumps could contribute to modifications of cellular membranes needed for survival in acidic conditions. It was previously found that either inactivation or overproduction of Ade pumps change dramatically the lipidome of *A. baumannii* ATCC17978 cells.[52] In addition, the AdeIJK pump was also implicated in the efflux of host fatty acids.[143] Thus, the role of RND and possibly Amf pumps could be in the modification of the fatty acid composition of the membranes during acidic stresses. Our NPN accumulation analyses are consistent with this conclusion and showed that inactivation of either AmfAB or AmfCD makes cells less permeable to this membrane probe (**Figure 3.12**). These changes in the permeability barrier were independent from the presence of RND pumps but the effect was the strongest when both Amf pumps were inactivated in Δ5 cells (**Figure 3.12-B**). This result is consistent with the finding that Amf pumps contribute to survival at pH 4.6.[113]

On the other hand, overproduction of these Amf pumps appears to impair *A. baumannii* growth under acidic conditions (**Figure 3.8**), perhaps because proton antiport leads to an influx of protons, making the cell interior even more acidic. Both AmfB and AmfD pumps share amino acid sequence similarity to MdfA efflux transporter, at 26.85% and 31.03%, respectively. Besides conferring antibiotic resistance when expressed in *E. coli*, MdfA also functions as a Na+ (K+)/H+ antiporter which helps maintain intracellular pH homeostasis.[148] It is also possible that the functions of these pumps are similar to those of RosA/RosB efflux pumps of *Yersinia*, in that they mediate a stress response (antibiotic or other) by pumping out said stressor and by inducing the acidification of the cytoplasm. The lower intracellular pH acts as a positive regulatory signal in *Yersinia* that then triggers other cellular stress response systems, perhaps involving modifications to the outer membrane.[132]

Interestingly, the two pumps AmfAB and AmfCD have non-overlapping physiological functions. The overproduction of AmfAB but not AmfCD is toxic to the cells (**Figures 3.7, 3.9, and 3.10**). The differences between the two pumps are also seen in the published RNAseq data.[67] Under normal conditions, the abundance of *amfC* transcripts is 4–5 times higher than that of *amfA* and further increases at pH 4.6, but decreases upon exposure to bile salts and low-iron conditions (data not shown here). In contrast, *amfA* transcription is induced by bile salts and low-iron conditions. The

AmfAB- and AmfCD-associated phenotypes were negated in the RND minus background, suggesting that the activity and/or components of the RND pumps are needed for Amf phenotypes. Since neither of these operons contains a gene encoding the outer membrane channel, it is possible that they engage AdeK for their activities and thus reduce the activity of AdeIJK.

It is already known that bacterial responses to different stress conditions often overlap. For example, the exposure to high osmolarity and acidic pH triggers the activation of the PhoPQ two-component response system as well as Fur activator regulating the expression of iron acquisition systems.[149–151] Perhaps all observed changes in growth due to deletions and overexpression of efflux pumps are caused by the same modifications or the lack thereof in the composition of bacterial membranes.

Our results suggest that the deletion of these Amf pumps under various stresses hinders the cells' capacity to maintain intracellular pH homeostasis and to export stress-associated small toxic molecules. This is in contrast to the membrane disruption seen in the overproduction of the Amf pumps. Overproduction also represents an inefficient management of cellular resources that could be used by stress response systems such as cell envelope remodeling that reduces permeability to reduce further stress damage.[152,153] Future studies of regulatory circuits in *A. baumannii* controlling the expression of efflux pumps could lead to the identification of underlying mechanisms. It is possible that the LuxR family transcriptional regulator (ABUW_1947) and two LysR family regulators (ABUW_1927 and ABUW_1936) could be involved in the regulation of the Amf efflux pumps. Identifying an outer membrane channel that functions with AmfAB and/or AmfCD could be an important missing piece in understanding the full functionality of these pumps.

These results highlight complex relationships between antibiotic non-susceptibility and *A. baumannii* metabolism.[153] Metabolomics studies could provide the insights needed for understanding the Amf pump–stress mechanisms.

Chapter 4 : Site-Directed Mutagenesis of RND Transporter AdeG from *Acinetobacter baumannii* Leads to Identification of Amino Acid Residues Essential for Norfloxacin, Nalidixic Acid, and 1-N-phenylnaphthylamine Efflux

4.1. Abstract

The RND-type transporter AdeG, of the operon AdeFGH, is one of three most prevalent efflux pumps in *Acinetobacter baumannii*. AdeFGH is known to contribute to acquired antibiotic resistance. Overproduction of this pump has been observed in clinical isolates and its efflux efficiency and limited substrate range promotes *A. baumannii* survival under high concentration antibiotic pressure. To gain insight into the transporter's mechanism of function, seven single and one double amino acid substitution mutants of the AdeG transporter were constructed and inserted onto the chromosomes of the RND efflux deficient strains AbΔ3 and AbΔ3-Pore. This study has identified amino acid residues in AdeG that are important for the transport of nalidixic acid, norfloxacin, and the fluorescent probe NPN. We found in 2-fold dilution antibiotic susceptibility assays that norfloxacin export involves the AdeG residues Q83, and I621 and G679, and that nalidixic acid export appears to involve Y725, I621, L138, P136, Q83A, and G679. From fluorescent probe uptake assays with increasing concentrations of NPN or increasing concentrations of the inhibitor SLUPP_1377, we found that AdeG G679I is likely a non-functional transporter. We also found that the AdeG substitutions Q83A, S620A, and Y725A made AdeG more sensitive to inhibition by SLUPP_1377. And lastly, we found that the AdeG mutant L138A appears to be resistant to inhibition by SLUPP_1377, but it also loses NPN efflux efficiency. We anticipate these findings will aid in future rational efflux pump inhibitor design and further functional characterization of this RND transporter.

4.2. Introduction

Upregulation of RND efflux pumps due to mutations in their regulators is commonly seen in clinical isolates of pathogenic bacteria.[104] The RND efflux pump AdeFGH has been seen to play a major role in *A. baumannii's* resistance to various antibiotics[131], including chloramphenicol, trimethoprim, tetracycline, tigecycline, clindamycin, and fluoroquinolones.[54] AdeFGH's association with decreased

susceptibility to tigecycline makes it an important research subject due to its clinical relevance[154], as well as the fact that researchers Coyne et al. found the *adeFGH* operon in 36 out of 40 *A. baumannii* clinical isolates.[54]

In RND transporter proteins, the transmembrane domains (**Figure 1.8**) carry out proton translocation by way of a proton-relay network composed of conserved protonated amino acid residues.[155] The proton-relay network is how the RND transporter uses the proton motive force of the inner membrane to drive substrate transport. The other main responsibility of the RND transporter protein is the substrate specificity of a pump[52], localized to the porter domain. There are several factors that impact the substrate specificity of transporters, including binding pocket volume, shape, lipophilicity, electrostatic potential, hydration, and distribution of multi-functional sites.

Numerous efflux pump inhibitors have been identified that inhibit AcrAB-TolC of *E. coli*,[108,109] but there have only been a few studies of AdeFGH inhibitor candidates.[156] The well studied PAβN efflux pump inhibitor (EPI) has been shown to inhibit AdeFGH and increases *A. baumannii*'s susceptibility to trimethoprim, chloramphenicol, and clindamycin.[157] Additionally, two quinolone-based compounds were found to potentiate chloramphenicol more than 16-fold in Ab5075-CHL, a strain of *A. baumannii* that overexpresses AdeG.[158] A previous unpublished study from the Zgurskaya lab found that the compound SLUPP_1377 potentiates the activity of novobiocin in *A. baumannii* strains with AdeIJK overproduction as well as in the hyperporinated wild-type strain ATCC17978. After further testing, the SLUPP_1377 compound was also found to inhibit AdeFGH. It is currently hypothesized that this inhibitor binds in a site which is different from the substrate binding site. The mechanism of action of this EPI is not yet known, but the following study aims to investigate its inhibition mechanism by testing SLUPP_1377 against various site-directed mutant AdeG transporters. Through these studies we have been able to identify specific AdeG binding pocket residues that define its substrate specificity and impact inhibition activity of SLUPP_1377.

There is currently no crystal structure of AdeG available so a homology model was generated using MODELLER version 10.1[159], the amino acid sequence of AdeG (ATCC 17978, Gen Bank Accession Code WP_001027060.1), and MexB of

Pseudomonas aeruginosa as a template (PDB code 3W9I). The following AdeG single amino acid substitution mutations were selected by using molecular docking and molecular dynamics simulations with chloramphenicol and SLUPP_1377.

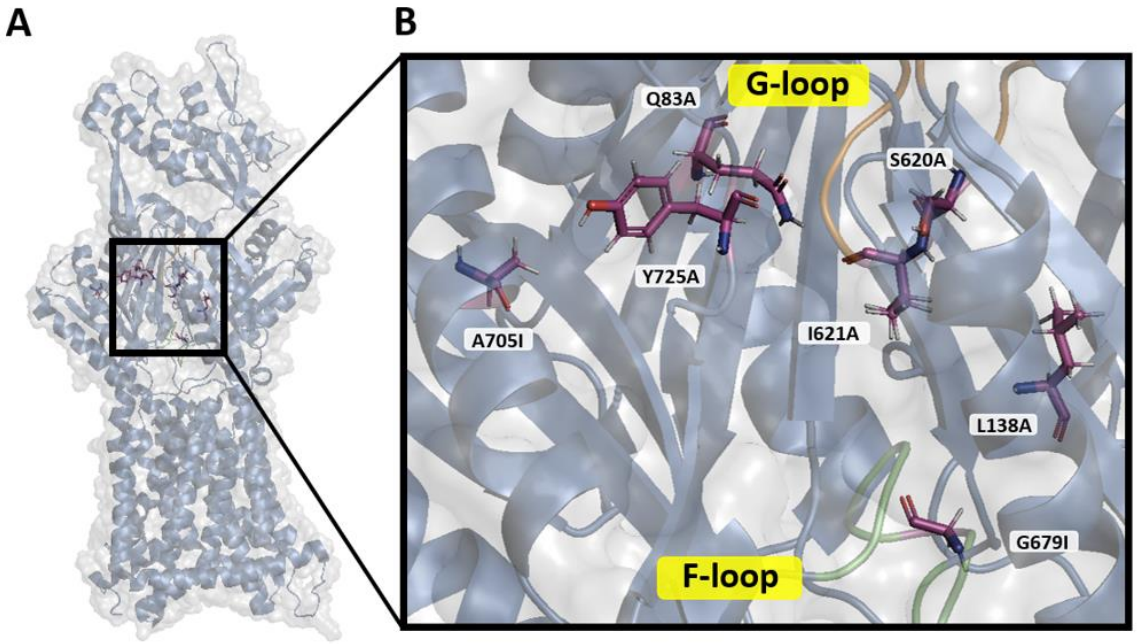

Figure 4.1 – Pymol-Wizard Mutated AdeJ protomer and select AdeG binding pocket residues

(**A**) An AdeG protomer (blue ribbon, based on AdeJ crystal structure PDB code: 7M4Q) with (**B**) highlighted amino acid residues (magenta) that were targeted in mutagenesis and labeled G-loop (orange) and F-loop (green).

4.3. Results

4.3.1. Chromosomal integration and expression of AdeG protein variants

Dr. Ayshegul Saral Sariyer has constructed the S620A, A705I, G679I, Y725A, And L138A mutants and I constructed the I621A and Q83A mutants in the plasmid encoded *adeG* genes (**Tables 2.1, 2.2**). The amino acid residues selected for mutagenesis are located in the proximal or distal binding pockets of the AdeG transporter. The AdeG residue G679I is located on the F-loop, which makes up part of the proximal binding site.[160] The three other residues also located in the proximal binding pocket are Y725A, A705I, and Q83A. The two binding pockets are separated by a flexible switch-loop[161] and is the location of residue I621A. The residues S620A and L138A are located in the distal binding pocket (**Figure 4.1**).

To analyze functional activities of AdeG mutants, my first goal was to integrate the mutated *adeG* genes into *A. baumannii* chromosomes. For this purpose, plasmids were integrated into the Tn7 site on the chromosome and expressed by growing the cell cultures in the presence of 1% L-arabinose. This amount of L-arabinose is needed to induce expression of the mutant transporters from both the plasmid-borne expression cassette and the chromosomally integrated efflux pump genes. Chromosomal insertions were confirmed by PCR using Ab (17978) *glmS* FWD, Ab (17978) *glmS* REV, and PTn7R primers (**Table 2.3**), as described before.[20] The expression of AdeG protein variants was determined by SDS-PAGE followed by immunoblotting with a custom AdeG monoclonal rabbit antibody serum (Thermo Fisher Scientific, Waltham, USA) made using AdeG protein antigen generated in the Zgurskaya lab (see Methods **2.15**) and followed by a secondary anti-rabbit immunoglobulin antibody (Sigma-Aldrich, St. Louis, USA). All AdeG mutants showed expression after a small volume (6 mL) membrane fraction purification (**Methods 2.9**) (data not shown here). Expression of each mutant was also verified after NPN uptake (**Figures 4.3, 4.10**). In conclusion, all mutant AdeG transporters were successfully integrated into the *A. baumannii* Δ3 chromosome, and all had confirmed expression.

Table 4.1 - Antibiotic susceptibilities of *A. Baumannii* Δ3-Pore AdeG site-directed mutants

Strains	MICs (μg/mL)		
	Chloramphenicol	Norfloxacin	Nalidixic Acid
AbΔ3-pore	8	0.25	2
AbΔ3-Pore (pAdeFGH)	16	1	8
AbΔ3-Pore (pAdeG) I621A	8	**0.25**	**2**
AbΔ3-Pore (pAdeG) S620A	16	1	8
AbΔ3-Pore (pAdeG) L138A	32	1	8
AbΔ3-Pore (pAdeG) G679I	16	**0.125-0.25**	**1-2**
AbΔ3-Pore (pAdeG) Y725A	8	0.5	4
AbΔ3-Pore (pAdeG) A705I	32	2	8
AbΔ3-Pore (pAdeG) Q83A	32	1	8

Minimal inhibitory concentrations [μg/mL] of AbΔ3-Pore cells containing control or AdeG mutant plasmids. MIC values that differ by four-fold or more are shown in underlined bold.

4.3.2. Functional characterization of mutant AdeG transporters

To test the function of the mutant AdeG transporters in *A. baumannii* Δ3-Pore cells, an antibiotic susceptibility assay was done using AdeG pump substrates Chloramphenicol (CHL), Norfloxacin (NOR), Nalidixic acid (NAL) (**Table 4.1**). The resulting minimum inhibitory concentrations (MICs) were compared to *A. baumannii* Δ3-Pore cells expressing an empty plasmid (pTJ1-MCS) or WT AdeFGH (pTJ1-AdeFGH). These two control strains represent the minimum efflux activity (empty plasmid) up to the maximum expected efflux activity (WT AdeFGH). These experiments were carried out at least twice, and the resulting MIC values were reproducible.

There were no significant changes in MICs of chloramphenicol in any of the tested strains. This was unexpected since this compound is a known substrate of the AdeFGH pump.[52] On the other hand, norfloxacin had a 4-8-fold increase in MIC and nalidixic acid had an 8-fold MIC increase in the WT (AbΔ3(pAdeFGH)) strain compared to the negative control (AbΔ3(pTJ1-MCS)).

The antibiotic susceptibility assays showed the AdeG mutants I621A and G679I were associated with a complete inability to efflux the pump substrate norfloxacin (NOR) and nalidixic acid (NAL) compared to WT, with each mutant pump showing a 4- to 8-fold decreasing in MIC. This suggests that the AdeG I621A and G679I mutants lost their ability to efflux norfloxacin and nalidixic acid. This made cells hosting the mutant pumps more susceptible to norfloxacin and nalidixic acid, thus the lower MIC values. The AdeG mutant Y725A showed a 2-fold higher susceptibility to both norfloxacin and nalidixic acid, suggesting that the Y725A substitution results in a slightly lower efflux ability. The remaining AdeG mutants (S620A, A705I, Q83A, and L138A) demonstrated antibiotic susceptibilities similar to WT AdeFGH.

4.3.3. Kinetic analysis of mutant AdeG transporters

Next, the kinetics of the AdeG mutants' ability to efflux NPN was measured (**Figure 4.3**). This uptake assay was conducted by preparing a non-binding 96 well plate with HMG buffer containing 0-16 μM of NPN. After 3 fluorescence readings without cells, 100 μL of OD_{600} = 1.0 cells were injected into the wells, one strain at a time, with each run going for about 10 minutes. The data sets were normalized by subtracting the first no-cell RFU reading from each well's time course. The data sets were then fitted using a script written for MatLab and the resulting fitted data sets were plotted as $[NPN]_{in}$, μM versus time, seconds.[122] The controls used for this kinetics uptake assay were the same as the inhibition uptake assay: AbΔ3-Pore (negative control) and AbΔ3-Pore (pAdeFGH) (positive control).

For most of the AdeG mutants, there was no noticeable NPN accumulation until at least 4 μM NPN. The increase from 4 μM NPN to 8 μM NPN saw a small jump in the steady-state levels of NPN accumulation, with AdeG mutants I621A and G679I (**Figure 4.3-F, H**) showing the largest increase in NPN accumulation. These two AdeG mutants also showed the highest maximum NPN accumulation at 16 μM NPN at almost 50K RFU. AdeG mutants I621A and G679I exhibiting NPN uptake profiles similar to the negative AbΔ3-Pore control suggests that these mutant pumps have a significant impairment to their ability to efflux NPN compared to other mutants. The AdeG mutants S620A and Y725A (**Figure 4.3-C, G**) exhibited NPN uptake profiles more similar to the positive control, but with higher NPN accumulation. This suggests that the AdeG mutants S620A and Y725A have an impaired ability to efflux NPN, but not to the degree of I621A and G679I. The AdeG mutants A705I, Q83A, and L138A (**Figure 4.3-D, E, I**) showed NPN uptake profiles most similar to WT, with the mutant Q83A even showing what appears to be improved efflux of 16 μM NPN, compared to the WT.

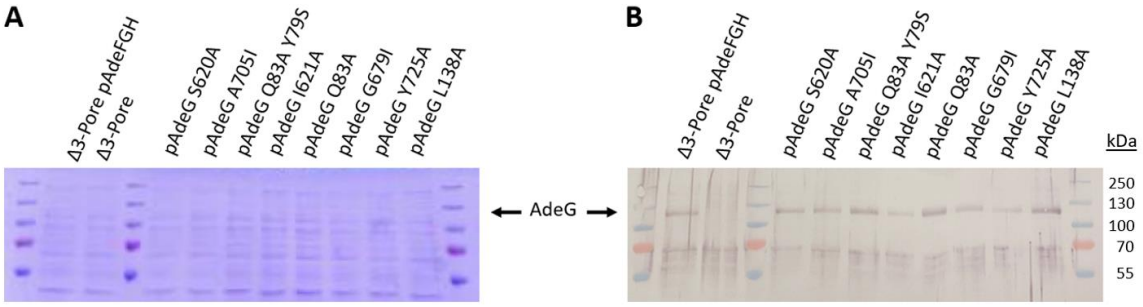

Figure 4.2 –AdeG expression in *A. baumannii* Δ3-Pore cells at time of NPN (0-16 µM) uptake

Whole cell expression of the AdeG mutants in *A. baumannii* Δ3-Pore cells washed in HMG buffer and resuspended to OD_{600} 1.0 +/- 0.05. AdeG protein was expressed in cells with permeabilized outer membranes. Plasmid expression of the AdeFGH operon was induced by 1% L-arabinose. Lysed cells were separated by SDS-PAGE on 12% gels and visualized by 1:5,000 anti-AdeG antibody serum.

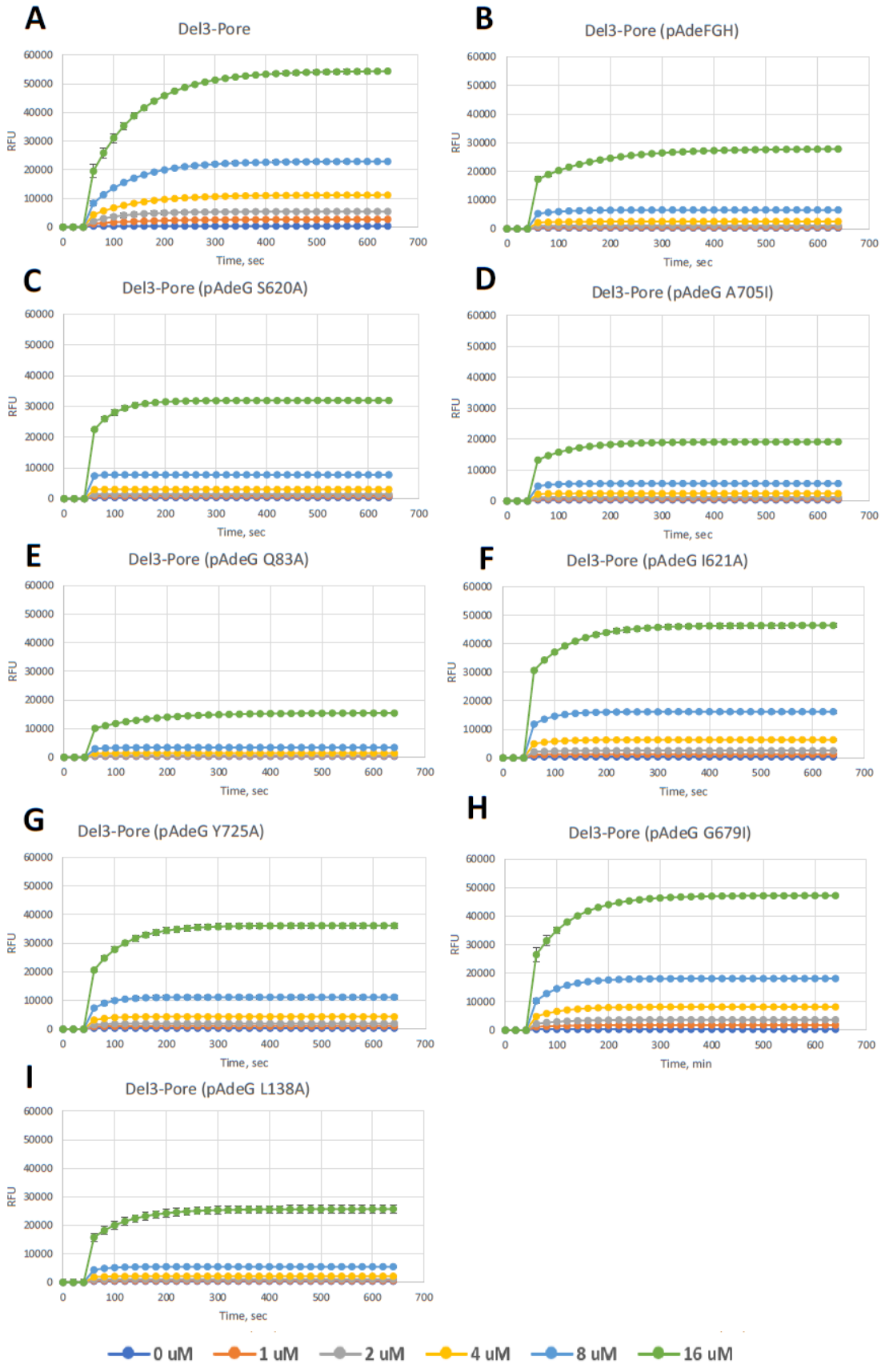
A
Del3-Pore
B
Del3-Pore (pAdeFGH)
C
Del3-Pore (pAdeG S620A)
D
Del3-Pore (pAdeG A705I)
E
Del3-Pore (pAdeG Q83A)
F
Del3-Pore (pAdeG I621A)
G
Del3-Pore (pAdeG Y725A)
H
Del3-Pore (pAdeG G679I)
I
Del3-Pore (pAdeG L138A)
RFU
Time, sec
Time, min
0 uM
1 uM
2 uM
4 uM
8 uM
16 uM

Figure 4.3 - Fluorescence uptake analysis of NPN (0-16 µM) with mutant AdeG transporters

Intracellular accumulation of fluorescent membrane probe NPN. Indicated strains were grown in LB broth and induced with 1% L-arabinose when appropriate. Washed cells were injected into HMG buffer containing 0-16 µM NPN. The resulting fluorescence was monitored continuously for 10 minutes. The uptake data sets were fitted using a script written for MatLab (**Methods 2.13**). The plots are changes in fluorescence intensity as a function of time. Error bars are SD (*n* = 3). (**A**) AbΔ3-Pore (**B**) AbΔ3-Pore (pAdeFGH) (**C**) AbΔ3-Pore (pAdeG S620A) (**D**) AbΔ3-Pore (pAdeG A705I) (**E**) AbΔ3-Pore (pAdeG Q83A) (**F**) AbΔ3-Pore (pAdeG I621A) (**G**) AbΔ3-Pore (pAdeG Y725A) (**H**) AbΔ3-Pore (pAdeG G679I) (**I**) AbΔ3-Pore (pAdeG L138A)

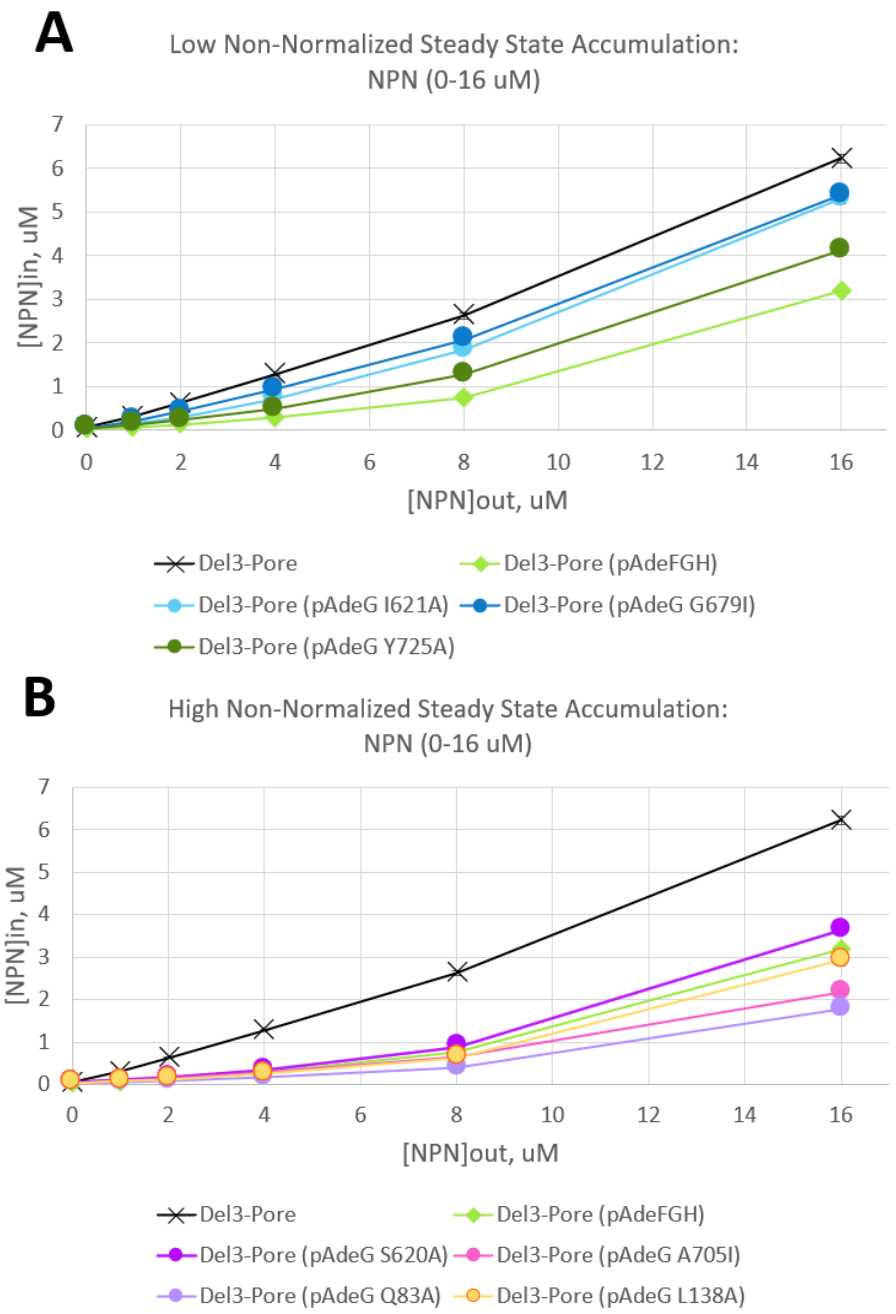

Figure 4.4 –Steady state accumulation of NPN (0-16 µM) uptake

Steady state concentrations of intra cellular NPN plotted against extracellular concentrations of NPN: (**A**) Low efflux efficiency AdeG mutants and (**B**) High efflux efficiency AdeG mutants. Steady state concentrations were normalized by subtracting the initial [NPN]in value (µM). The steady state data sets were calculated using a script written for MatLab (**Methods 2.13**). Error bars are SD (n=2).

Next, we compared the steady state accumulation between the strains based on their kinetics time courses (**Figure 4.4**). These concentrations were calculated in MatLab

using the same script used to calculate the uptake data set fittings (**Methods 2.13, Figure 4.3**). The steady state accumulations were then normalized by subtracting the initial $[NPN]_{in}$ value (μM). The normalized steady state curves for the AdeG mutants appear to mostly group either above or below the cells producing the WT AdeG (light green diamonds). These two groups have been labeled as "low efficiency" (I621A, G679I, and Y725A) and "high efficiency" (S620A, A705I, Q83A, and L138A). Low efficiency AdeG mutants (**Figure 4.4-A)** are distributed between the efflux deficient cells (black "x" markers) and WT AdeG (light green diamonds) and generally showed lower efflux efficiency compared to WT AdeG. The high efficiency AdeG mutants (**Figure 4.4-B**) grouped at or below the WT AdeG levels and generally demonstrated efflux efficiency similar to or higher than WT AdeG. At the higher 16 μM concentration of NPN, the differences between the mutants became more obvious. The only normalized curve shown as having higher steady state accumulation compared to WT was the AdeG S620A mutant (dark purple). When the NPN concentration was increased from 8 μM to 16 μM, AdeG S620A had the greatest increase in steady state NPN accumulation of the high efficiency group.

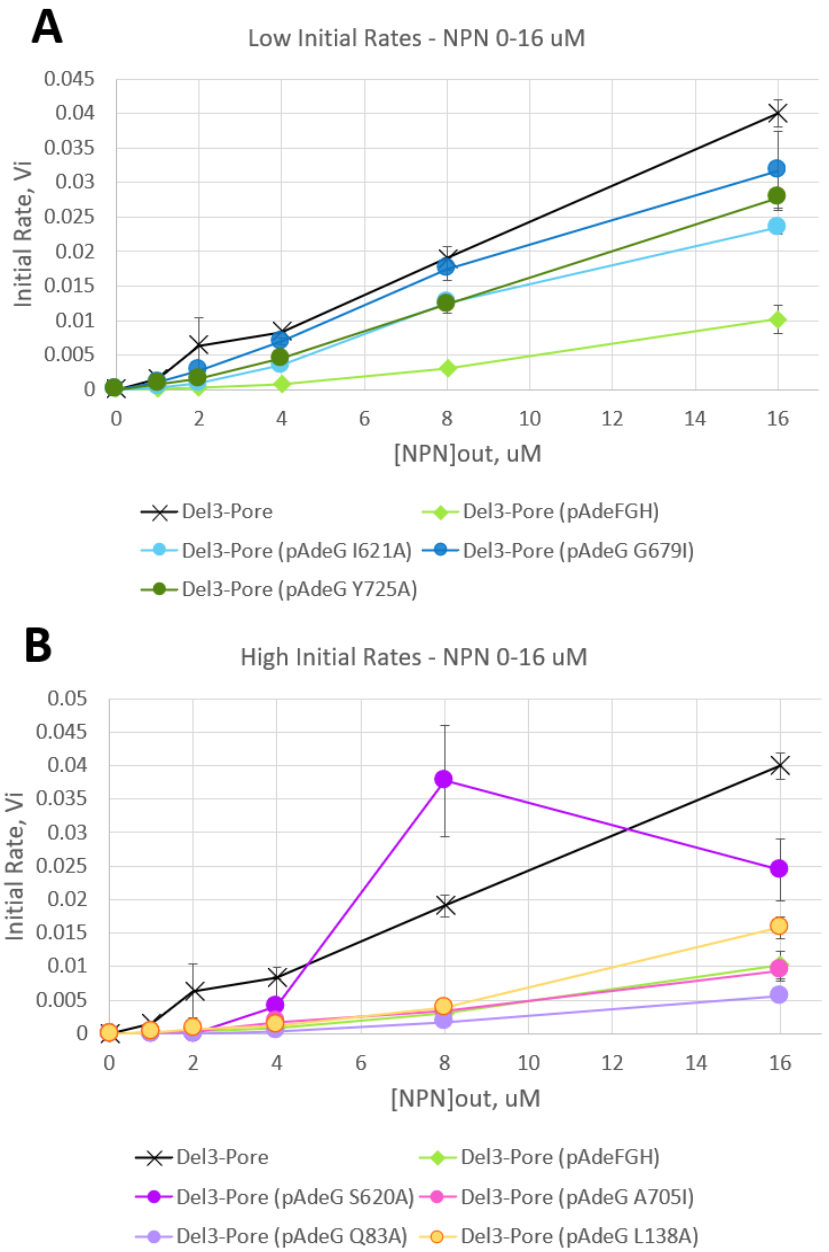

Figure 4.5 – Initial rates of NPN (0-16 µM) uptake

Initial rates of uptake of all *A. baumannii* Δ3-Pore AdeG mutant strains and controls: (**A**) Low efflux efficiency AdeG mutants, (**B**) High efflux efficiency AdeG mutants. The uptake data sets were fitted using a script written for MatLab (**Methods 2.13**). Error bars are SD (n = 2).

We also calculated the initial rates (Vi) using the same model in MatLab. The initial rates of the strains were plotted verses external concentration of NPN (**Figure 4.5**). The initial rates for the low efficiency AdeG mutants (**Figure 4.5-A**) are distributed between the negative control strain (AbΔ3-Pore, black "x" markers) and the positive

control strain (AbΔ3-Pore(pAdeFGH), light green diamonds). The higher initial rates show that these AdeG mutants are less efficient at exporting NPN than the WT AdeG.

The initial rates for the high efficiency AdeG mutants (**Figure 4.5-B**) are distributed above and below the WT AdeG cells (light green diamonds). The two AdeG mutants S620A and L138A show initial rates higher than the WT, suggesting that they are less efflux efficient than WT AdeG and the other "high efficiency" mutants. The AdeG mutant L138A showed the fastest initial rate change. When doubling the external NPN concentration from 8 μM to 16 μM, AdeG L138A saw its initial rate quadruple. This suggests that even though AdeG L138A was efflux efficient at lower NPN concentrations, 16 μM NPN is likely to be above its K_D resulting in a greater increase in NPN uptake. The AdeG mutant A705I shows initial rates that line up very closely with the WT AdeG curve, suggesting that this amino acid substitution did not have much impact on the export rate of the transporter. The AdeG mutant Q83A appears to have the lowest initial rates across all tested NPN concentrations, suggesting that this single residue substitution slightly improves efflux efficiency of the AdeG transporter.

4.3.4. The effect of mutations in AdeG on the inhibitory activity of SLUPP_1377

In an ongoing effort to discover new and effective EPIs, Zgurskaya previously reported a substituted phthalanilide NSC-60339 and a substituted diaminoquinoline NSC-33353 targeting AcrAB-TolC efflux system in *E. coli*.[109,162] These compounds exhibited weak antibacterial activity, improved the potency of antibiotics, and inhibited efflux in a biochemical assay. The attractive profiles of these AcrAB-TolC EPIs and the homology between *E. coli* AcrB and *A. baumannii* AdeG and AdeJ[45,163] has prompted us to initiate efforts in designing inhibitors that target major RND efflux systems, including AdeFGH in *A. baumannii*.

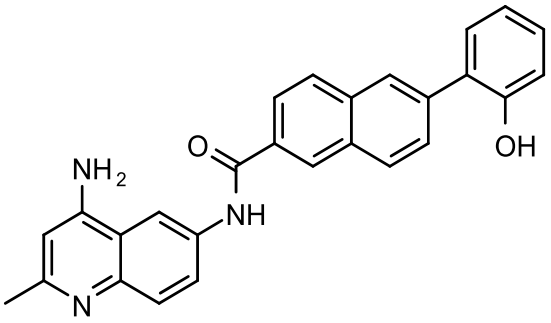

Figure 4.6 – Structure of putative efflux pump inhibitor SLUPP_1377

Molecule name: OU-0000008, Synonym: SLUPP-0001377

Dr. Rushikesh Tambat has identified SLUPP_1377 as an inhibitor of AdeFGH. He determined the minimum potentiating concentration of SLUPP_1377 that decreases the MICS of chloramphenicol, erythromycin, or nalidixic acid by four-fold (MPC_4) in AbΔ3-Pore cells with and without the mutant plasmid-expressed AdeG transporters (**Table 4.2**). All three of the above antibiotics are known substrates of the AdeG pump and they have the same MICs in AbΔ3 as in AbΔ3-Pore, meaning cell permeability does not significantly impact the efficacy of these antibiotics. As expected, there is no difference in SLUPP_1377 MICs and MPC_4 values in the AbΔ3-Pore strain because there are no RND pumps for SLUPP_1377 to inhibit. The compound SLUPP_1377 potentiated the activity of chloramphenicol in the positive control strain AbΔ3-Pore(pAdeFGH) and had MPC_4 values 4-fold lower than the respective MIC value. In the strains producing AdeG mutants described in Section 4.3.1. above, SLUPP_1377 potentiated the activity of chloramphenicol in the AdeG mutants S620A and Q83A with MPC_4 values 8-fold lower than their corresponding MIC values. The SLUPP_1377 MPC_4 values were 4-fold lower than MICs in the AdeG mutants L138A and A705I, and 2-fold lower for Y725A. There was no difference in MPC_4 values versus MIC values in AdeG mutants I621A and G679I.

SLUPP_1377 potentiated the activity of norfloxacin in the AdeG mutant Q83A with MPC_4 values 32-fold lower than its corresponding MIC value. The AdeG mutant S620A showed an MPC_4 value 16-fold lower. The AdeG mutants A705I and L138A showed norfloxacin potentiation similar to WT AdeFGH with MPC_4 values 8-fold lower.

AdeG mutant Y725A showed an MPC_4 value 4-fold lower. Lastly, the AdeG mutants I621A and G679I showed no difference between MPC_4 and MIC values for norfloxacin.

SLUPP_1377 potentiated the activity of nalidixic acid in AdeG mutants S620A and Q83A with MPC_4 values 8-fold lower than their corresponding MIC values. The AdeG mutants L138A and A705I showed similar nalidixic acid potentiation as WT AdeFGH with MPC_4 values 4-fold lower. The AdeG mutant Y725A showed an MPC_4 value 2-fold lower. Lastly, the AdeG mutants I621A and G679I showed no difference between MPC_4 and MIC values for nalidixic acid.

In conclusion, the AdeG mutants I621A and G679I were not susceptible to potentiation by SLUPP_1377, which supports the previous results suggesting that they are non-functional mutants. The AdeG mutant Y725A was slightly less susceptible to potentiation by SLUPP_1377 compared to WT AdeFGH. The AdeG mutants L138A and A705I were as susceptible to potentiation by SLUPP_1377 as the WT AdeG. Lastly, the AdeG mutants S620A and Q83A were the most susceptible to potentiation by SLUPP_1377.

Table 4.2 – MPC_4 values of SLUPP_1377 with CHL, NOR, and NAL in AbΔ3-Pore AdeG mutants

Strains	**SLUPP-1377 (MIC, µM)**	**MPC_4 (µM)**		
		CHL	NOR	NAL
AbΔ3-Pore	3.125	3.125	3.125	3.125
AbΔ3-Pore (pAdeFGH)	12.5	3.125	1.56	3.125
AbΔ3-Pore (pAdeG) I621A	3.125	3.125	3.125	3.125
AbΔ3-Pore (pAdeG) S620A	12.5	1.56	0.78	1.56
AbΔ3-Pore (pAdeG) L138A	12.5	3.125	1.56	3.125
AbΔ3-Pore (pAdeG) G679I	3.125	3.125	3.125	3.125
AbΔ3-Pore (pAdeG) Y725A	6.25	3.125	1.56	3.125
AbΔ3-Pore (pAdeG) A705I	12.5	3.125	1.56	3.125
AbΔ3-Pore (pAdeG) Q83A	12.5	1.56	0.39	1.56

MPC_4: minimal potentiating concentration (MPC), a concentration of compound that decreases minimum inhibitory concentration (MIC) of an antibiotic by 4-fold. CHL – Chloramphenicol, NOR – Norfloxacin, NAL – Nalidixic acid.

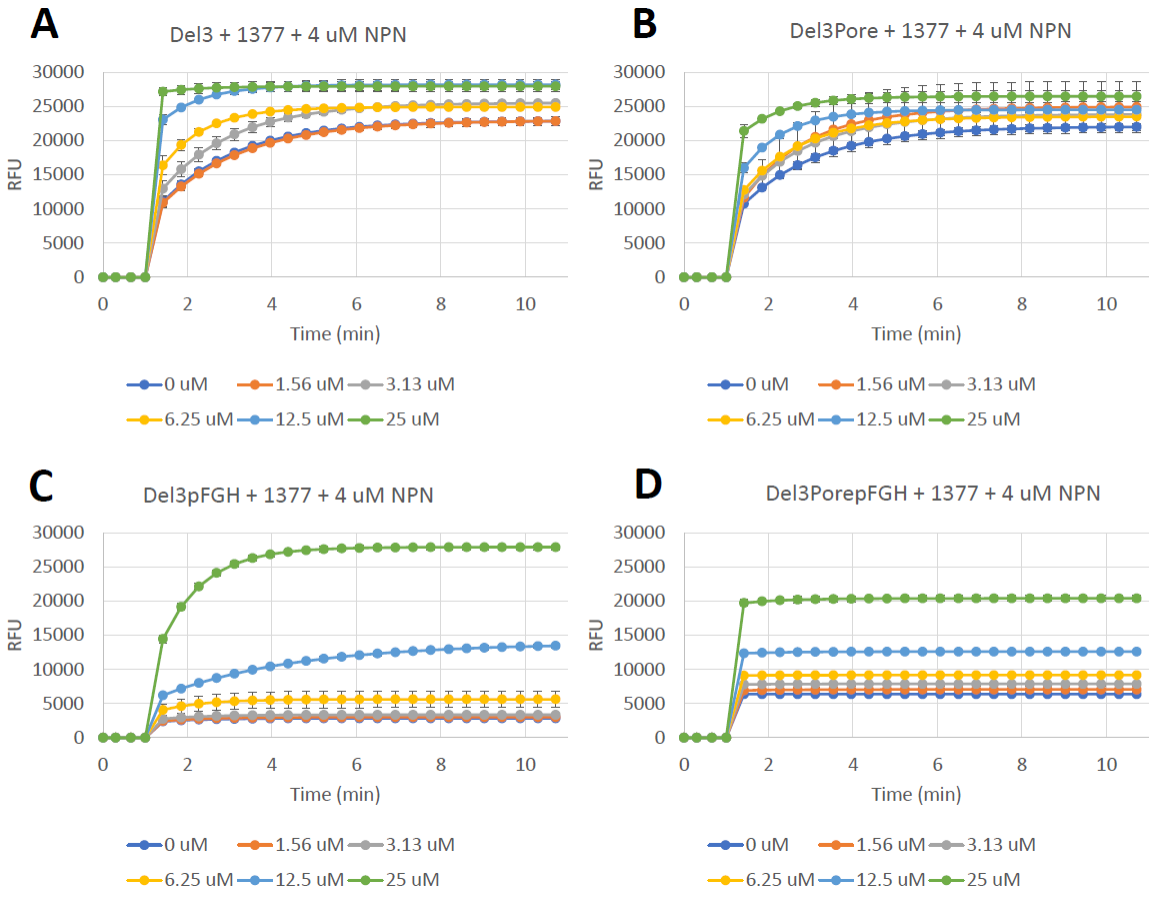

Figure 4.7 - Fluorescence uptake analysis of NPN in combination with SLUPP_1377

Intracellular accumulation of fluorescent membrane probe NPN. Indicated strains were grown in LB broth and induced with 1% L-arabinose when appropriate. Washed cells were injected into HMG buffer containing 4 µM NPN and 0-25 µM SLUPP_1377. The resulting fluorescence was monitored continuously for 10 minutes. The uptake data sets were fitted using a script written for MatLab (**Methods 2.13**). Error bars are SD (n = 2). (**A**) AbΔ3 (**B**) AbΔ3-Pore (**C**) AbΔ3 (pAdeFGH) (**D**) AbΔ3-Pore (pAdeFGH)

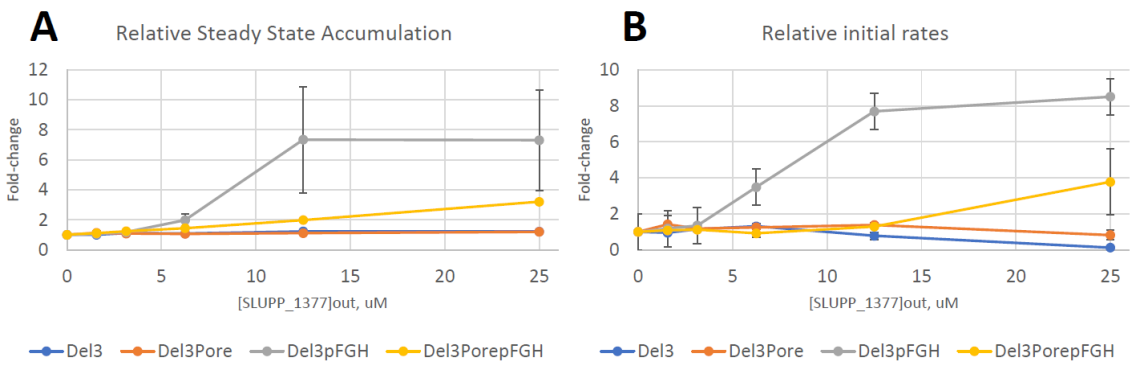

Figure 4.8 – Relative steady state accumulation and initial rates for NPN and SLUPP_1377 optimization

(**A**) Relative steady state fits of intracellular NPN (fold-change) plotted against extracellular concentrations of SLUPP_1377. Steady state concentrations were normalized by dividing each steady state value by the initial steady state value. Error bars are Std dev (n=2). (**B**) Relative initial rates of uptake (fold-change) plotted against extracellular concentrations of SLUPP_1377. The initial rates were normalized by dividing each initial rate by the initial rate value at 0 µM SLUPP_1377. Error bars are SD (n = 2). Both the steady state and initial rate data sets were fitted using a script written for MatLab (**Methods 2.13**).

4.3.5. SLUPP_1377 inhibits efflux of NPN in cells overproducing AdeFGH

We next measured the intracellular accumulation of the fluorescent probe NPN in combination with SLUPP_1377, a compound suspected to inhibit the efflux activity of AdeG. First the NPN uptake profiles of AbΔ3 and AbΔ3-Pore strains, with and without overexpression of pAdeFGH, were examined to see if we could see a concentration dependent trend with the potential inhibitor SLUPP_1377. The compound SLUPP_1377 showed inherent fluorescence when measured in wells containing HMG buffer and cells (data not shown). The fluorescence contribution of SLUPP_1377 was removed from the assay by running control wells containing SLUPP_1377 and cells in HMG buffer (no NPN) alongside experimental wells containing the same concentrations of SLUPP_1377 and cells in HMG buffer, with a final concentration of 4 µM NPN. The RFU values from the control wells were subtracted from the experimental NPN wells. As seen in **Figure 4.7-A,B**, both the AbΔ3 cells and the AbΔ3-Pore cells have high levels of NPN accumulation across all concentrations of SLUPP_1377. The increasing NPN accumulation seen when increasing concentration of SLUPP_1377 is likely due to the inherent fluorescence of SLUPP_1377 rather than efflux inhibition. The panels in **Figure**

4.7-C,D show a concentration dependent intracellular accumulation of NPN in both AbΔ3 and AbΔ3-Pore cells.

Next, I compared the normalized steady state accumulation between the strains based on their time courses (**Figure 4.8-A**). This plot shows the relative steady state accumulation of NPN (fold-change) on the y-axis and $[SLUPP\_1377]_{out}$ (μM) on the x-axis. The steady state accumulation data sets were normalized by dividing each value by the initial steady state value. The two efflux deficient strains, AbΔ3 and AbΔ3-Pore, did not see a change in relative steady state accumulation with increasing concentrations of SLUPP_1377. This result was expected since SLUPP_1377 is believed to inhibit the RND transporter AdeG, which is not present in either strain. Both strains overproducing AdeFGH did show increased relative steady state accumulation with increasing concentration of inhibitor, but to different degrees. AbΔ3-Pore (pAdeFGH) saw a 2-fold increase with 12.5 μM SLUPP_1377 and a 3-fold increase with 25 μM SLUPP_1377. AbΔ3 (pAdeFGH) had a much more dramatic increase with a 7-fold increase with 12.5 μM SLUPP_1377 and with 25 μM SLUPP_1377. The standard deviation error bars were very large for the highest two inhibitor concentrations in AbΔ3 (pAdeFGH) cells, and for this reason we decided to conduct future NPN uptake experiments with porinated AbΔ3 strains.

Lastly, initial rates for the NPN uptake in combination with SLUPP_1377 time courses (**Figure 4.8-B**) were calculated using a script made for MatLab (**Methods 2.13**). The initial rate data sets were normalized by dividing the initial rate value at 0 μM SLUPP_1377 from each initial rate value. Similar to the trends seen in the relative steady state plot (**Figure 4.8-A**), the two efflux deficient strains, AbΔ3 and AbΔ3-Pore, had either no change or a slight decrease in relative initial rates. AbΔ3-Pore (pAdeFGH) did not have a noticeable change in relative initial rate until 25 μM SLUPP_1377 where it had a 4-fold increase. AbΔ3 (pAdeFGH) had noticeable changes to its initial rates starting at 6.25 μM SLUPP_1377 with a 3.5-fold increase, a 7.5-fold increase at 12.5 μM SLUPP_1377, and a 8.5-fold increase at 25 μM SLUPP_1377, thus indicating a significant loss of efflux efficiency. This plot shows that the strain AbΔ3 (pAdeFGH) had by far the most dramatic increase in relative initial rates with increasing concentrations of

inhibitor, suggesting that out of the four tested strains it had the highest sensitivity to efflux inhibition by SLUPP_1377.

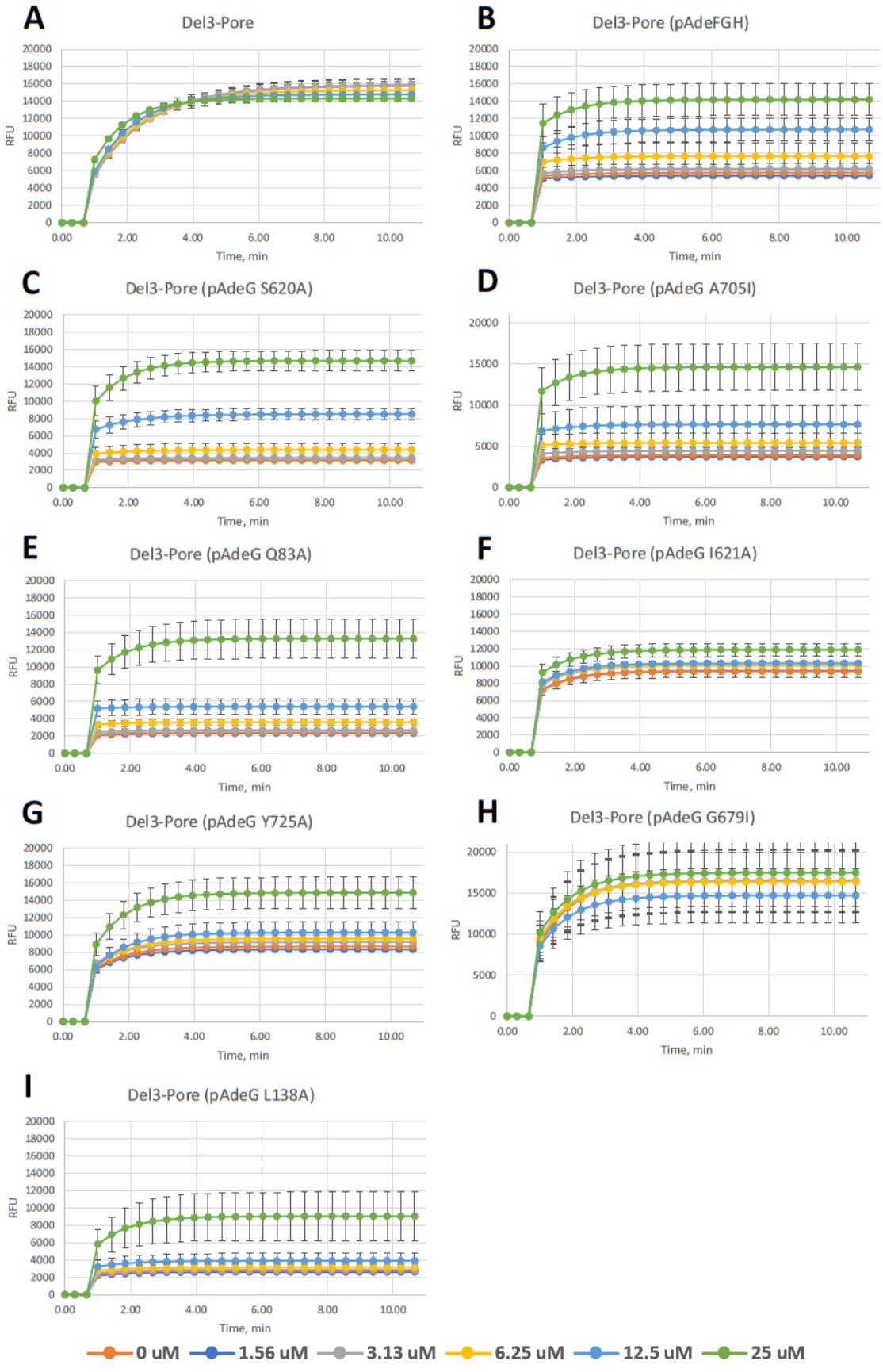
A
Del3-Pore
B
Del3-Pore (pAdeFGH)
C
Del3-Pore (pAdeG S620A)
D
Del3-Pore (pAdeG A705I)
E
Del3-Pore (pAdeG Q83A)
F
Del3-Pore (pAdeG I621A)
G
Del3-Pore (pAdeG Y725A)
H
Del3-Pore (pAdeG G679I)
I
Del3-Pore (pAdeG L138A)
RFU
Time, min
0 uM
1.56 uM
3.13 uM
6.25 uM
12.5 uM
25 uM

Figure 4.9 - Fluorescence uptake analysis of NPN and SLUPP_1377 in AbΔ3-Pore cells expressing mutant AdeG transporters

Intracellular accumulation of fluorescent membrane probe NPN. Indicated strains were grown in LB broth and induced with 1% L-arabinose when appropriate. Washed cells were injected into HMG buffer containing 4 μM NPN and 0-25 μM SLUPP_1377. The resulting fluorescence was monitored continuously for 10 minutes. The uptake data sets were fitted using a script written for MatLab. The plots are changes in fluorescence intensity as a function of time. Error bars are SE (n = 4). (**A**) AbΔ3-Pore (**B**) AbΔ3-Pore (pAdeFGH) (**C**) AbΔ3-Pore (pAdeG S620A) (**D**) AbΔ3-Pore (pAdeG A705I) (**E**) AbΔ3-Pore (pAdeG Q83A) (**F**) AbΔ3-Pore (pAdeG I621A) (**G**) AbΔ3-Pore (pAdeG Y725A) (**H**) AbΔ3-Pore (pAdeG G679I) (**I**) AbΔ3-Pore (pAdeG L138A)

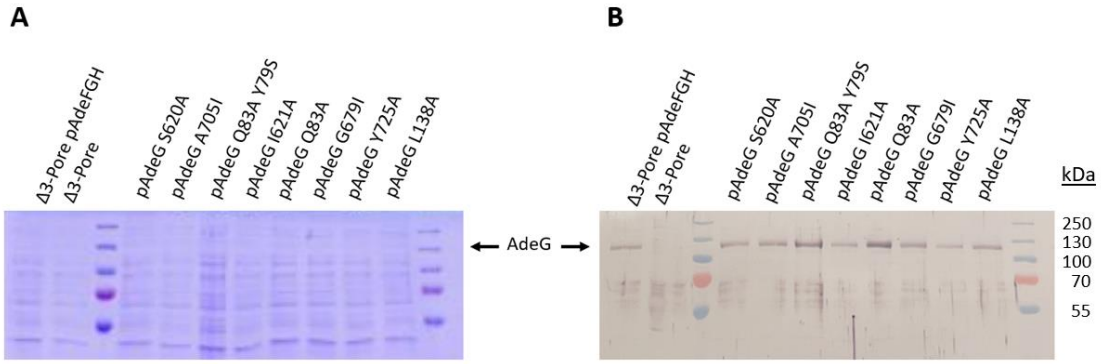

Figure 4.10 –AdeG expression in *A. baumannii* Δ3-Pore cells at time of NPN + SLUPP_1377 uptake

Whole cell expression of the AdeG mutants in *A. baumannii* Δ3-Pore cells washed in HMG buffer and resuspended to OD_{600} 1.0 +/- 0.05. AdeG protein was expressed in cells with permeabilized outer membranes. Plasmid expression of the AdeFGH operon was induced by 1% L-arabinose. Lysed cells were separated by SDS-PAGE on 12% gels and visualized by 1:5,000 anti-AdeG antibody serum.

4.3.6. Mutations in the substrate binding pockets of AdeG change inhibition efficiency of SLUPP_1377

One of the challenges faced during the development of efflux pump inhibitors (EPIs) comes from targeting the highly hydrophobic binding pocket of the transporter. Potential EPI molecules that successfully interact with this region have been characterized by their insolubility or amphiphilicity, as well as issues with their pharmacokinetics and toxicity. Plus, EPIs that bind to substrate binding sites are more likely to have properties similar to pump substrates, resulting in lower inhibition efficiency due to being exported by the pump. But thanks to published crystal structures of two EPIs bound to major RND transporters (pyranopyridine core MBX inhibitors

bound to *E. coli*'s AcrB[164], and pyridopyrimidine derivatives bound to *E.coli*'s AcrB and *P. aeruginosa*'s MexB[165]) we now know that EPIs can bind to the phenylalanine-rich hydrophobic trap deep within the distal binding pocket.[166] This enables the design of EPIs that specifically target this hydrophobic trap and avoid being exported by the pump.

We next analyzed how mutations in the proximal and distal binding sites of AdeG affect the efficiency of SLUPP_1377's action. As a method of measuring efflux activity, the intracellular accumulation of NPN was analyzed in AbΔ3-Pore cells carrying the mutant AdeFGH operons and compared to NPN uptake of AbΔ3-Pore (negative control) and AbΔ3-Pore (pAdeFGH) (positive control). All wells contained the final concentration of 4 μM NPN. This NPN fluorescence assay was run in combination with increasing concentrations of SLUPP_1377: 0 μM, 1.56 μM, 3.13 μM, 6.25 μM, 12.5 μM, and 25 μM.

Most mutants exhibited similar steady state NPN accumulation ($[NPN]_{in}$, **Figure 4.9**) at the highest concentration of SLUPP_1377 (25 μM) to the steady state NPN accumulation seen in the cells expressing the WT AdeFGH efflux pump (~14k RFU). The AdeG A705I mutant showed similar NPN accumulation compared to WT at 25 μM of SLUPP_1377, but 12.5 μM SLUPP_1377 was not effective (**Figure 4.9-D**). Unlike in Δ3-Pore(pAdeFGH) cells, the intracellular accumulation of NPN in AdeG A705I cells was not increased by 12.5 μM SLUPP_1377. This phenotype was also seen in the AdeG mutants Q83A, and Y725A (**Figure 4.9-E, G**). Thus, for all these mutants only 25 μM of SLUPP_1377 was enough significantly increase intracellular accumulation of NPN.

The AdeG mutant I621A did not have much difference in NPN accumulation with increasing concentrations of SLUPP_1377 (**Figure 4.9-F**). The NPN accumulation profile of this mutant appears similar to the negative control, but with lower RFU values, suggesting the mutant pump is still functional, but SLUPP-1377 is no longer active against this AdeG variant.

Two of the AdeG mutants showed increased maximum intracellular NPN accumulation, but with quite different accumulation profiles. The accumulation curves of AdeG S620A (**Figure 4.9-C**) had a similar trend to those of Δ3-Pore

(pAdeFGH) cells (**Figure 4.9-B**). SLUPP_1377 concentrations 0 μM to 6.25 μM had no impact on NPN accumulation. AdeG S620A cells added to wells containing 12.5 μM did show a ~4,000 RFU increase, which is about the same increase in NPN accumulation seen in WT AdeFGH cells with 12.5 μM SLUPP_1377. Notably, the NPN accumulation in AdeG S620A cells with 25 μM SLUPP_1377 saw an increase of ~6,000 RFU compared to the ~1,500 μM increase in Δ3-Pore(pAdeFGH) cells. It appears that 25 μM SLUPP_1377 may be more effective at inhibiting efflux in the mutant AdeG S620A cells compared to the WT AdeG pump.

The MIC values (**Table 4.1**) and NPN uptake (**Figure 4.3**) showed that AdeG mutant G679I lost its efflux activity. In agreement with those results, I found that cells overproducing this mutant resemble the negative control cells more than the cells with fully functioning WT AdeG transporter (**Figure 4.9**). AdeG G679I had the highest maximum NPN accumulation of all the mutants at about 17,000 RFU, which is similar to the negative control max of ~18,000 RFU. In both the AdeG G679I mutant and AbΔ3-Pore cells lacking the AdeFGH pump, the cells with the highest NPN accumulation were those in wells with 0 μM SLUPP_1377. The AdeG G679I mutant also followed the no efflux trend where increasing concentrations of SLUPP_1377 resulted in lower maximum RFU values due to the quenching effect of SLUPP_1377 fluorescence (see above Section 4.3.5.).

While the AdeG Y725A mutant (**Figure 4.9-G**) showed similar maximum NPN accumulation values with 25 μM SLUPP_1377 to the WT cells, it showed an increase in RFU values at the lower concentrations of SLUPP_1377. For example, AbΔ3-Pore(pAdeFGH) cells exhibited maximum NPN accumulation values at around 5,000 RFU for SLUPP_1377 concentrations 0 μM – 6.25 μM. AdeG Y725A cells in wells containing 0 μM – 6.25 μM SLUPP_1377 saw an increase in maximum NPN accumulation to about 8,000 RFU. Effectively, the 0 μM – 6.25 μM SLUPP_1377 uptake curves shifted up to match the 12.5 μM RFU values, which in both AdeG Y725A and AbΔ3-Pore (pAdeFGH) cells were ~8,000 RFU. This suggests that the AdeG Y725A mutant has a lowered ability to efflux NPN compared to WT, leading to the higher baseline NPN accumulation. But since the maximum RFU values with 25 μM

SLUPP_1377 is only a bit higher than WT, it is likely that SLUPP_1377 has similar inhibitory activity in the AdeG Y725A mutant as the WT AdeFGH pump.

The AdeG Q83A mutant (**Figure 4.9-E**) had very similar NPN accumulation at 25 μM SLUPP_1377 as WT AdeG, but showed comparatively lower NPN accumulation at SLUPP_1377 concentrations of 12.5 μM and below. This suggests that the AdeG Q83A mutant is less susceptible to inhibition by SLUPP_1377 at lower concentrations compared to WT AdeG.

Lastly, the AdeG L138A mutant (**Figure 4.9-I**) showed a significant decrease in NPN accumulation at all concentrations of SLUPP_1377 compared to WT AdeG. All SLUPP_1377 concentrations except 25 μM exhibited max NPN accumulation at around 3,000 RFU. This is about half of the baseline NPN accumulation seen in the positive control. These data suggest that the AdeG L138A mutant is resistant to inhibition by SLUPP_1377.

Next, we compared the normalized steady state accumulation between the strains based on their inhibition time courses (**Figure 4.11**). This plot shows relative steady state accumulation of NPN (fold-change) on the y-axis and $[SLUPP\_1377]_{out}$ μM on the x-axis. Like the previous steady state accumulation data, the data sets used for this plot were calculated in MatLab using the same script used to calculate the uptake data set fittings (**Methods 2.13**). The steady state accumulations were then normalized by dividing each steady state value by the initial value. The AdeG mutants I621A, G679I, and Y725A curves distributed between the negative control (AbΔ3-Pore, black "x" markers) and the positive control (AbΔ3-Pore(pAdeFGH), light green diamonds), demonstrating that, for these three mutants, increasing the concentration of SLUPP_1377 inhibitor did not have as dramatic an increase in maximum NPN accumulation compared to other mutants (**Figure 4.11-A**). This supports the classification of these three mutants as "low efflux efficiency".

The "high efficiency" AdeG mutants all had similar relative steady state NPN accumulation up until 12.5 μM SLUPP_1377 where they start to show their separation (**Figure 4.11-B**). Their differences in sensitivity to the inhibitor is apparent at 25 μM SLUPP_1377. AdeG Q83A showed the largest increase in relative steady state

accumulation, indicating that this substitution was most sensitive to inhibition by SLUPP_1377. The AdeG mutants S620A, A705I, Q83A Y79S, and L138A had relative steady state accumulations higher than WT AdeG at 25 μM SLUPP_1377, suggesting that they were more susceptible to inhibition by SLUPP_1377 than WT AdeG, but they were still less sensitive than AdeG Q83A.

Lastly, initial rates for the NPN uptake in combination with SLUPP_1377 time courses were calculated using the same steady state process script in MatLab (**Methods 2.13**) The initial rates of the strains were normalized by dividing each initial rate with the initial rate at 0 μM SLUPP_1377. The resulting relative initial rates were plotted verses external concentration of SLUPP_1377 (**Figure 4.12**). Similar to their trends without inhibitor, the AdeG mutants I621A, G679I, and Y725A relative initial rate curves distributed below the WT AdeG (**Figure 4.12-A**). The relative initial rates of AdeG I621A and G679I remained unchanged with increasing concentrations of SLUPP_1377, suggesting that the inhibitor did not impact the mutants' efflux efficiency. AdeG Y725A did show increases in relative initial rates with increasing concentrations of inhibitor, suggesting that this substitution is still susceptible to inhibition by SLUPP_1377.

All of the "high efficiency" AdeG mutants demonstrated relative initial rates similar to or above WT AdeG (**Figure 4.12-B**). The AdeG mutants S620A and Q83A showed the by far the largest jump in relative initial rates when comparing their values at 12.5 μM to 25 μM SLUPP_1377. This suggests that AdeG mutants S620A and Q83A are very susceptible to inhibition by SLUPP_1377 since it appears that the inhibitor overwhelms the mutant transporters at 25 μM SLUPP_1377, resulting in large initial rate fold-changes. The AdeG mutant A705I has a relative initial rate curve similar to WT AdeG, suggesting that it is similarly susceptible to efflux inhibition by SLUPP_1377. And lastly, the AdeG mutants L138A and Q83A Y79S showed relative initial rate curves above WT AdeG, suggesting that they are more susceptible to inhibition by SLUPP_1377, but not to the same degree as AdeG mutants S620A and Q83A. There is a significant difference in inhibitor sensitivity between the single AdeG mutant Q83A and the double AdeG mutant Q83A Y79S, which may suggest that the Y79S substitution is responsible for the decreased susceptibility to SLUPP_1377 inhibition.

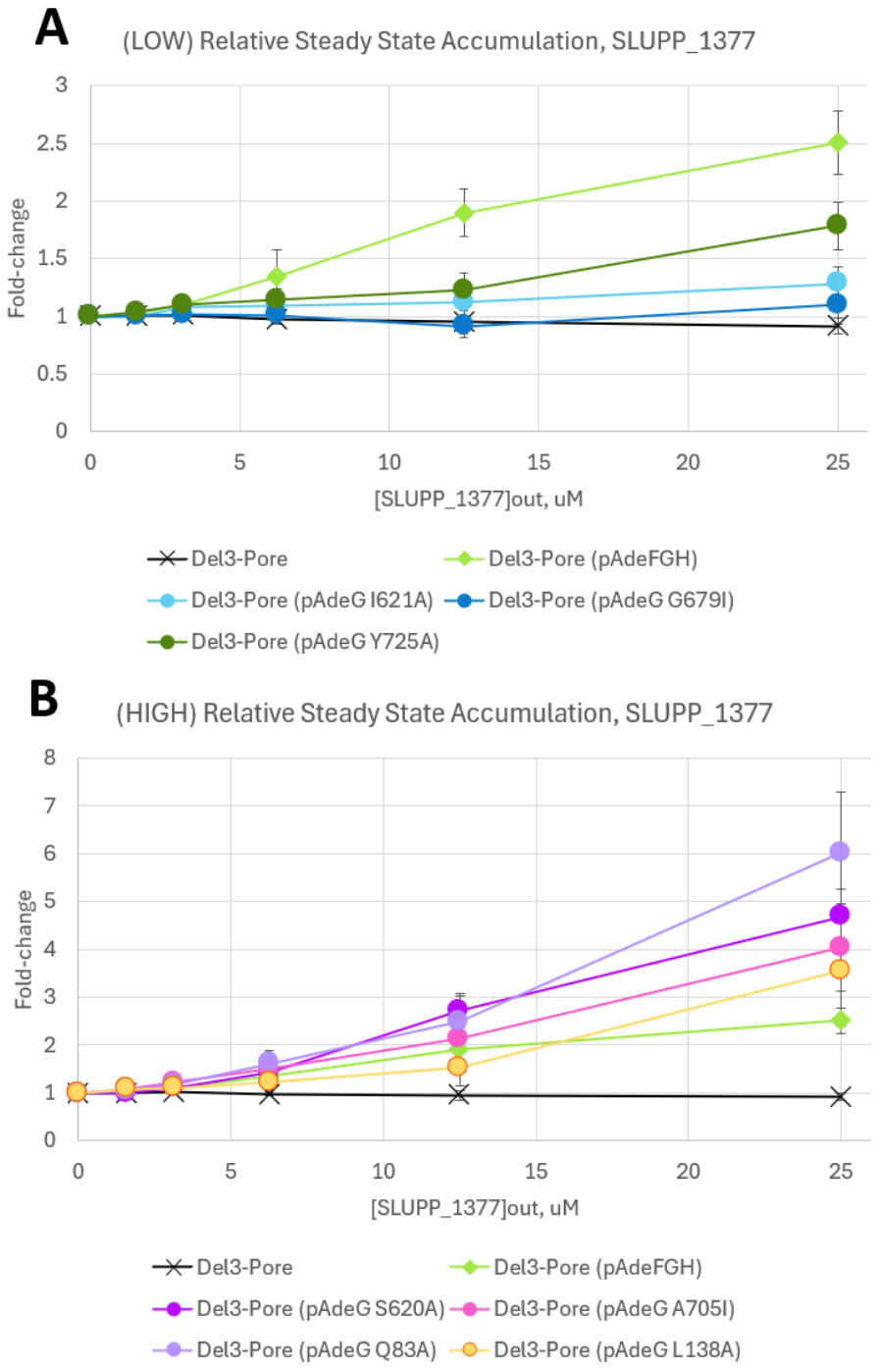

Figure 4.11 –Steady state accumulation of NPN (4 µM) in combination with SLUPP_1377 (0-25 µM)

Steady state concentrations of intra cellular NPN plotted against extracellular concentrations of SLUPP_1377. Steady state concentrations were normalized by dividing each steady state value by the initial steady state value. Error bars are SE (n=4).

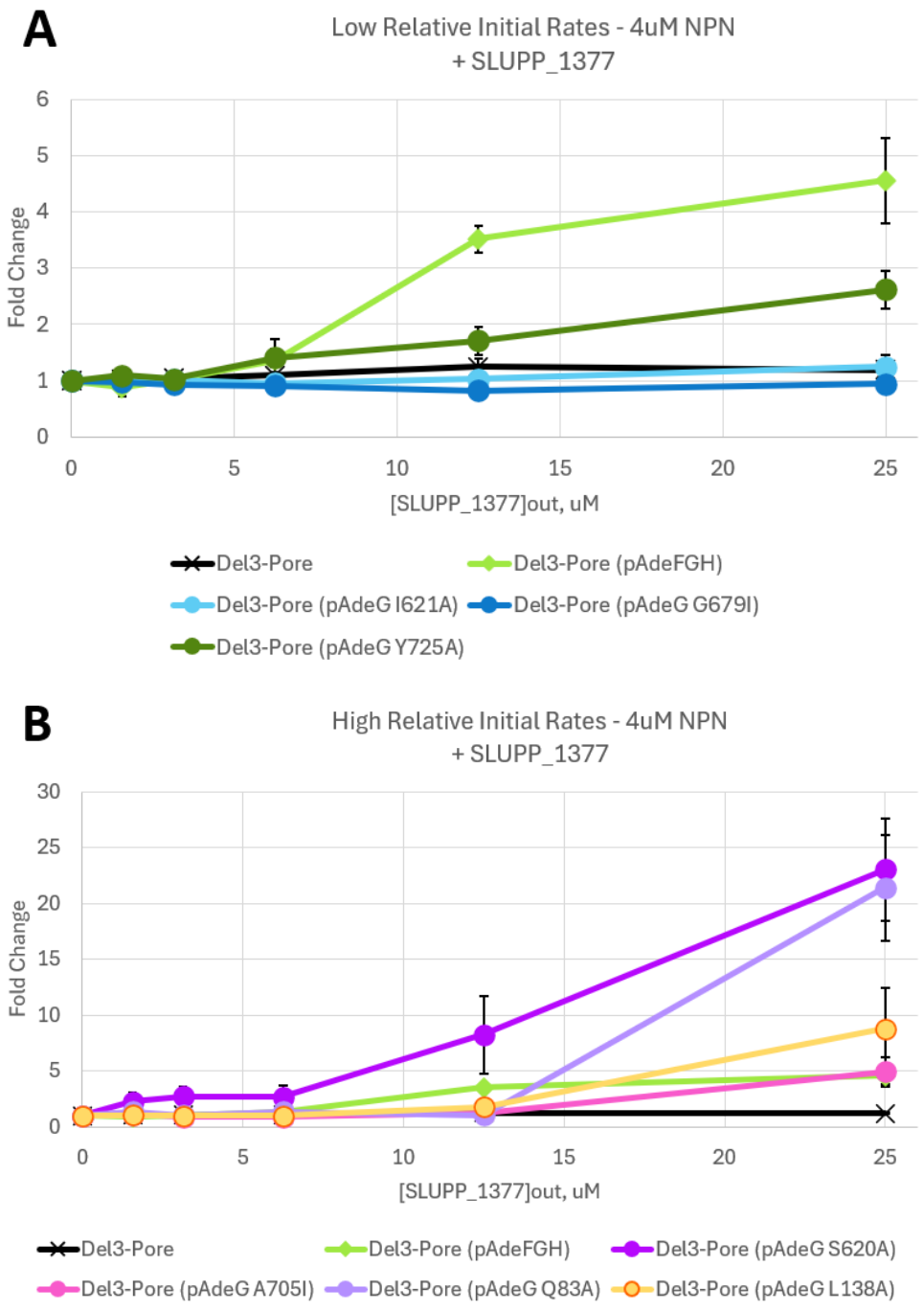

Figure 4.12 –Initial rates of NPN (4 µM) uptake in combination with SLUPP_1377

Initial rates of uptake of all *A. baumannii* Δ3-Pore AdeG mutant strains and controls. The uptake data sets were fitted using a script written for MatLab. Error bars are SE (n = 4).

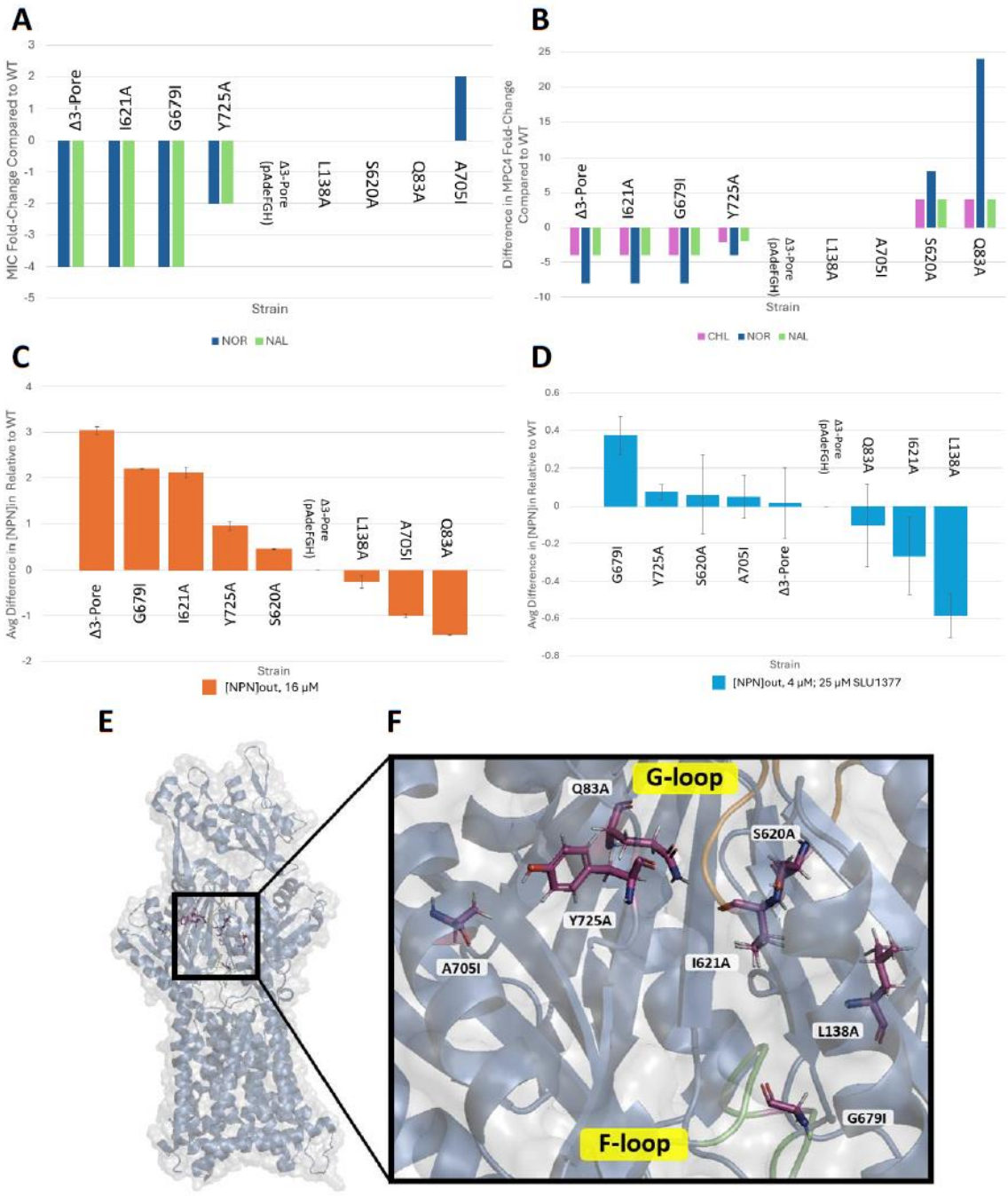

Figure 4.13 – Summary of AdeG binding pocket mutations

Graphical summaries of AdeG mutant properties relative to WT AbΔ3-Pore (pAdeFGH). (**A**) Ratio of Norfloxacin (NOR) and Nalidixic acid (NAL) MIC values for each strain relative to WT MIC values. (**B**) Difference in MPC4 fold-change for Chloramphenicol (CHL), NOR, and NAL potentiation by SLUPP_1377. (**C**) Average difference in

maximum intracellular NPN accumulation relative to WT. [NPN]out is 16 μM. (**D**) Average difference in maximum intracellular NPN accumulation with inhibition by 25 μM SLUPP_1377. [NPN]out is 4 μM. (**E**) An AdeG protomer (blue ribbon, based on AdeJ crystal structure PDB code: 7M4Q) with (**F**) highlighted amino acid residues (magenta) that were targeted in mutagenesis and labeled G-loop (orange) and F-loop (green).

4.4. Discussion

Infections caused by multidrug resistant pathogens like *A. baumannii* will continue to pose a significant threat to patients that must interact with a hospital setting and especially to individuals who have already compromised immune systems.[21] This threat will become more worrying as clinical *A. baumannii* continues to develop increased resistances to antibiotics regularly used in its treatment.[167] Therefore, it is imperative that the research community continues its work to discover and develop more effective treatments for *A. baumannii*. Gram-negative bacteria like *A. baumannii* are particularly good evaders of antimicrobials due to their double membranes.[168] The combination of the inner and outer membranes creates a synergistic effect of keeping drugs out with the low permeability barrier of the outer membrane and keeping intracellular drug accumulation low with the export activity of efflux pumps.[117] The RND superfamily of efflux pumps are transporters which have a very wide range of pump substrates.[27]

This study focused on the substrate specificity and inhibition of the major RND efflux pump AdeG of *A. baumannii* and how specific residues within its hydrophobic binding pocket interact with AdeG pump substrates and the inhibitor SLUPP_1377. Of the seven constructed single substitution AdeG mutants, AdeG I621A (G-loop) and G679I (F-loop) both appeared to be non-functional mutants since they exhibited efflux activity levels that were close to the negative control strain AbΔ3-Pore. This aligns with previous findings which show that the F-loop and G-loop are critical for RND transporter function.[40] Perhaps substituting the small glycine side chain with the bulkier and more hydrophobic isoleucine side chain resulted in protein-misfolding or blocked pump substrates from moving further into the proximal binding site from the entrance site.[169] All other AdeG mutants demonstrated at least low levels of efflux activity.

The two AdeG mutants located in the distal binding pocket (DBP), S620A and L138A, both exhibited similar antibiotic susceptibilities compared to WT AdeG. AdeG mutant L138A exhibited similar potentiation activity by SLUPP_1377 as WT AdeG, while S620A appeared more sensitive to potentiation by SLUPP_1377 compared to WT AdeG (**Figure 4.13-B**). These two mutants also showed efflux activity similar to WT AdeG (**Figure 4.13-C**). AdeG mutant S620A showed similar SLUPP_1377 inhibitor susceptibility compared to WT AdeG while L138A appeared the most susceptible to SLUPP_1377 inhibition (**Figure 4.13-D**). Analysis of additional substitutions located within the hydrophobic trap could provide more detail on where the SLUPP_1377 compound is binding.

The remaining AdeG residues located in the proximal binding pocket did not demonstrate a unifying trend. The antibiotic susceptibilities of AdeG mutants Y725A, A705I, and Q83A were all within 2-fold of WT AdeG (**Figure 4.13-A**). AdeG mutants Y725A and A705I were about as sensitive to antibiotic potentiation by SLUPP_1377 as WT AdeG, while AdeG Q83A showed significantly higher norfloxacin potentiation and relatively higher chloramphenicol and nalidixic acid potentiation compared to WT AdeG (**Figure 4.13-B**). While AdeG Y725A showed a significant decrease in efflux efficiency, A705I and Q83A showed improved efflux efficiency compared to WT AdeG (**Figure 4.13-C**). Lastly, AdeG mutants Y725A, A705I, and Q83A all appeared about as susceptible to SLUPP_1377 inhibition at WT AdeG (**Figure 4.13-D**).

In conclusion, we found that most of the binding pocket residue substitutions had an impact on the AdeG transporter's efflux efficiency and substrate specificity (**Figure 4.13**). The AdeG mutant A705I appeared to have the most similar efflux activity as WT AdeG. The AdeG F-loop mutant G679I and AdeG G-loop mutant I621A both resulted in a non-functional transporter. Both DBP mutants S620A and L138A resulted in higher EPI susceptibility. Lastly, the PBP AdeG mutants Y725A and Q83A demonstrated various efflux efficiencies and inhibitor susceptibilities, with Q83A exhibiting significantly improved norfloxacin potentiation by SLUPP_1377.

Chapter 5: Site-Directed Mutagenesis of RND Transporter AdeJ from *Acinetobacter baumannii* Leads to Identification of Amino Acid Residues that Hinder Erythromycin Efflux

5.1. Abstract

The RND type transporter AdeJ, of the operon AdeIJK, is the most prevalent efflux pump in *A. baumannii*. AdeIJK is responsible for high levels of intrinsic resistance against small toxic molecule accumulation within the *A. baumannii* cell. Overproduction of this pump has also been observed in clinical isolates[170] and its high export efficiency and wide substrate range promotes *A. baumannii*'s survival under high concentration antibiotic pressure. To better understand the substrate specificity determinants in RND transporters, seven single amino acid substitution mutants of the AdeJ binding sites were constructed. I inserted plasmids carrying the mutant AdeJ transporters into RND deficient strains AbΔ3 and AbΔ3-Pore and I compared their characteristics to WT AdeJ and AdeG.

This study identified two amino acid residues in AdeJ whose substitution improved the transporter's export efficiency of erythromycin. We found in 2-fold dilution antibiotic susceptibility assays that the AdeJ mutants R701A and F136A improved the efflux of erythromycin by 4-fold. Both of these mutants could be improving erythromycin export by removing physical bulk and/or electrostatic repulsive forces to better accommodate the erythromycin molecule into and through the transporter binding pocket. We anticipate these findings will aid in future rational efflux pump inhibitor design and further functional characterization of this RND transporter.

5.2. Introduction

The AdeIJK efflux pump of *A. baumannii* is clinically significant due to its role in multidrug resistance.[51] Unlike AdeABC and AdeFGH, AdeIJK is found in all *A. baumannii* strains as part of its intrinsic resistance to various antibiotics.[171] This complicates how *A. baumannii* infections are treated due to AdeIJK's ability to pump out clinically relevant drugs like cephalosporins, fluoroquinolones, tetracyclines, tigecycline, lincosamindes, chloramphenicol, and co-trimoxazole.[51] Ongoing investigations into AdeIJK, including this one, aim to understand its mechanism of action and to find ways

to counteract its effects, which is crucial for developing effective treatments against MDR strains of *A. baumannii*.

Of the efflux pump classes, the RND superfamily have the broadest substrates ranges and their overexpression has been linked to MDR in *A. baumannii*.[154] In addition to the clinically relevant substrates listed above, AdeIJK has also been found to export acridine, pyronine, safranin, and sodium dodecyl sulfate (SDS). The AdeJ transporter protein is a homologue of *E. coli*'s AcrB (58% identity), and Coyne et al. found the following amino acids to be conserved based on sequence alignment and comparison between AdeJ and AdeB: Phe 386, Phe 388, Phe 458, Phe 459, Leu 25, Lys 29, Asp 99, and Asp 101. These conserved residues correspond mostly to the transmembrane domains (TMDs). This is in contrast to the loop regions which were seen to have greater variability.[51]

5.3. Results

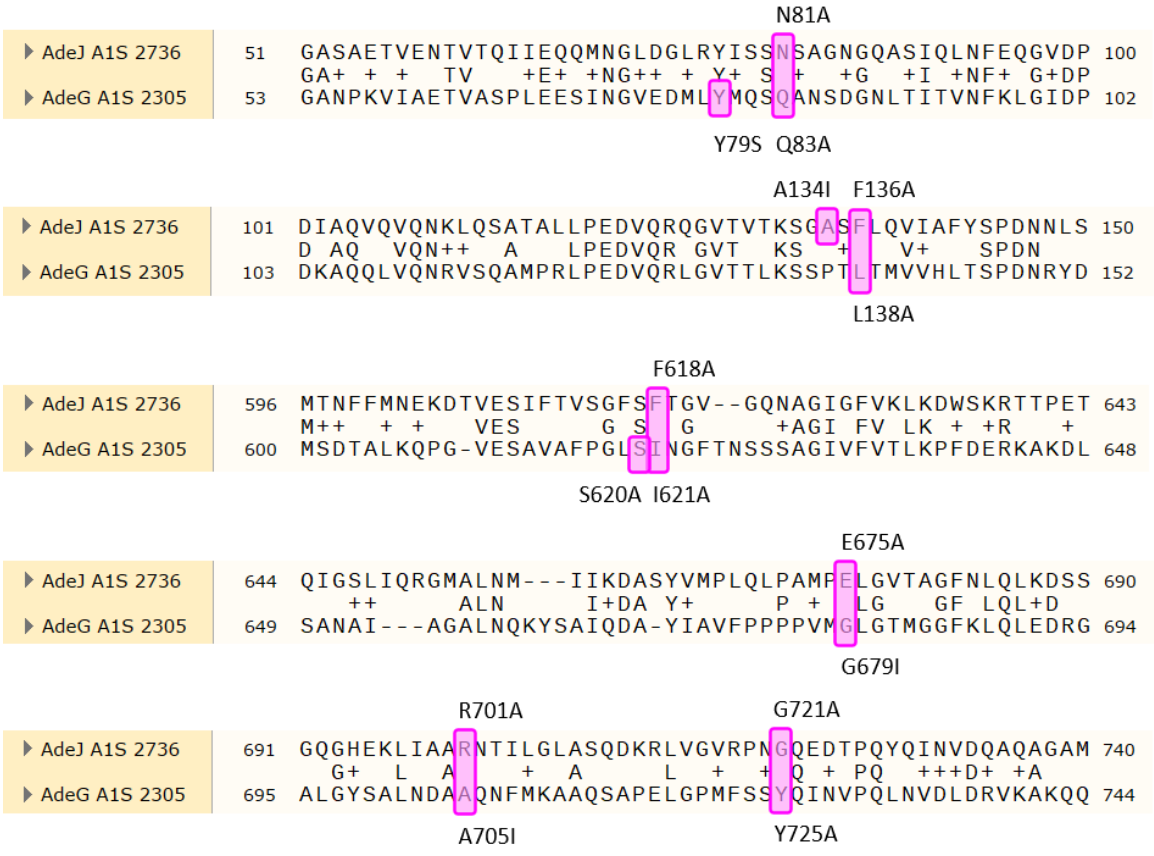

Figure 5.1 – Alignment of mutated AdeJ and AdeG residues

An alignment of AdeJ and AdeG residues with highlighted amino acid residues (pink) that were targeted in mutagenesis. Protein sequence alignment was done in SnapGene (San Diego, USA)

The following AdeJ single amino acid substitution mutants were selected based on molecular docking and molecular dynamics simulations with chloramphenicol and SLUPP_1377. The residues that were most likely to be involved in interacting with the docked chloramphenicol/SLUPP_1377 within the binding pocket were chosen for mutagenesis. All of the selected mutants were successfully constructed by Dr. Ayshegul Saral Sariyer using the L-arabinose inducible overproduction vector pTJ1 as the backbone. Then, I inserted the constructed plasmids in AbΔ3 and AbΔ3-Pore strains and continued with functional characterization of the AdeJ mutants.

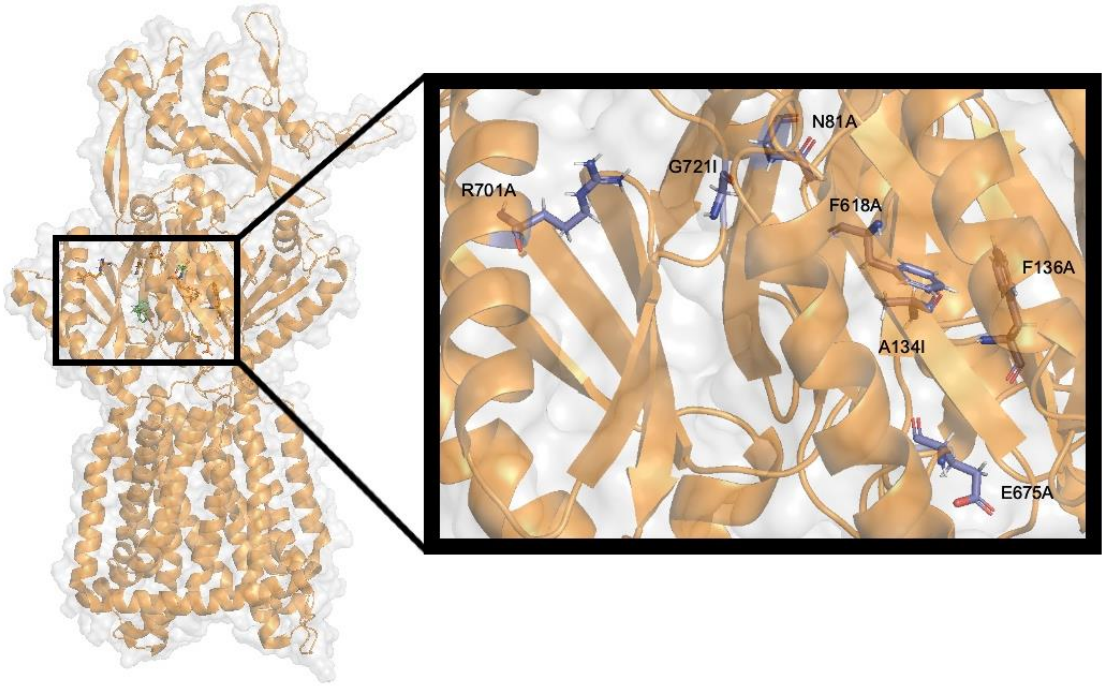

Figure 5.2 – AdeJ protomer crystal structure and select binding pocket residues

An AdeJ protomer (orange ribbon, PDB code: 7M4Q) with highlighted amino acid residues (blue) that were targeted in mutagenesis.

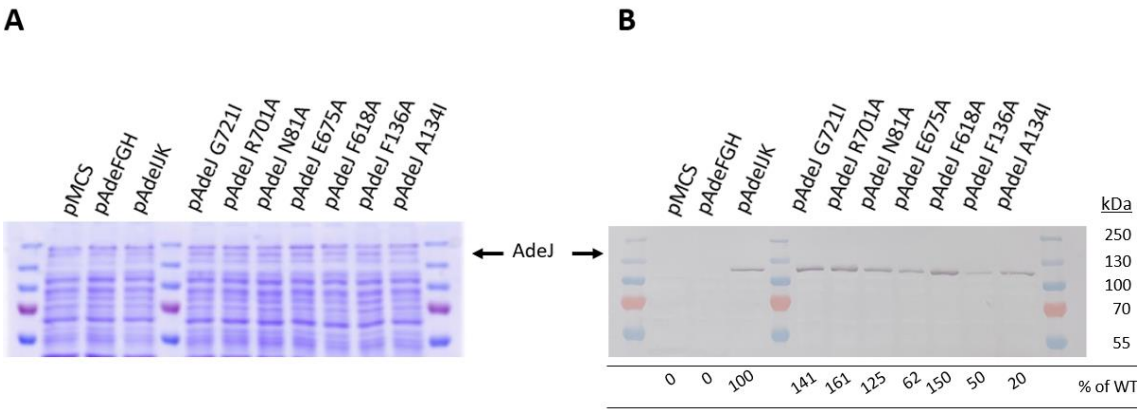

Figure 5.3 - AdeJ mutant expression in *A. baumannii* Δ3-Pore cells

Whole cell expression of the AdeJ mutants in *A. baumannii* Δ3-Pore cells washed in HMG buffer and resuspended to OD_{600} 1.0 +/- 0.05. AdeJ protein was expressed in cells with permeabilized outer membranes. Plasmid expression of the pAdeIJK operon was induced by 1% L-arabinose. Lysed cells were separated by SDS-PAGE on 12% gels and visualized by 1:5,000 anti-AdeJ antibody serum. The western blot membrane was scanned using a Canon CanoScan 9000F and the band intensities were measured using Quantity One (Bio Rad). The relative band intensities are shown as a percentage of the AbΔ3-Pore(pAdeIJK) band intensity (adjusted volume, INT*mm2).

We found that all AdeJ single substitution mutants expressed in AbΔ3-Pore cells. As was the case in the previous chapter, AdeJ expression was only from the plasmid since the chromosomal insertion site was already occupied by the modified *fhuA* in AbΔ3-Pore cells. While all AdeJ mutants had confirmed expression, they expressed at varying levels. AdeJ mutants G721I (141%), R701A (161%), N81A (125%), and F618A (150%) showed AdeJ expressions levels higher than the positive control AbΔ3-Pore (pAdeIJK) cells (100%). AdeJ mutants E675A (62%), F136A (50%), and A134I (20%) showed AdeJ expression levels lower than the control cells (100%), meaning any demonstrated increase in antibiotic susceptibility or reduced NPN uptake could be due to lower levels of transporter expression.

TABLE 5.1 - Antibiotic susceptibilities of *A. baumannii* AdeJ site-directed mutants to different classes of antibiotics

Strain	CHL (μM)	NOR (μM)	NOV (μM)	ERY (μM)	SDS (μM)
AbΔ3 (pTJ1-MCS)	6.25 – 12.5	0.195	≤ 0.098	0.78	16
AbΔ3 (pAdeIJK)	12.5	3.13 – 6.25	3.13 – 6.25	6.25	256
AbΔ3 (pAdeJ G721I)	12.5 – 25	3.13	6.25	12.5	256 – 1024
AbΔ3 (pAdeJ R701A)	12.5 – 25	3.13 – 6.25	6.25	**25**	128 – 256
AbΔ3 (pAdeJ N81A)	12.5 – 25	3.13 – 6.25	6.25	12.5	128 – 256
AbΔ3 (pAdeJ E675A)	12.5	3.13	6.25	12.5	128
Ab Δ3 (pAdeJ F618A)	12.5 – 25	6.25	3.13 – 6.25	12.5	256 – 1024
Ab Δ3 (pAdeJ F136A)	25 – 50	6.25 – 12.5	3.13	**25**	256
Ab Δ3 (pAdeJ A134I)	12.5 - 25	6.25	3.13 – 6.25	6.25 – 12.5	128 - 256

CHL – Chloramphenicol, NOR – Norfloxacin, NOV – Novobiocin, ERY – Erythromycin, SDS – Sodium dodecyl sulfate

The antibiotic susceptibility assay of the AdeJ mutants and control strains resulted in mostly unchanged MICs for chloramphenicol, norfloxacin, novobiocin and SDS (**Table 5.1**). There were two AdeJ mutants that saw an increase in erythromycin MIC values. Both AdeJ mutants R701A and F136A had a 4-fold decrease in erythromycin susceptibility (up to 25 μM from 6.25 μM). This suggests that the WT AdeJ residues R701 and F136 may have been hindering the export efficiency of erythromycin.

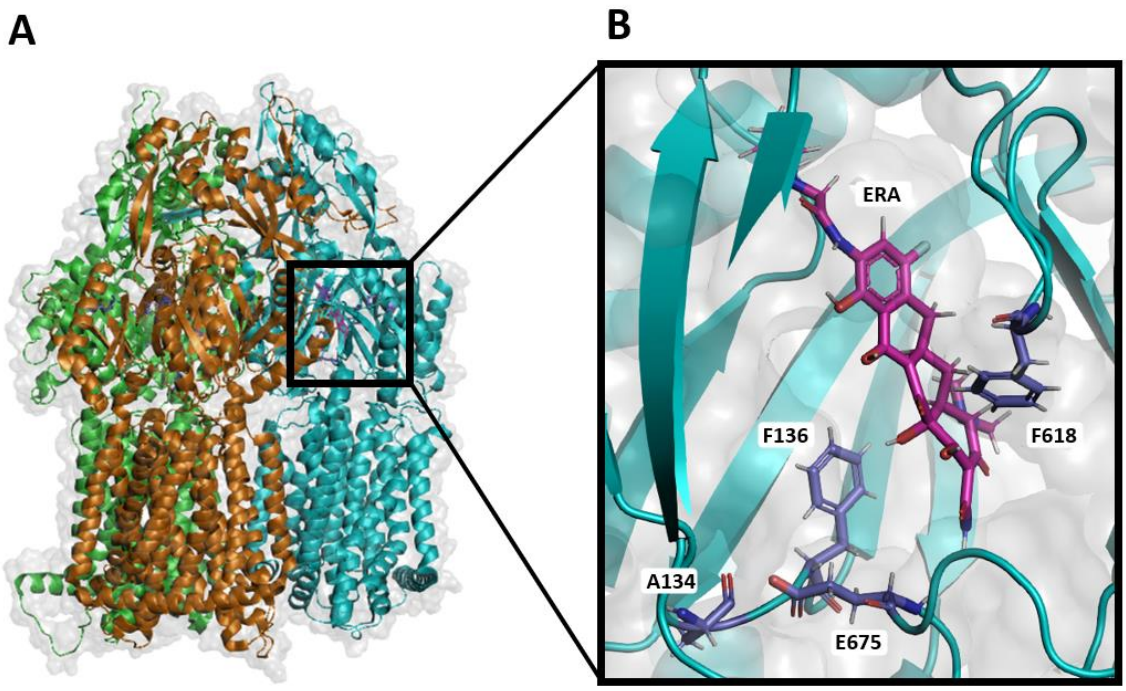

Figure 5.4 – Crystal structure of AdeJ-Era and binding site

Crystal structure of AdeJ-Era: **A** A cartoon view of the AdeJ trimer with Eravacycline bound (magenta stick) (PDB code: 7M4P). The protein surface is colored light grey, 80% transparency. The access, binding, and extrusion state protomers are colored orange, cyan, and green, respectively. **B** A zoomed in view of Era-binding site. Residues that were selected for mutagenesis are highlighted as blue sticks and labeled.

5.4. Discussion

Using a published PDB file for the structure of AdeJ bound to eravacycline, **Figure 5.4-A** shows the eravacycline molecule (magenta) bound to the AdeJ protomer that is in the binding state (cyan). The other two protomers are in access (orange) and extrusion (green) transport states and were not seen to contain an eravacycline molecule. The accompanying panel (**Figure 5.4-B**) shows a zoomed in view of the eravacycline binding site within the cyan colored AdeJ protomer. The eravacycline molecule is labeled as ERA. Of the residues that were seen to participate in eravacycline binding, two were among our selected AdeJ substitutions: F136 and F618. These two residues, along with V139, F178, G179, G180, F277, A326, Y327, F611, V613, F616, and F629, were found to anchor the eravacycline molecule to the binding pocket.

To better understand how certain Gram-negative bacteria use drug export as a significant part of their antibiotic resistance repertoire, we selected seven residues located within the AdeJ binding pocket to substitute as a method of determining substrate-residue specificity.

Erythromycin is a large macrolide antibiotic that is still used by clinicians today to treat chest infections, like pneumonia, skin infections, and sexually transmitted infections[172] and it is a substrate of the AdeJ pump. Recently in 2023, Zhang et al. published a solved Cryo-EM crystal structure of the *Klebsiella pneumoniae* AcrB efflux pump, another RND transporter similar to AdeJ, bound with erythromycin.[173] They found that the erythromycin molecule bound to a region deep within the distal binding pocket. There were many residues found to be involved in binding with erythromycin, including four phenylalanine residues. Perhaps it was the removal of one of the AdeJ binding pocket phenylalanine residues that resulted in a change in the transporter's ability to export erythromycin. It is possible that the AdeJ substitution F136A still allowed for enough erythromycin-binding pocket interactions to transport the ERY molecule but also allowed for improved ERY export by reducing volume taken up by residue sidechains in the binding pocket enough to better accommodate the ERY molecule into and through the transporter. This result contrasts with the homologous AdeG substitution mutant L138A (**Figure 5.1**), which showed less efficient substrate efflux.

As for the decreased erythromycin susceptibility in the AdeJ R701A mutant, this could be due to better accommodation of the ERY molecule into the distal binding pocket. The substitution of the arginine for an alanine at residue #701 could reduce the electrostatic repulsive forces against ERY enough to significantly improve export. This is in contrast to the homologous AdeG substitution mutant A705I (**Figure 5.1**) which did not show any changes in antibiotic substrate susceptibility.

Another recent publication of an antibiotic bound transporter structure, published by the same authors as the *Klebsiella* AcrB-ERY structure, shows the tetracycline derivative eravacycline bound to AdeJ of *A. baumannii*. [174] Two of the AdeJ residues we selected for mutagenesis (F136 and F618), along with V139, F178, G179, G180, F277, A326, Y327, F611, V613, F616, and F629, were found to anchor the eravacycline

molecule to the binding pocket. It is apparent that the many hydrophobic amino acid residues found in the AdeJ binding pocket play an important role in the transporter's ability to export such a wide variety of substrates. Some of the residues we selected for mutagenesis, including F618, E675, and G721, have been found to be conserved among *A. baumannii*'s AdeJ and AdeB pumps[175,176], so it is a bit surprising that substitutions of AdeJ F618A saw a decrease in erythromycin susceptibility. But previous publications have uncovered examples of mutations leading to increased expression of efflux genes resulting in an increase in resistance to antibiotics, such as quinolone resistance in *norA* mutants of *S. aureus*[177], so this result was not out of the question of possible outcomes for the mutagenesis.

Chapter 6: Overall Discussion and Conclusions

The studies discussed in this work have demonstrated efflux pump mediated survival strategies of *Acinetobacter baumannii* in regard to antibiotic and human-infection related stress conditions. *A. baumannii* uses both RND and MFS family of efflux pumps to export small toxic molecules before they can accumulate within the cell to cytotoxic levels. In the case of the two newly characterized MFS pumps, AmfAB and AmfCD were not found to significantly contribute to *A. baumannii*'s antibiotic susceptibility profile. This result was unexpected since these transporters were initially identified as being upregulated in efflux deficient strains.[64] We had thought that perhaps AmfAB and AmfCD were being upregulated to compensate for at least some of the lost substrate range of AdeB or AdeIJK. This may still be the case, but for substrates besides the antibiotic classes we tested here. One possible experimental avenue we could have explored is the effects of Amf pump deletion and overproduction under starvation. This could have been done using the same growth curve method used here, but a deficient media. Perhaps the Amf pumps become even more crucial to *A. baumannii*'s survival under starvation conditions.

Another potential future research avenue for the AmfAB and AmfCD pumps is to investigate the metabolome of the different stress responses studied here. This could illuminate what specific role these MFS pumps are playing in *A. baumannii* and what specific substrates the pumps are responsible for transporting. It would also be beneficial

to determine if any of the known outer membrane channels encoded in the *A. baumannii* genome could be the missing piece of the AmfAB/CD complexes. It is possible that we missed substrate specific efflux activity by these two pumps because we did not overexpress their corresponding outer membrane protein along with the transporters and membrane fusion proteins.

We also demonstrated specific substrate specificities of selected AdeG and AdeJ binding pocket residues. This research is important both because it provides more information on how these RND transporters are able to export such a wide range of differently shaped and sized substrates, but it also assists in the future development of efflux pump inhibitors. So far no efflux pump inhibitor (EPI) has made it into clinical trials, but we hope our findings can help guide their refinement. The compound SLUPP_1377 was found to inhibit the efflux activity of both AdeJ and AdeG, but it was selected for inhibition studies in AdeG because there are already a number of compounds that have been identified as possible inhibitors of AdeJ but there are none for AdeG. Our studies demonstrated that SLUPP_1377 does have significant inhibitory activity in AdeG and potentiates the activity of chloramphenicol in AbΔ3(pAdeFGH).

References

(1) Peleg, A. Y.; Seifert, H.; Paterson, D. L. Acinetobacter Baumannii: Emergence of a Successful Pathogen. *Clin. Microbiol. Rev.* **2008**, *21* (3), 538–582. https://doi.org/10.1128/CMR.00058-07.

(2) Glew, R. H.; Moellering, R. C.; Kunz, L. J. Infections with Acinetobacter Calcoaceticus (Herellea Vaginicola): Clinical and Laboratory Studies. *Medicine (Baltimore)* **1977**, *56* (2), 79–97. https://doi.org/10.1097/00005792-197703000-00001.

(3) Zin, E. B.-B. R.; Towner, K. J. Acinetobacter Spp. as Nosocomial Pathogens: Microbiological, Clinical, and Epidemiological Features. *CLIN MICROBIOL REV* **1996**, *9*.

(4) Nocera, F. P.; Attili, A.-R.; De Martino, L. Acinetobacter Baumannii: Its Clinical Significance in Human and Veterinary Medicine. *Pathogens* **2021**, *10* (2), 127. https://doi.org/10.3390/pathogens10020127.

(5) Vester, B.; Long, K. S. Antibiotic Resistance in Bacteria Caused by Modified Nucleosides in 23S Ribosomal RNA. In *Madame Curie Bioscience Database [Internet]*; Landes Bioscience, 2013.

(6) Hillyer, T.; Benin, B. M.; Sun, C.; Aguirre, N.; Willard, B.; Sham, Y. Y.; Shin, W. S. A Novel Strategy to Characterize the Pattern of β-Lactam Antibiotic-Induced Drug Resistance in Acinetobacter Baumannii. *Sci. Rep.* **2023**, *13* (1), 9177. https://doi.org/10.1038/s41598-023-36475-9.

(7) Bush, K.; Bradford, P. A. β-Lactams and β-Lactamase Inhibitors: An Overview. *Cold Spring Harb. Perspect. Med.* **2016**, *6* (8), a025247. https://doi.org/10.1101/cshperspect.a025247.
(8) Novović, K.; Jovčić, B. Colistin Resistance in Acinetobacter Baumannii: Molecular Mechanisms and Epidemiology. *Antibiotics* **2023**, *12* (3), 516. https://doi.org/10.3390/antibiotics12030516.
(9) Evans, M. E.; Feola, D. J.; Rapp, R. P. Polymyxin B Sulfate and Colistin: Old Antibiotics for Emerging Multiresistant Gram-Negative Bacteria. *Ann. Pharmacother.* **1999**, *33* (9), 960–967. https://doi.org/10.1345/aph.18426.
(10) Sauvage, E.; Kerff, F.; Terrak, M.; Ayala, J. A.; Charlier, P. The Penicillin-Binding Proteins: Structure and Role in Peptidoglycan Biosynthesis. *FEMS Microbiol. Rev.* **2008**, *32* (2), 234–258. https://doi.org/10.1111/j.1574-6976.2008.00105.x.
(11) Cayô, R.; Rodríguez, M.-C.; Espinal, P.; Fernández-Cuenca, F.; Ocampo-Sosa, A. A.; Pascual, Á.; Ayala, J. A.; Vila, J.; Martínez-Martínez, L. Analysis of Genes Encoding Penicillin-Binding Proteins in Clinical Isolates of Acinetobacter Baumannii ▿. *Antimicrob. Agents Chemother.* **2011**, *55* (12), 5907–5913. https://doi.org/10.1128/AAC.00459-11.
(12) Mcstrother. Methicillin-Resistant *Staphylococcus Aureus*. *Wikipedia*; 2024.
(13) Fernández, L.; Hancock, R. E. W. Adaptive and Mutational Resistance: Role of Porins and Efflux Pumps in Drug Resistance. *Clin. Microbiol. Rev.* **2012**, *25* (4), 661. https://doi.org/10.1128/CMR.00043-12.
(14) Sarshar, M.; Behzadi, P.; Scribano, D.; Palamara, A. T.; Ambrosi, C. Acinetobacter Baumannii: An Ancient Commensal with Weapons of a Pathogen. *Pathogens* **2021**, *10* (4), 387. https://doi.org/10.3390/pathogens10040387.
(15) Abdi, S. N.; Ghotaslou, R.; Ganbarov, K.; Mobed, A.; Tanomand, A.; Yousefi, M.; Asgharzadeh, M.; Kafil, H. S. Acinetobacter Baumannii Efflux Pumps and Antibiotic Resistance. *Infect. Drug Resist.* **2020**, *13*, 423–434. https://doi.org/10.2147/IDR.S228089.
(16) Hirsch, E. B.; Tam, V. H. Impact of Multidrug-Resistant Pseudomonas Aeruginosa Infection on Patient Outcomes. *Expert Rev. Pharmacoecon. Outcomes Res.* **2010**, *10* (4), 441–451. https://doi.org/10.1586/erp.10.49.
(17) Bickenbach, J.; Schöneis, D.; Marx, G.; Marx, N.; Lemmen, S.; Dreher, M. Impact of Multidrug-Resistant Bacteria on Outcome in Patients with Prolonged Weaning. *BMC Pulm. Med.* **2018**, *18* (1), 141. https://doi.org/10.1186/s12890-018-0708-3.
(18) Nelson, R. E.; Hatfield, K. M.; Wolford, H.; Samore, M. H.; Scott, R. D.; Reddy, S. C.; Olubajo, B.; Paul, P.; Jernigan, J. A.; Baggs, J. National Estimates of Healthcare Costs Associated With Multidrug-Resistant Bacterial Infections Among Hospitalized Patients in the United States. *Clin. Infect. Dis. Off. Publ. Infect. Dis. Soc. Am.* **2021**, *72* (Suppl 1), S17–S26. https://doi.org/10.1093/cid/ciaa1581.
(19) CDC. *COVID-19 & Antibiotic Resistance*. Centers for Disease Control and Prevention. https://www.cdc.gov/drugresistance/covid19.html (accessed 2023-12-06).
(20) Krishnamoorthy, G.; Leus, I. V.; Weeks, J. W.; Wolloscheck, D.; Rybenkov, V. V.; Zgurskaya, H. I. Synergy between Active Efflux and Outer Membrane Diffusion Defines Rules of Antibiotic Permeation into Gram-Negative Bacteria. *mBio* **2017**, *8* (5). https://doi.org/10.1128/mBio.01172-17.
(21) Centers for Disease Control and Prevention (U.S.). *Antibiotic Resistance Threats in the United States, 2019*; Centers for Disease Control and Prevention (U.S.), 2019. https://doi.org/10.15620/cdc:82532.
(22) Pearson, J. P.; Van Delden, C.; Iglewski, B. H. Active Efflux and Diffusion Are Involved in Transport of Pseudomonas Aeruginosa Cell-to-Cell Signals. *J. Bacteriol.* **1999**, *181* (4), 1203–1210. https://doi.org/10.1128/JB.181.4.1203-1210.1999.
(23) Vila, J.; Martí, S.; Sánchez-Céspedes, J. Porins, Efflux Pumps and Multidrug Resistance in Acinetobacter Baumannii. *J. Antimicrob. Chemother.* **2007**, *59* (6), 1210–1215. https://doi.org/10.1093/jac/dkl509.

(24) Huang, L.; Wu, C.; Gao, H.; Xu, C.; Dai, M.; Huang, L.; Hao, H.; Wang, X.; Cheng, G. Bacterial Multidrug Efflux Pumps at the Frontline of Antimicrobial Resistance: An Overview. *Antibiotics* **2022**, *11* (4), 520. https://doi.org/10.3390/antibiotics11040520.
(25) Nishino, K.; Yamasaki, S.; Nakashima, R.; Zwama, M.; Hayashi-Nishino, M. Function and Inhibitory Mechanisms of Multidrug Efflux Pumps. *Front. Microbiol.* **2021**, *12*, 3390. https://doi.org/10.3389/fmicb.2021.737288.
(26) Wang, Z.; Fan, G.; Hryc, C. F.; Blaza, J. N.; Serysheva, I. I.; Schmid, M. F.; Chiu, W.; Luisi, B. F.; Du, D. An Allosteric Transport Mechanism for the AcrAB-TolC Multidrug Efflux Pump. *eLife* **2017**, *6*, e24905. https://doi.org/10.7554/eLife.24905.
(27) Nikaido, H.; Takatsuka, Y. Mechanisms of RND Multidrug Efflux Pumps. *Biochim. Biophys. Acta* **2009**, *1794* (5), 769–781. https://doi.org/10.1016/j.bbapap.2008.10.004.
(28) Nikaido, H.; Zgurskaya, H. I. AcrAB and Related Multidrug Efflux Pumps of Escherichia Coli. *J. Mol. Microbiol. Biotechnol.* **2001**, *3* (2), 215–218.
(29) Du, D.; van Veen, H. W.; Murakami, S.; Pos, K. M.; Luisi, B. F. Structure, Mechanism and Cooperation of Bacterial Multidrug Transporters. *Curr. Opin. Struct. Biol.* **2015**, *33*, 76–91. https://doi.org/10.1016/j.sbi.2015.07.015.
(30) Russell Lewis, B.; Uddin, M. R.; Moniruzzaman, M.; Kuo, K. M.; Higgins, A. J.; Shah, L. M. N.; Sobott, F.; Parks, J. M.; Hammerschmid, D.; Gumbart, J. C.; Zgurskaya, H. I.; Reading, E. Conformational Restriction Shapes the Inhibition of a Multidrug Efflux Adaptor Protein. *Nat. Commun.* **2023**, *14* (1), 3900. https://doi.org/10.1038/s41467-023-39615-x.
(31) Daury, L.; Orange, F.; Taveau, J.-C.; Verchère, A.; Monlezun, L.; Gounou, C.; Marreddy, R. K. R.; Picard, M.; Broutin, I.; Pos, K. M.; Lambert, O. Tripartite Assembly of RND Multidrug Efflux Pumps. *Nat. Commun.* **2016**, *7* (1), 10731. https://doi.org/10.1038/ncomms10731.
(32) Eda, S.; Maseda, H.; Yoshihara, E.; Nakae, T. Assignment of the Outer-Membrane-Subunit-Selective Domain of the Membrane Fusion Protein in the Tripartite Xenobiotic Efflux Pump of Pseudomonas Aeruginosa. *FEMS Microbiol. Lett.* **2006**, *254* (1), 101–107. https://doi.org/10.1111/j.1574-6968.2005.00010.x.
(33) Stegmeier, J. F.; Polleichtner, G.; Brandes, N.; Hotz, C.; Andersen, C. Importance of the Adaptor (Membrane Fusion) Protein Hairpin Domain for the Functionality of Multidrug Efflux Pumps. *Biochemistry* **2006**, *45* (34), 10303–10312. https://doi.org/10.1021/bi060320g.
(34) Lobedanz, S.; Bokma, E.; Symmons, M. F.; Koronakis, E.; Hughes, C.; Koronakis, V. A Periplasmic Coiled-Coil Interface Underlying TolC Recruitment and the Assembly of Bacterial Drug Efflux Pumps. *Proc. Natl. Acad. Sci. U. S. A.* **2007**, *104* (11), 4612–4617. https://doi.org/10.1073/pnas.0610160104.
(35) Ge, Q.; Yamada, Y.; Zgurskaya, H. The C-Terminal Domain of AcrA Is Essential for the Assembly and Function of the Multidrug Efflux Pump AcrAB-TolC. *J. Bacteriol.* **2009**, *191* (13), 4365–4371. https://doi.org/10.1128/JB.00204-09.
(36) Alav, I.; Kobylka, J.; Kuth, M. S.; Pos, K. M.; Picard, M.; Blair, J. M. A.; Bavro, V. N. Structure, Assembly, and Function of Tripartite Efflux and Type 1 Secretion Systems in Gram-Negative Bacteria. *Chem. Rev.* **2021**, *121* (9), 5479–5596. https://doi.org/10.1021/acs.chemrev.1c00055.
(37) Murakami, S.; Nakashima, R.; Yamashita, E.; Matsumoto, T.; Yamaguchi, A. Crystal Structures of a Multidrug Transporter Reveal a Functionally Rotating Mechanism. *Nature* **2006**, *443* (7108), 173–179. https://doi.org/10.1038/nature05076.
(38) Pos, K. M. Drug Transport Mechanism of the AcrB Efflux Pump. *Biochim. Biophys. Acta* **2009**, *1794* (5), 782–793. https://doi.org/10.1016/j.bbapap.2008.12.015.
(39) Cha, H.; Müller, R. T.; Pos, K. M. Switch-Loop Flexibility Affects Transport of Large Drugs by the Promiscuous AcrB Multidrug Efflux Transporter. *Antimicrob. Agents Chemother.* **2014**, *58* (8), 4767–4772. https://doi.org/10.1128/AAC.02733-13.

(40) Klenotic, P. A.; Moseng, M. A.; Morgan, C. E.; Yu, E. W. Structural and Functional Diversity of RND Transporters. *Chem. Rev.* **2021**, *121* (9), 5378–5416. https://doi.org/10.1021/acs.chemrev.0c00621.
(41) Schulz, R.; Kleinekathöfer, U. Transitions between Closed and Open Conformations of TolC: The Effects of Ions in Simulations. *Biophys. J.* **2009**, *96* (8), 3116–3125. https://doi.org/10.1016/j.bpj.2009.01.021.
(42) Andersen, C.; Koronakis, E.; Hughes, C.; Koronakis, V. An Aspartate Ring at the TolC Tunnel Entrance Determines Ion Selectivity and Presents a Target for Blocking by Large Cations. *Mol. Microbiol.* **2002**, *44* (5), 1131–1139. https://doi.org/10.1046/j.1365-2958.2002.02898.x.
(43) Krishnamoorthy, G.; Tikhonova, E. B.; Dhamdhere, G.; Zgurskaya, H. I. On the Role of TolC in Multidrug Efflux: The Function and Assembly of AcrAB-TolC Tolerate Significant Depletion of Intracellular TolC Protein. *Mol. Microbiol.* **2013**, *87* (5), 982–997. https://doi.org/10.1111/mmi.12143.
(44) Seeger, M. A.; Schiefner, A.; Eicher, T.; Verrey, F.; Diederichs, K.; Pos, K. M. Structural Asymmetry of AcrB Trimer Suggests a Peristaltic Pump Mechanism. *Science* **2006**, *313* (5791), 1295–1298. https://doi.org/10.1126/science.1131542.
(45) Du, D.; Wang-Kan, X.; Neuberger, A.; Van Veen, H. W.; Pos, K. M.; Piddock, L. J. V.; Luisi, B. F. Multidrug Efflux Pumps: Structure, Function and Regulation. *Nat. Rev. Microbiol.* **2018**, *16* (9), 523–539. https://doi.org/10.1038/s41579-018-0048-6.
(46) Yao, X.-Q.; Kimura, N.; Murakami, S.; Takada, S. Drug Uptake Pathways of Multidrug Transporter AcrB Studied by Molecular Simulations and Site-Directed Mutagenesis Experiments. *J. Am. Chem. Soc.* **2013**, *135* (20), 7474–7485. https://doi.org/10.1021/ja310548h.
(47) Kobylka, J.; Kuth, M. S.; Müller, R. T.; Geertsma, E. R.; Pos, K. M. AcrB: A Mean, Keen, Drug Efflux Machine. *Ann. N. Y. Acad. Sci.* **2020**, *1459* (1), 38–68. https://doi.org/10.1111/nyas.14239.
(48) Chen, M.; Shi, X.; Yu, Z.; Fan, G.; Serysheva, I. I.; Baker, M. L.; Luisi, B. F.; Ludtke, S. J.; Wang, Z. In Situ Structure of the AcrAB-TolC Efflux Pump at Subnanometer Resolution. *Struct. Lond. Engl. 1993* **2022**, *30* (1), 107-113.e3. https://doi.org/10.1016/j.str.2021.08.008.
(49) Yousefian, N.; Ornik-Cha, A.; Poussard, S.; Decossas, M.; Berbon, M.; Daury, L.; Taveau, J.-C.; Dupuy, J.-W.; Đorđević-Marquardt, S.; Lambert, O.; Pos, K. M. Structural Characterization of the EmrAB-TolC Efflux Complex from E. Coli. *Biochim. Biophys. Acta BBA - Biomembr.* **2021**, *1863* (1), 183488. https://doi.org/10.1016/j.bbamem.2020.183488.
(50) Sulavik, M. C.; Houseweart, C.; Cramer, C.; Jiwani, N.; Murgolo, N.; Greene, J.; DiDomenico, B.; Shaw, K. J.; Miller, G. H.; Hare, R.; Shimer, G. Antibiotic Susceptibility Profiles of Escherichia Coli Strains Lacking Multidrug Efflux Pump Genes. *Antimicrob. Agents Chemother.* **2001**, *45* (4), 1126–1136. https://doi.org/10.1128/AAC.45.4.1126-1136.2001.
(51) Damier-Piolle, L.; Magnet, S.; Brémont, S.; Lambert, T.; Courvalin, P. AdeIJK, a Resistance-Nodulation-Cell Division Pump Effluxing Multiple Antibiotics in *Acinetobacter Baumannii*. *Antimicrob. Agents Chemother.* **2008**, *52* (2), 557–562. https://doi.org/10.1128/AAC.00732-07.
(52) Leus, I. V.; Weeks, J. W.; Bonifay, V.; Smith, L.; Richardson, S.; Zgurskaya, H. I. Substrate Specificities and Efflux Efficiencies of RND Efflux Pumps of Acinetobacter Baumannii. *J. Bacteriol.* **2018**, *200* (13). https://doi.org/10.1128/JB.00049-18.
(53) Yoon, E.-J.; Chabane, Y. N.; Goussard, S.; Snesrud, E.; Courvalin, P.; Dé, E.; Grillot-Courvalin, C. Contribution of Resistance-Nodulation-Cell Division Efflux Systems to Antibiotic Resistance and Biofilm Formation in Acinetobacter Baumannii. *mBio* **2015**, *6* (2), e00309-15. https://doi.org/10.1128/mBio.00309-15.

(54) Coyne, S.; Rosenfeld, N.; Lambert, T.; Courvalin, P.; Périchon, B. Overexpression of Resistance-Nodulation-Cell Division Pump AdeFGH Confers Multidrug Resistance in Acinetobacter Baumannii. *Antimicrob. Agents Chemother.* **2010**, *54* (10), 4389–4393. https://doi.org/10.1128/AAC.00155-10.
(55) Pao, S. S.; Paulsen, I. T.; Saier, M. H. Major Facilitator Superfamily. *Microbiol. Mol. Biol. Rev. MMBR* **1998**, *62* (1), 1–34.
(56) Drew, D.; North, R. A.; Nagarathinam, K.; Tanabe, M. Structures and General Transport Mechanisms by the Major Facilitator Superfamily (MFS). *Chem. Rev.* **2021**, *121* (9), 5289–5335. https://doi.org/10.1021/acs.chemrev.0c00983.
(57) Lekshmi, M.; Ammini, P.; Adjei, J.; Sanford, L. M.; Shrestha, U.; Kumar, S.; Varela, M. F. Modulation of Antimicrobial Efflux Pumps of the Major Facilitator Superfamily in Staphylococcus Aureus. *AIMS Microbiol.* **2018**, *4* (1), 1. https://doi.org/10.3934/microbiol.2018.1.1.
(58) Wan, Y.; Wang, M.; Chan, E. W. C.; Chen, S. Membrane Transporters of the Major Facilitator Superfamily Are Essential for Long-Term Maintenance of Phenotypic Tolerance to Multiple Antibiotics in E. Coli. *Microbiol. Spectr.* **2021**, *9* (3), e0184621. https://doi.org/10.1128/Spectrum.01846-21.
(59) Kumar, S.; Lekshmi, M.; Parvathi, A.; Ojha, M.; Wenzel, N.; Varela, M. F. Functional and Structural Roles of the Major Facilitator Superfamily Bacterial Multidrug Efflux Pumps. *Microorganisms* **2020**, *8* (2), 266. https://doi.org/10.3390/microorganisms8020266.
(60) Lomovskaya, O.; Lewis, K. Emr, an Escherichia Coli Locus for Multidrug Resistance. *Proc. Natl. Acad. Sci. U. S. A.* **1992**, *89* (19), 8938–8942. https://doi.org/10.1073/pnas.89.19.8938.
(61) Lewis, K. Multidrug Resistance Pumps in Bacteria: Variations on a Theme. *Trends Biochem. Sci.* **1994**, *19* (3), 119–123. https://doi.org/10.1016/0968-0004(94)90204-6.
(62) Nishino, K.; Yamaguchi, A. Analysis of a Complete Library of Putative Drug Transporter Genes in Escherichia Coli. *J. Bacteriol.* **2001**, *183* (20), 5803–5812. https://doi.org/10.1128/JB.183.20.5803-5812.2001.
(63) Nishino, K.; Yamaguchi, A. Role of Histone-like Protein H-NS in Multidrug Resistance of Escherichia Coli. *J. Bacteriol.* **2004**, *186* (5), 1423–1429. https://doi.org/10.1128/JB.186.5.1423-1429.2004.
(64) Leus, I. V.; Adamiak, J.; Trinh, A. N.; Smith, R. D.; Smith, L.; Richardson, S.; Ernst, R. K.; Zgurskaya, H. I. Inactivation of AdeABC and AdeIJK Efflux Pumps Elicits Specific Nonoverlapping Transcriptional and Phenotypic Responses in Acinetobacter Baumannii. *Mol. Microbiol.* **2020**, *114* (6), 1049–1065. https://doi.org/10.1111/mmi.14594.
(65) Fang, F. C.; Frawley, E. R.; Tapscott, T.; Vazquez-Torres, A. Bacterial Stress Responses during Host Infection. *Cell Host Microbe* **2016**, *20* (2), 133–143. https://doi.org/10.1016/j.chom.2016.07.009.
(66) Dawan, J.; Ahn, J. Bacterial Stress Responses as Potential Targets in Overcoming Antibiotic Resistance. *Microorganisms* **2022**, *10* (7), 1385. https://doi.org/10.3390/microorganisms10071385.
(67) Avican, K.; Aldahdooh, J.; Togninalli, M.; Mahmud, A. K. M. F.; Tang, J.; Borgwardt, K. M.; Rhen, M.; Fällman, M. RNA Atlas of Human Bacterial Pathogens Uncovers Stress Dynamics Linked to Infection. *Nat. Commun.* **2021**, *12* (1), 3282. https://doi.org/10.1038/s41467-021-23588-w.
(68) Gaurav, A.; Bakht, P.; Saini, M.; Pandey, S.; Pathania, R. Role of Bacterial Efflux Pumps in Antibiotic Resistance, Virulence, and Strategies to Discover Novel Efflux Pump Inhibitors. *Microbiology* **2023**, *169* (5), 001333. https://doi.org/10.1099/mic.0.001333.
(69) Vabulas, R. M.; Raychaudhuri, S.; Hayer-Hartl, M.; Hartl, F. U. Protein Folding in the Cytoplasm and the Heat Shock Response. *Cold Spring Harb. Perspect. Biol.* **2010**, *2* (12), a004390. https://doi.org/10.1101/cshperspect.a004390.

(70) Tedesco, B.; Ferrari, V.; Cozzi, M.; Chierichetti, M.; Casarotto, E.; Pramaggiore, P.; Mina, F.; Galbiati, M.; Rusmini, P.; Crippa, V.; Cristofani, R.; Poletti, A. The Role of Small Heat Shock Proteins in Protein Misfolding Associated Motoneuron Diseases. *Int. J. Mol. Sci.* **2022**, *23* (19), 11759. https://doi.org/10.3390/ijms231911759.
(71) Bromberg, Z.; Weiss, Y. The Role of the Membrane-Initiated Heat Shock Response in Cancer. *Front. Mol. Biosci.* **2016**, *3*, 12. https://doi.org/10.3389/fmolb.2016.00012.
(72) Zügel, U.; Kaufmann, S. H. E. Role of Heat Shock Proteins in Protection from and Pathogenesis of Infectious Diseases. *Clin. Microbiol. Rev.* **1999**, *12* (1), 19–39.
(73) Sottile, M. L.; Nadin, S. B. Heat Shock Proteins and DNA Repair Mechanisms: An Updated Overview. *Cell Stress Chaperones* **2018**, *23* (3), 303–315. https://doi.org/10.1007/s12192-017-0843-4.
(74) Wang, M.; Lu, J.; Qin, P.; Wang, S.; Ding, W.; Fu, H.-H.; Zhang, Y.-Z.; Zhang, W. Biofilm Formation Stabilizes Metabolism in a Roseobacteraceae Bacterium under Temperature Increase. *Appl. Environ. Microbiol.* **2023**, *89* (10), e00601-23. https://doi.org/10.1128/aem.00601-23.
(75) Sobanski, T.; Rose, M.; Suraweera, A.; O'Byrne, K.; Richard, D. J.; Bolderson, E. Cell Metabolism and DNA Repair Pathways: Implications for Cancer Therapy. *Front. Cell Dev. Biol.* **2021**, *9*, 633305. https://doi.org/10.3389/fcell.2021.633305.
(76) Guan, N.; Liu, L. Microbial Response to Acid Stress: Mechanisms and Applications. *Appl. Microbiol. Biotechnol.* **2020**, *104* (1), 51–65. https://doi.org/10.1007/s00253-019-10226-1.
(77) Kar, N. S.; Dasgupta, A. K. The Possible Role of Surface Charge in Membrane Organization in an Acidophile. *Indian J. Biochem. Biophys.* **1996**, *33* (5), 398–402.
(78) Richard, H.; Foster, J. W. Escherichia Coli Glutamate- and Arginine-Dependent Acid Resistance Systems Increase Internal pH and Reverse Transmembrane Potential. *J. Bacteriol.* **2004**, *186* (18), 6032–6041. https://doi.org/10.1128/JB.186.18.6032-6041.2004.
(79) Aquino, P.; Honda, B.; Jaini, S.; Lyubetskaya, A.; Hosur, K.; Chiu, J. G.; Ekladious, I.; Hu, D.; Jin, L.; Sayeg, M. K.; Stettner, A. I.; Wang, J.; Wong, B. G.; Wong, W. S.; Alexander, S. L.; Ba, C.; Bensussen, S. I.; Bernstein, D. B.; Braff, D.; Cha, S.; Cheng, D. I.; Cho, J. H.; Chou, K.; Chuang, J.; Gastler, D. E.; Grasso, D. J.; Greifenberger, J. S.; Guo, C.; Hawes, A. K.; Israni, D. V.; Jain, S. R.; Kim, J.; Lei, J.; Li, H.; Li, D.; Li, Q.; Mancuso, C. P.; Mao, N.; Masud, S. F.; Meisel, C. L.; Mi, J.; Nykyforchyn, C. S.; Park, M.; Peterson, H. M.; Ramirez, A. K.; Reynolds, D. S.; Rim, N. G.; Saffie, J. C.; Su, H.; Su, W. R.; Su, Y.; Sun, M.; Thommes, M. M.; Tu, T.; Varongchayakul, N.; Wagner, T. E.; Weinberg, B. H.; Yang, R.; Yaroslavsky, A.; Yoon, C.; Zhao, Y.; Zollinger, A. J.; Stringer, A. M.; Foster, J. W.; Wade, J.; Raman, S.; Broude, N.; Wong, W. W.; Galagan, J. E. Coordinated Regulation of Acid Resistance in Escherichia Coli. *BMC Syst. Biol.* **2017**, *11* (1), 1. https://doi.org/10.1186/s12918-016-0376-y.
(80) Foster, J. W. Escherichia Coli Acid Resistance: Tales of an Amateur Acidophile. *Nat. Rev. Microbiol.* **2004**, *2* (11), 898–907. https://doi.org/10.1038/nrmicro1021.
(81) Wiebe, M. A.; Brannon, J. R.; Steiner, B. D.; Bamidele, A.; Schrimpe-Rutledge, A. C.; Codreanu, S. G.; Sherrod, S. D.; McLean, J. A.; Hadjifrangiskou, M. Serine Deamination Is a New Acid Tolerance Mechanism Observed in Uropathogenic Escherichia Coli. *mBio 13* (6), e02963-22. https://doi.org/10.1128/mbio.02963-22.
(82) Caza, M.; Kronstad, J. W. Shared and Distinct Mechanisms of Iron Acquisition by Bacterial and Fungal Pathogens of Humans. *Front. Cell. Infect. Microbiol.* **2013**, *3*, 80. https://doi.org/10.3389/fcimb.2013.00080.
(83) Murdoch, C. C.; Skaar, E. P. Nutritional Immunity: The Battle for Nutrient Metals at the Host–Pathogen Interface. *Nat. Rev. Microbiol.* **2022**, *20* (11), 657–670. https://doi.org/10.1038/s41579-022-00745-6.
(84) Haschka, D.; Hoffmann, A.; Weiss, G. Iron in Immune Cell Function and Host Defense. *Semin. Cell Dev. Biol.* **2021**, *115*, 27–36. https://doi.org/10.1016/j.semcdb.2020.12.005.

(85) Khasheii, B.; Mahmoodi, P.; Mohammadzadeh, A. Siderophores: Importance in Bacterial Pathogenesis and Applications in Medicine and Industry. *Microbiol. Res.* **2021**, *250*, 126790. https://doi.org/10.1016/j.micres.2021.126790.
(86) Zeng, X.; Xu, F.; Lin, J. Specific TonB-ExbB-ExbD Energy Transduction Systems Required for Ferric Enterobactin Acquisition in Campylobacter. *FEMS Microbiol. Lett.* **2013**, *347* (1), 83–91. https://doi.org/10.1111/1574-6968.12221.
(87) Andrews, S. C.; Robinson, A. K.; Rodríguez-Quiñones, F. Bacterial Iron Homeostasis. *FEMS Microbiol. Rev.* **2003**, *27* (2–3), 215–237. https://doi.org/10.1016/S0168-6445(03)00055-X.
(88) Wood, J. M. Bacterial Responses to Osmotic Challenges. *J. Gen. Physiol.* **2015**, *145* (5), 381–388. https://doi.org/10.1085/jgp.201411296.
(89) Auer, G. K.; Weibel, D. B. Bacterial Cell Mechanics. *Biochemistry* **2017**, *56* (29), 3710–3724. https://doi.org/10.1021/acs.biochem.7b00346.
(90) Saum, S. H.; Müller, V. Salinity-Dependent Switching of Osmolyte Strategies in a Moderately Halophilic Bacterium: Glutamate Induces Proline Biosynthesis in Halobacillus Halophilus. *J. Bacteriol.* **2007**, *189* (19), 6968–6975. https://doi.org/10.1128/JB.00775-07.
(91) Gregory, G. J.; Boyd, E. F. Stressed out: Bacterial Response to High Salinity Using Compatible Solute Biosynthesis and Uptake Systems, Lessons from Vibrionaceae. *Comput. Struct. Biotechnol. J.* **2021**, *19*, 1014–1027. https://doi.org/10.1016/j.csbj.2021.01.030.
(92) Wood, J. M. Bacterial Osmoregulation: A Paradigm for the Study of Cellular Homeostasis. *Annu. Rev. Microbiol.* **2011**, *65*, 215–238. https://doi.org/10.1146/annurev-micro-090110-102815.
(93) Robin, B.; Nicol, M.; Le, H.; Tahrioui, A.; Schaumann, A.; Vuillemenot, J.-B.; Vergoz, D.; Lesouhaitier, O.; Jouenne, T.; Hardouin, J.; Potron, A.; Perrot, V.; Dé, E. MacAB-TolC Contributes to the Development of Acinetobacter Baumannii Biofilm at the Solid–Liquid Interface. *Front. Microbiol.* **2022**, *12*.
(94) Achouak, W.; Heulin, T.; Pagès, J.-M. Multiple Facets of Bacterial Porins. *FEMS Microbiol. Lett.* **2001**, *199* (1), 1–7. https://doi.org/10.1111/j.1574-6968.2001.tb10642.x.
(95) Masi, M.; Pagès, J.-M. Structure, Function and Regulation of Outer Membrane Proteins Involved in Drug Transport in Enterobactericeae: The OmpF/C – TolC Case. *Open Microbiol. J.* **2013**, *7*, 22–33. https://doi.org/10.2174/1874285801307010022.
(96) Chen, C.; Yu, L.; Tian, F.; Zhao, J.; Zhai, Q. Identification of Novel Bile Salt-Tolerant Genes in Lactobacillus Using Comparative Genomics and Its Application in the Rapid Screening of Tolerant Strains. *Microorganisms* **2022**, *10* (12), 2371. https://doi.org/10.3390/microorganisms10122371.
(97) Sistrunk, J. R.; Nickerson, K. P.; Chanin, R. B.; Rasko, D. A.; Faherty, C. S. Survival of the Fittest: How Bacterial Pathogens Utilize Bile To Enhance Infection. *Clin. Microbiol. Rev.* **2016**, *29* (4), 819–836. https://doi.org/10.1128/CMR.00031-16.
(98) Begley, M.; Gahan, C. G. M.; Hill, C. The Interaction between Bacteria and Bile. *FEMS Microbiol. Rev.* **2005**, *29* (4), 625–651. https://doi.org/10.1016/j.femsre.2004.09.003.
(99) Thanassi, D. G.; Cheng, L. W.; Nikaido, H. Active Efflux of Bile Salts by Escherichia Coli. *J. Bacteriol.* **1997**, *179* (8), 2512–2518. https://doi.org/10.1128/jb.179.8.2512-2518.1997.
(100) Dussurget, O.; Cabanes, D.; Dehoux, P.; Lecuit, M.; Buchrieser, C.; Glaser, P.; Cossart, P.; European Listeria Genome Consortium. Listeria Monocytogenes Bile Salt Hydrolase Is a PrfA-Regulated Virulence Factor Involved in the Intestinal and Hepatic Phases of Listeriosis. *Mol. Microbiol.* **2002**, *45* (4), 1095–1106. https://doi.org/10.1046/j.1365-2958.2002.03080.x.
(101) Jung, H.-J.; Sorbara, M. T.; Pamer, E. G. TAM Mediates Adaptation of Carbapenem-Resistant Klebsiella Pneumoniae to Antimicrobial Stress during Host Colonization and Infection. *PLoS Pathog.* **2021**, *17* (2), e1009309. https://doi.org/10.1371/journal.ppat.1009309.
(102) Lomovskaya, O.; Warren, M. S.; Lee, A.; Galazzo, J.; Fronko, R.; Lee, M.; Blais, J.; Cho, D.; Chamberland, S.; Renau, T.; Leger, R.; Hecker, S.; Watkins, W.; Hoshino, K.; Ishida, H.;

Lee, V. J. Identification and Characterization of Inhibitors of Multidrug Resistance Efflux Pumps in Pseudomonas Aeruginosa: Novel Agents for Combination Therapy. *Antimicrob. Agents Chemother.* **2001**, *45* (1), 105–116. https://doi.org/10.1128/AAC.45.1.105-116.2001.
(103) Zhang, S.; Wang, J.; Ahn, J. Advances in the Discovery of Efflux Pump Inhibitors as Novel Potentiators to Control Antimicrobial-Resistant Pathogens. *Antibiotics* **2023**, *12* (9), 1417. https://doi.org/10.3390/antibiotics12091417.
(104) Piddock, L. J. V. Multidrug-Resistance Efflux Pumps - Not Just for Resistance. *Nat. Rev. Microbiol.* **2006**, *4* (8), 629–636. https://doi.org/10.1038/nrmicro1464.
(105) Renau, T. E.; Léger, R.; Flamme, E. M.; Sangalang, J.; She, M. W.; Yen, R.; Gannon, C. L.; Griffith, D.; Chamberland, S.; Lomovskaya, O.; Hecker, S. J.; Lee, V. J.; Ohta, T.; Nakayama, K. Inhibitors of Efflux Pumps in Pseudomonas Aeruginosa Potentiate the Activity of the Fluoroquinolone Antibacterial Levofloxacin. *J. Med. Chem.* **1999**, *42* (24), 4928–4931. https://doi.org/10.1021/jm9904598.
(106) Radchenko, M.; Symersky, J.; Nie, R.; Lu, M. Structural Basis for the Blockade of MATE Multidrug Efflux Pumps. *Nat. Commun.* **2015**, *6* (1), 7995. https://doi.org/10.1038/ncomms8995.
(107) Compagne, N.; Vieira Da Cruz, A.; Müller, R. T.; Hartkoorn, R. C.; Flipo, M.; Pos, K. M. Update on the Discovery of Efflux Pump Inhibitors against Critical Priority Gram-Negative Bacteria. *Antibiotics* **2023**, *12* (1), 180. https://doi.org/10.3390/antibiotics12010180.
(108) Green, A. T.; Moniruzzaman, M.; Cooper, C. J.; Walker, J. K.; Smith, J. C.; Parks, J. M.; Zgurskaya, H. I. Discovery of Multidrug Efflux Pump Inhibitors with a Novel Chemical Scaffold. *Biochim. Biophys. Acta Gen. Subj.* **2020**, *1864* (6), 129546. https://doi.org/10.1016/j.bbagen.2020.129546.
(109) Abdali, N.; Parks, J. M.; Haynes, K. M.; Chaney, J. L.; Green, A. T.; Wolloscheck, D.; Walker, J. K.; Rybenkov, V. V.; Baudry, J.; Smith, J. C.; Zgurskaya, H. I. Reviving Antibiotics: Efflux Pump Inhibitors That Interact with AcrA, a Membrane Fusion Protein of the AcrAB-TolC Multidrug Efflux Pump. *ACS Infect. Dis.* **2017**, *3* (1), 89–98. https://doi.org/10.1021/acsinfecdis.6b00167.
(110) Grenier, F.; Matteau, D.; Baby, V.; Rodrigue, S. Complete Genome Sequence of Escherichia Coli BW25113. *Genome Announc.* **2014**, *2* (5), 10.1128/genomea.01038-14. https://doi.org/10.1128/genomea.01038-14.
(111) Taylor, R. G.; Walker, D. C.; McInnes, R. R. E. Coli Host Strains Significantly Affect the Quality of Small Scale Plasmid DNA Preparations Used for Sequencing. *Nucleic Acids Res.* **1993**, *21* (7), 1677–1678. https://doi.org/10.1093/nar/21.7.1677.
(112) Simon, R.; Priefer, U.; Pühler, A. A Broad Host Range Mobilization System for In Vivo Genetic Engineering: Transposon Mutagenesis in Gram Negative Bacteria. *Bio/Technology* **1983**, *1* (9), 784–791. https://doi.org/10.1038/nbt1183-784.
(113) Leus, I. V.; Olvera, M.; Adamiak, J. W.; Nguyen, L. L.; Zgurskaya, H. I. Acinetobacter Baumannii Survival under Infection-Associated Stresses Depends on the Expression of Resistance–Nodulation–Division and Major Facilitator Superfamily Efflux Pumps. *Antibiotics* **2024**, *13* (1), 7. https://doi.org/10.3390/antibiotics13010007.
(114) Kyriakidis, I.; Vasileiou, E.; Pana, Z. D.; Tragiannidis, A. Acinetobacter Baumannii Antibiotic Resistance Mechanisms. *Pathogens* **2021**, *10* (3), 373. https://doi.org/10.3390/pathogens10030373.
(115) Houang, E. T.; Sormunen, R. T.; Lai, L.; Chan, C. Y.; Leong, A. S. Effect of Desiccation on the Ultrastructural Appearances of Acinetobacter Baumannii and Acinetobacter Lwoffii. *J. Clin. Pathol.* **1998**, *51* (10), 786–788. https://doi.org/10.1136/jcp.51.10.786.
(116) Jacobs, A. C.; Thompson, M. G.; Black, C. C.; Kessler, J. L.; Clark, L. P.; McQueary, C. N.; Gancz, H. Y.; Corey, B. W.; Moon, J. K.; Si, Y.; Owen, M. T.; Hallock, J. D.; Kwak, Y. I.; Summers, A.; Li, C. Z.; Rasko, D. A.; Penwell, W. F.; Honnold, C. L.; Wise, M. C.;

Waterman, P. E.; Lesho, E. P.; Stewart, R. L.; Actis, L. A.; Palys, T. J.; Craft, D. W.; Zurawski, D. V. AB5075, a Highly Virulent Isolate of Acinetobacter Baumannii, as a Model Strain for the Evaluation of Pathogenesis and Antimicrobial Treatments. *mBio* **2014**, *5* (3), 10.1128/mbio.01076-14. https://doi.org/10.1128/mbio.01076-14.

(117) Krishnamoorthy, G.; Wolloscheck, D.; Weeks, J. W.; Croft, C.; Rybenkov, V. V.; Zgurskaya, H. I. Breaking the Permeability Barrier of Escherichia Coli by Controlled Hyperporination of the Outer Membrane. *Antimicrob. Agents Chemother.* **2016**, *60* (12), 7372–7381. https://doi.org/10.1128/AAC.01882-16.

(118) Ram, Y.; Dellus-Gur, E.; Bibi, M.; Karkare, K.; Obolski, U.; Feldman, M. W.; Cooper, T. F.; Berman, J.; Hadany, L. Predicting Microbial Growth in a Mixed Culture from Growth Curve Data. *Proc. Natl. Acad. Sci. U. S. A.* **2019**, *116* (29), 14698–14707. https://doi.org/10.1073/pnas.1902217116.

(119) Sprouffske, K.; Wagner, A. Growthcurver: An R Package for Obtaining Interpretable Metrics from Microbial Growth Curves. *BMC Bioinformatics* **2016**, *17*, 172. https://doi.org/10.1186/s12859-016-1016-7.

(120) Leus, I. V.; Adamiak, J.; Chandar, B.; Bonifay, V.; Zhao, S.; Walker, S. S.; Squadroni, B.; Balibar, C. J.; Kinarivala, N.; Standke, L. C.; Voss, H. U.; Tan, D. S.; Rybenkov, V. V.; Zgurskaya, H. I. Functional Diversity of Gram-Negative Permeability Barriers Reflected in Antibacterial Activities and Intracellular Accumulation of Antibiotics. *Antimicrob. Agents Chemother.* **2023**, *67* (2), e0137722. https://doi.org/10.1128/aac.01377-22.

(121) Koronakis, V.; Li, J.; Koronakis, E.; Stauffer, K. Structure of TolC, the Outer Membrane Component of the Bacterial Type I Efflux System, Derived from Two-Dimensional Crystals. *Mol. Microbiol.* **1997**, *23* (3), 617–626. https://doi.org/10.1046/j.1365-2958.1997.d01-1880.x.

(122) Westfall, D. A.; Krishnamoorthy, G.; Wolloscheck, D.; Sarkar, R.; Zgurskaya, H. I.; Rybenkov, V. V. Bifurcation Kinetics of Drug Uptake by Gram-Negative Bacteria. *PLoS ONE* **2017**, *12* (9). https://doi.org/10.1371/journal.pone.0184671.

(123) Yang, J.; Yan, R.; Roy, A.; Xu, D.; Poisson, J.; Zhang, Y. The I-TASSER Suite: Protein Structure and Function Prediction. *Nat. Methods* **2015**, *12* (1), 7–8. https://doi.org/10.1038/nmeth.3213.

(124) Roy, A.; Kucukural, A.; Zhang, Y. I-TASSER: A Unified Platform for Automated Protein Structure and Function Prediction. *Nat. Protoc.* **2010**, *5* (4), 725–738. https://doi.org/10.1038/nprot.2010.5.

(125) Zhang, Y. I-TASSER Server for Protein 3D Structure Prediction. *BMC Bioinformatics* **2008**, *9* (1), 40. https://doi.org/10.1186/1471-2105-9-40.

(126) Rice, L. B. Federal Funding for the Study of Antimicrobial Resistance in Nosocomial Pathogens: No ESKAPE. *J. Infect. Dis.* **2008**, *197* (8), 1079–1081. https://doi.org/10.1086/533452.

(127) Pendleton, J. N.; Gorman, S. P.; Gilmore, B. F. Clinical Relevance of the ESKAPE Pathogens. *Expert Rev. Anti Infect. Ther.* **2013**, *11* (3), 297–308. https://doi.org/10.1586/eri.13.12.

(128) De Oliveira, D. M. P.; Forde, B. M.; Kidd, T. J.; Harris, P. N. A.; Schembri, M. A.; Beatson, S. A.; Paterson, D. L.; Walker, M. J. Antimicrobial Resistance in ESKAPE Pathogens. *Clin. Microbiol. Rev.* **2020**, *33* (3), e00181-19. https://doi.org/10.1128/CMR.00181-19.

(129) Kornelsen, V.; Kumar, A. Update on Multidrug Resistance Efflux Pumps in Acinetobacter Spp. *Antimicrob. Agents Chemother.* **2021**, *65* (7), e00514-21. https://doi.org/10.1128/AAC.00514-21.

(130) Geisinger, E.; Huo, W.; Hernandez-Bird, J.; Isberg, R. R. Acinetobacter Baumannii: Envelope Determinants That Control Drug Resistance, Virulence, and Surface Variability.

Annu. Rev. Microbiol. **2019**, *73*, 481–506. https://doi.org/10.1146/annurev-micro-020518-115714.
(131) Yoon, E.-J.; Courvalin, P.; Grillot-Courvalin, C. RND-Type Efflux Pumps in Multidrug-Resistant Clinical Isolates of Acinetobacter Baumannii: Major Role for AdeABC Overexpression and AdeRS Mutations. *Antimicrob. Agents Chemother.* **2013**, *57* (7), 2989–2995. https://doi.org/10.1128/AAC.02556-12.
(132) Lin, M.-F.; Lin, Y.-Y.; Lan, C.-Y. Contribution of EmrAB Efflux Pumps to Colistin Resistance in Acinetobacter Baumannii. *J. Microbiol. Seoul Korea* **2017**, *55* (2), 130–136. https://doi.org/10.1007/s12275-017-6408-5.
(133) Moreno-Hagelsieb, G.; Collado-Vides, J. A Powerful Non-Homology Method for the Prediction of Operons in Prokaryotes. *Bioinforma. Oxf. Engl.* **2002**, *18 Suppl 1*, S329-336. https://doi.org/10.1093/bioinformatics/18.suppl_1.s329.
(134) *tolC - Outer membrane protein TolC - Escherichia coli (strain K12) | UniProtKB | UniProt*. https://www.uniprot.org/uniprotkb/P02930/entry#sequences (accessed 2023-11-23).
(135) Buroni, S.; Pasca, M. R.; Flannagan, R. S.; Bazzini, S.; Milano, A.; Bertani, I.; Venturi, V.; Valvano, M. A.; Riccardi, G. Assessment of Three Resistance-Nodulation-Cell Division Drug Efflux Transporters of Burkholderia Cenocepacia in Intrinsic Antibiotic Resistance. *BMC Microbiol.* **2009**, *9*, 200. https://doi.org/10.1186/1471-2180-9-200.
(136) Ozer, B.; Duran, N.; Onlen, Y.; Savas, L. Efflux Pump Genes and Antimicrobial Resistance of Pseudomonas Aeruginosa Strains Isolated from Lower Respiratory Tract Infections Acquired in an Intensive Care Unit. *J. Antibiot. (Tokyo)* **2012**, *65* (1), 9–13. https://doi.org/10.1038/ja.2011.102.
(137) Hinchliffe, P.; Greene, N. P.; Paterson, N. G.; Crow, A.; Hughes, C.; Koronakis, V. Structure of the Periplasmic Adaptor Protein from a Major Facilitator Superfamily (MFS) Multidrug Efflux Pump. *FEBS Lett.* **2014**, *588* (17), 3147–3153. https://doi.org/10.1016/j.febslet.2014.06.055.
(138) Jumper, J.; Evans, R.; Pritzel, A.; Green, T.; Figurnov, M.; Ronneberger, O.; Tunyasuvunakool, K.; Bates, R.; Žídek, A.; Potapenko, A.; Bridgland, A.; Meyer, C.; Kohl, S. A. A.; Ballard, A. J.; Cowie, A.; Romera-Paredes, B.; Nikolov, S.; Jain, R.; Adler, J.; Back, T.; Petersen, S.; Reiman, D.; Clancy, E.; Zielinski, M.; Steinegger, M.; Pacholska, M.; Berghammer, T.; Bodenstein, S.; Silver, D.; Vinyals, O.; Senior, A. W.; Kavukcuoglu, K.; Kohli, P.; Hassabis, D. Highly Accurate Protein Structure Prediction with AlphaFold. *Nature* **2021**, *596* (7873), 583–589. https://doi.org/10.1038/s41586-021-03819-2.
(139) Varadi, M.; Bertoni, D.; Magana, P.; Paramval, U.; Pidruchna, I.; Radhakrishnan, M.; Tsenkov, M.; Nair, S.; Mirdita, M.; Yeo, J.; Kovalevskiy, O.; Tunyasuvunakool, K.; Laydon, A.; Žídek, A.; Tomlinson, H.; Hariharan, D.; Abrahamson, J.; Green, T.; Jumper, J.; Birney, E.; Steinegger, M.; Hassabis, D.; Velankar, S. AlphaFold Protein Structure Database in 2024: Providing Structure Coverage for over 214 Million Protein Sequences. *Nucleic Acids Res.* **2024**, *52* (D1), D368–D375. https://doi.org/10.1093/nar/gkad1011.
(140) Varadi, M.; Anyango, S.; Deshpande, M.; Nair, S.; Natassia, C.; Yordanova, G.; Yuan, D.; Stroe, O.; Wood, G.; Laydon, A.; Žídek, A.; Green, T.; Tunyasuvunakool, K.; Petersen, S.; Jumper, J.; Clancy, E.; Green, R.; Vora, A.; Lutfi, M.; Figurnov, M.; Cowie, A.; Hobbs, N.; Kohli, P.; Kleywegt, G.; Birney, E.; Hassabis, D.; Velankar, S. AlphaFold Protein Structure Database: Massively Expanding the Structural Coverage of Protein-Sequence Space with High-Accuracy Models. *Nucleic Acids Res.* **2022**, *50* (D1), D439–D444. https://doi.org/10.1093/nar/gkab1061.
(141) The PyMOL Molecular Graphics System.
(142) Zgurskaya, H. I. Multicomponent Drug Efflux Complexes: Architecture and Mechanism of Assembly. *Future Microbiol.* **2009**, *4*, 919–932. https://doi.org/10.2217/fmb.09.62.
(143) Jiang, J.-H.; Hassan, K. A.; Begg, S. L.; Rupasinghe, T. W. T.; Naidu, V.; Pederick, V. G.; Khorvash, M.; Whittall, J. J.; Paton, J. C.; Paulsen, I. T.; McDevitt, C. A.; Peleg, A. Y.;

Eijkelkamp, B. A. Identification of Novel Acinetobacter Baumannii Host Fatty Acid Stress Adaptation Strategies. *mBio* **2019**, *10* (1), e02056-18. https://doi.org/10.1128/mBio.02056-18.
(144) Schumacher, K.; Brameyer, S.; Jung, K. Bacterial Acid Stress Response: From Cellular Changes to Antibiotic Tolerance and Phenotypic Heterogeneity. *Curr. Opin. Microbiol.* **2023**, *75*, 102367. https://doi.org/10.1016/j.mib.2023.102367.
(145) Fanelli, G.; Pasqua, M.; Colonna, B.; Prosseda, G.; Grossi, M. Expression Profile of Multidrug Resistance Efflux Pumps During Intracellular Life of Adherent-Invasive Escherichia Coli Strain LF82. *Front. Microbiol.* **2020**, *11*. https://doi.org/10.3389/fmicb.2020.01935.
(146) Pasqua, M.; Grossi, M.; Scinicariello, S.; Aussel, L.; Barras, F.; Colonna, B.; Prosseda, G. The MFS Efflux Pump EmrKY Contributes to the Survival of Shigella within Macrophages. *Sci. Rep.* **2019**, *9* (1), 2906. https://doi.org/10.1038/s41598-019-39749-3.
(147) Distel, J. S.; Di Venanzio, G.; Mackel, J. J.; Rosen, D. A.; Feldman, M. F. Replicative Acinetobacter Baumannii Strains Interfere with Phagosomal Maturation by Modulating the Vacuolar pH. *PLoS Pathog.* **2023**, *19* (6), e1011173. https://doi.org/10.1371/journal.ppat.1011173.
(148) Lewinson, O.; Padan, E.; Bibi, E. Alkalitolerance: A Biological Function for a Multidrug Transporter in pH Homeostasis. *Proc. Natl. Acad. Sci. U. S. A.* **2004**, *101* (39), 14073–14078. https://doi.org/10.1073/pnas.0405375101.
(149) Murata, T.; Tseng, W.; Guina, T.; Miller, S. I.; Nikaido, H. PhoPQ-Mediated Regulation Produces a More Robust Permeability Barrier in the Outer Membrane of Salmonella Enterica Serovar Typhimurium. *J. Bacteriol.* **2007**, *189* (20), 7213–7222. https://doi.org/10.1128/JB.00973-07.
(150) Van Riet, S.; Tadesse, W.; Mortier, J.; Schlegel, S.; Simoens, K.; Bernaerts, K.; Dal Co, A.; Aertsen, A. Heterogeneity and Evolutionary Tunability of Escherichia Coli Resistance against Extreme Acid Stress. *Microbiol. Spectr.* **2022**, *10* (6), e0375722. https://doi.org/10.1128/spectrum.03757-22.
(151) Bearson, S.; Bearson, B.; Foster, J. W. Acid Stress Responses in Enterobacteria. *FEMS Microbiol. Lett.* **1997**, *147* (2), 173–180. https://doi.org/10.1111/j.1574-6968.1997.tb10238.x.
(152) Ren, X.; Palmer, L. D. Acinetobacter Metabolism in Infection and Antimicrobial Resistance. *Infect. Immun. 91* (6), e00433-22. https://doi.org/10.1128/iai.00433-22.
(153) Whittle, E. E.; McNeil, H. E.; Trampari, E.; Webber, M.; Overton, T. W.; Blair, J. M. A. Efflux Impacts Intracellular Accumulation Only in Actively Growing Bacterial Cells. *mBio* **2021**, *12* (5), e0260821. https://doi.org/10.1128/mBio.02608-21.
(154) Coyne, S.; Courvalin, P.; Périchon, B. Efflux-Mediated Antibiotic Resistance in Acinetobacter Spp. *Antimicrob. Agents Chemother.* **2011**, *55* (3), 947–953. https://doi.org/10.1128/AAC.01388-10.
(155) Su, C.-C.; Li, M.; Gu, R.; Takatsuka, Y.; McDermott, G.; Nikaido, H.; Yu, E. W. Conformation of the AcrB Multidrug Efflux Pump in Mutants of the Putative Proton Relay Pathway. *J. Bacteriol.* **2006**, *188* (20), 7290–7296. https://doi.org/10.1128/JB.00684-06.
(156) Sharma, A.; Gupta, V. K.; Pathania, R. Efflux Pump Inhibitors for Bacterial Pathogens: From Bench to Bedside. *Indian J. Med. Res.* **2019**, *149* (2), 129–145. https://doi.org/10.4103/ijmr.IJMR_2079_17.
(157) Reza, A.; Sutton, J. M.; Rahman, K. M. Effectiveness of Efflux Pump Inhibitors as Biofilm Disruptors and Resistance Breakers in Gram-Negative (ESKAPEE) Bacteria. *Antibiot. Basel Switz.* **2019**, *8* (4), 229. https://doi.org/10.3390/antibiotics8040229.
(158) Zhu, Y. *Development and evaluation of bacterial efflux pump inhibitors*. King's College London. https://kclpure.kcl.ac.uk/portal/en/studentTheses/development-and-evaluation-of-bacterial-efflux-pump-inhibitors (accessed 2024-01-31).

(159) Webb, B.; Sali, A. Comparative Protein Structure Modeling Using MODELLER. *Curr. Protoc. Bioinforma.* **2016**, *54*, 5.6.1-5.6.37. https://doi.org/10.1002/cpbi.3.
(160) Su, C.-C.; Morgan, C. E.; Kambakam, S.; Rajavel, M.; Scott, H.; Huang, W.; Emerson, C. C.; Taylor, D. J.; Stewart, P. L.; Bonomo, R. A.; Yu, E. W. Cryo-Electron Microscopy Structure of an Acinetobacter Baumannii Multidrug Efflux Pump. *mBio* **2019**, *10* (4), e01295-19. https://doi.org/10.1128/mBio.01295-19.
(161) Nakashima, R.; Sakurai, K.; Yamasaki, S.; Nishino, K.; Yamaguchi, A. Structures of the Multidrug Exporter AcrB Reveal a Proximal Multisite Drug-Binding Pocket. *Nature* **2011**, *480* (7378), 565–569. https://doi.org/10.1038/nature10641.
(162) D'Cunha, N.; Moniruzzaman, M.; Haynes, K.; Malloci, G.; Cooper, C. J.; Margiotta, E.; Vargiu, A. V.; Uddin, M. R.; Leus, I. V.; Cao, F.; Parks, J. M.; Rybenkov, V. V.; Ruggerone, P.; Zgurskaya, H. I.; Walker, J. K. Mechanistic Duality of Bacterial Efflux Substrates and Inhibitors: Example of Simple Substituted Cinnamoyl and Naphthyl Amides. *ACS Infect. Dis.* **2021**, *7* (9), 2650–2665. https://doi.org/10.1021/acsinfecdis.1c00100.
(163) Wang-Kan, X.; Rodríguez-Blanco, G.; Southam, A. D.; Winder, C. L.; Dunn, W. B.; Ivens, A.; Piddock, L. J. V. Metabolomics Reveal Potential Natural Substrates of AcrB in Escherichia Coli and Salmonella Enterica Serovar Typhimurium. *mBio* **2021**, *12* (2), 10.1128/mbio.00109-21. https://doi.org/10.1128/mbio.00109-21.
(164) Sjuts, H.; Vargiu, A. V.; Kwasny, S. M.; Nguyen, S. T.; Kim, H.-S.; Ding, X.; Ornik, A. R.; Ruggerone, P.; Bowlin, T. L.; Nikaido, H.; Pos, K. M.; Opperman, T. J. Molecular Basis for Inhibition of AcrB Multidrug Efflux Pump by Novel and Powerful Pyranopyridine Derivatives. *Proc. Natl. Acad. Sci. U. S. A.* **2016**, *113* (13), 3509–3514. https://doi.org/10.1073/pnas.1602472113.
(165) Nakashima, R.; Sakurai, K.; Yamasaki, S.; Hayashi, K.; Nagata, C.; Hoshino, K.; Onodera, Y.; Nishino, K.; Yamaguchi, A. Structural Basis for the Inhibition of Bacterial Multidrug Exporters. *Nature* **2013**, *500* (7460), 102–106. https://doi.org/10.1038/nature12300.
(166) Aron, Z.; Opperman, T. J. The Hydrophobic Trap—the Achilles Heel of RND Efflux Pumps. *Res. Microbiol.* **2018**, *169* (7–8), 393–400. https://doi.org/10.1016/j.resmic.2017.11.001.
(167) Harding, C. M.; Hennon, S. W.; Feldman, M. F. Uncovering the Mechanisms of Acinetobacter Baumannii Virulence. *Nat. Rev. Microbiol.* **2018**, *16* (2), 91–102. https://doi.org/10.1038/nrmicro.2017.148.
(168) Breijyeh, Z.; Jubeh, B.; Karaman, R. Resistance of Gram-Negative Bacteria to Current Antibacterial Agents and Approaches to Resolve It. *Molecules* **2020**, *25* (6), 1340. https://doi.org/10.3390/molecules25061340.
(169) Zack, K. M.; Sorenson, T.; Joshi, S. G. Types and Mechanisms of Efflux Pump Systems and the Potential of Efflux Pump Inhibitors in the Restoration of Antimicrobial Susceptibility, with a Special Reference to Acinetobacter Baumannii. *Pathogens* **2024**, *13* (3), 197. https://doi.org/10.3390/pathogens13030197.
(170) He, X.; Lu, F.; Yuan, F.; Jiang, D.; Zhao, P.; Zhu, J.; Cheng, H.; Cao, J.; Lu, G. Biofilm Formation Caused by Clinical Acinetobacter Baumannii Isolates Is Associated with Overexpression of the AdeFGH Efflux Pump. *Antimicrob. Agents Chemother.* **2015**, *59* (8), 4817–4825. https://doi.org/10.1128/AAC.00877-15.
(171) Rosenfeld, N.; Bouchier, C.; Courvalin, P.; Périchon, B. Expression of the Resistance-Nodulation-Cell Division Pump AdeIJK in Acinetobacter Baumannii Is Regulated by AdeN, a TetR-Type Regulator. *Antimicrob. Agents Chemother.* **2012**, *56* (5), 2504–2510. https://doi.org/10.1128/aac.06422-11.
(172) *About erythromycin*. nhs.uk. https://www.nhs.uk/medicines/erythromycin/about-erythromycin/ (accessed 2024-01-12).

(173) Zhang, Z.; Morgan, C. E.; Bonomo, R. A.; Yu, E. W. Cryo-EM Structures of the Klebsiella Pneumoniae AcrB Multidrug Efflux Pump. *mBio* **2023**, *14* (3), e0065923. https://doi.org/10.1128/mbio.00659-23.
(174) Zhang, Z.; Morgan, C. E.; Bonomo, R. A.; Yu, E. W. Cryo-EM Determination of Eravacycline-Bound Structures of the Ribosome and the Multidrug Efflux Pump AdeJ of Acinetobacter Baumannii. *mBio* **2021**, *12* (3), e0103121. https://doi.org/10.1128/mbio.01031-21.
(175) Su, C.-C.; Morgan, C. E.; Kambakam, S.; Rajavel, M.; Scott, H.; Huang, W.; Emerson, C. C.; Taylor, D. J.; Stewart, P. L.; Bonomo, R. A.; Yu, E. W. Cryo-Electron Microscopy Structure of an Acinetobacter Baumannii Multidrug Efflux Pump. *mBio* **2019**, *10* (4), 10.1128/mbio.01295-19. https://doi.org/10.1128/mbio.01295-19.
(176) Morgan, C. E.; Glaza, P.; Leus, I. V.; Trinh, A.; Su, C.-C.; Cui, M.; Zgurskaya, H. I.; Yu, E. W. Cryoelectron Microscopy Structures of AdeB Illuminate Mechanisms of Simultaneous Binding and Exporting of Substrates. *mBio* **2021**, *12* (1), e03690-20. https://doi.org/10.1128/mBio.03690-20.
(177) Kaatz, G. W.; Seo, S. M.; Ruble, C. A. Efflux-Mediated Fluoroquinolone Resistance in Staphylococcus Aureus. *Antimicrob. Agents Chemother.* **1993**, *37* (5), 1086–1094.

Appendices

List of Tables and Figures

Nucleotide sequences used for cloning and mutagenesis:

>A1S_2304 (*adeF*) GenBank: CP000521.1

```
atgtcatttt cccgcaaaca gtttgcactg tctgccatct ttgttgctat tttagcaacc
ggtggcagtt ttatgttgtt acatgaaaat gccgatgcaa aagctgcacc aaccgctgcc
caacaagctg ctactgttga tgtagcccca gtagtaagca aaaccattac cgattggcaa
gaatattccg gtcgtttaga agcaattgat caagttgata ttcggcctca agtttcagga
aaactcattg ccgtacattt caaagatgga agcctcgtta aaaaaggtga tttacttttc
acaatcgacc ctcgtccttt tgaagcagaa ctgaaccgtg caaaagccca gcttgcttca
gctgaagcac aggtaacata taccgccagc aatctttcgc gtattcaacg tctcattcag
```

agtaatgctg tttctcgtca agaactggat ttagccgaaa atgatgcacg ttcagcgaat
gctaacctac aagccgctag agctgctgtc caatctgcac gtttaaatct ggaatacacc
cgtattactg caccagtcag cggccggatt tcacgagctg aagtgaccgt gggtaatgtc
gtctctgcag gtaatggcgc acaggtttta acaagtttag tgtctgtatc acgcctatac
gcatctttcg atgttgatga acaaacttac ctgaaatata tcagtaatca gcgtaattca
gcacaagtac ctgtctatat gggacttgcc aatgaaacag gctttactcg cgaaggtaca
atcaactcaa tcgataacaa cctgaataca acctcaggaa caatccgtgt tcgtgcaact
tttgacaatc caaacggtgt tttattaccg ggcctatatg cacgaattcg tttaggtgga
ggtcaacctc gcccagcgat tctgattagt ccaaccgcgg ttggcgtcga ccaagataaa
cgttttgtcg tagtagttga tgcgaaaaat caaactgctt atcgcgaagt aaaactcggt
gcccaacaag atggcttgca aatcgtaaat agcggattac aagcgggtga tcgtattgta
gtgaatggtt tacagcgaat tcgtccgggt gaccctgtta caccgcatct cgttcctatg
ccaaattcac aaatcactgc taacgctact cctcaacctc agccaacaga taaaacatca
actccggcaa aaggttaa

>A1S_2305 (*adeG*) GenBank: CP000521.1

atgaatattt ctaagttttt tattgatcgg ccgatctttg ctggtgtttt atcagtattg
attttactcg ccggtctgct ttcggtattc caattaccga tttctgaata tcccgaggtt
gttccaccat ctgtggtggt acgcgcccaa tatccgggtg caaacccaaa agtgattgct
gaaacggttg catctccgct cgaagagtca atcaacggcg tcgaagacat gctgtatatg
caatctcaag caaacagcga cggtaaccta accattacgg tgaactttaa gctcggtatc
gacccagata aagcccaaca attggttcaa aaccgtgtgt ctcaggccat gccccgttta
cctgaagatg tacagcgctt aggtgtaacc acactaaaaa gctcacctac tctaactatg
gtagtgcatc tgacctcacc agataatcgc tatgacatga cctacttacg taactatgcg
gtgctcaacg tgaaagaccg tttagcgcgt ttacaagggg ttggtgaagt cggattattt
ggttctggtg actacgcgat gcgtgtatgg cttgacccgc aaaaagtagc acagcgtaac
cttacagcca ctgaaattgt gaatgcaatc cgtgaacaaa acattcaggt tgcagcgggt
acaatcggtg catcaccaag taattcacct ttacagcttt cggtcaatgc tcaaggtcgt
ttaaccactg agcaagaatt tgccgatatc attttaaaaa ctgctcccga cggtgcagtc
acccgattgg gtgatgttgc acgtgttgaa ctcgcagctt cacaatatgg cttacgttca
ttgcttgata ataaacaagc tgtcgcaatt ccaattttcc aagctccggg tgcgaatgct
ttacaagttt ccgatcaagt gcgtagcaca atgaaggagc tttcaaaaga ttttccatct
tcaattaaat acgacattgt ttatgacccg actcagttcg tacgggccag tattaaagcc
gtcgttcata ccttacttga agcaattgca ctggttgttg tggttgttat tttattctta
caaacatggc gcgcctcaat cattccattg cttgccgtac cggtttcaat tattggtaca
ttcgcgctca tgctcgcttt tggttactca atcaatgcgc tatcactgtt cgggatggtg
cttgccatcg gcattgtcgt cgatgacgcg attgtggtcg tcgaaaatgt cgagaggaat
attgaagcag gcttaaaccc aagggaggcg acttaccgtg ccatgcgaga agtcagtgga
ccgattattg ccattgcttt aacacttgtt gcagtattcg tacctcttgc ctttatgaca
ggcttaacag ggcaattcta taaacaattt gccatgacca ttgccatttc aacggttatt
tcggctttta actcactcac cctatctcca gctttggcag cgctgttact taaaggacac
gatgctaaac ctgatgcctt aacacgtatt atgaatcgtg tattcggtcg tttctttgca
ctgtttaacc gtgtgttttc acgtgcttca gaccgttata gtcaaggcgt cagccgtgtc
atttcccata aagcttcggc aatgggtgtc tatgcagcac ttctaggttt aaccgttggt
atttcctata ttgttccggg cggtttcgtt cctgcgcagg acaaacaata tttaattagc
tttgcgcagc taccaaacgg cgcatcatta gatcgtaccg aagcagtcat tcgtaaaatg
agtgacactg cacttaaaca gcctggtgta gaaagtgctg ttgccttccc tggcctctca
attaatggtt tcaccaatag ctctagcgct ggtattgtct ttgtgacttt aaagccattt
gatgaacgta aggcaaaaga cttatctgca aatgcaattg caggtgcgct caaccagaaa
tattcagcta ttcaagatgc ctatatcgcg gttttcccac caccaccagt gatgggctta
ggtactatgg gcggctttaa actgcaactt gaagaccgag gtgccttagg ctattcagcc
ttgaacgatg ctgctcaaaa ctttatgaag gcagcacaat cagcccctga acttggtcca
atgttctcaa gttatcaaat taacgtgcct caactcaatg tagatctgga ccgtgtaaaa
gctaaacagc aaggcgttgc tgtgacagat gttttcaaca ctatgcagat ttatttaggt
tctcagtacg ttaacgactt taaccgtttt ggacgtgttt atcaggtccg tgcacaagcc

gatgcgcctt tccgtgctaa ccctgaagat attttgcagc ttaaaacccg taatagtgcc
ggacaaatgg tgccattatc ttcattggtg aatgtaactc aaacctatgg tcctgaaatg
gtcgttcgtt ataacggtta cacatcagca gatattaacg gcggccctgc cccaggttat
tcatctagcc aagcagaagc tgcggttgaa cgtattgctg cacaaactct accgcgtggt
atcaagtttg aatggacaga tttaacttac caaaaaatct tggctggtaa tgctggactt
tgggtattcc ctattagcgt attactcgtg ttcttagtat tagctgctca gtatgaaagc
ttaaccctac cattagcagt tatcttaatt gtaccaatgg gaatcttagc ggctctgaca
ggtgtctggt tgacagctgg agataacaac atctttaccc aaatcggtct aatggtactg
gtggggctag cctgtaaaaa tgctattttg attgtcgaat ttgcgcggga acttgaaatg
caaggtgcga ctgcctttaa agcagccgtt gaagcaagtc gtctacgttt acgcccaatt
ttaatgacct ctattgcatt tattatgggt gtagtgccac tggttacttc aactggcgca
ggttctgaaa tgcgacatgc gatgggtgtt gccgtattct tcggtatgat cggtgtaaca
ttctttggtt tattcctcac cccggccttt tacgttctga ttcgtaccct caacagcaaa
cataaactac attctgcggc agttcatgaa gcgccgttag ctagcccaca cgatcattaa

>A1S_2306 (*adeH*) GenBank: CP000521.1

gtgattacat caaaacaaaa ctggttgttg tcctcactca tgggaagcct gctccttgca
ggctgctcat tggccccaga atatcaacct gcaaaagtta tagtgccagt caaattcaaa
gaatctgacc ccaaacttga agataataac tggaagattg cccaacctgc cgatcaacaa
actcgtggtg aatggtggcg catttacaat gatactcaac tgaatgaact tgaacagcaa
gctatcgcag gcaaccagaa cctaaaagcg gtggcagcaa atattcaggc ttcacgtgca
ctacgttcgg cagctcaagc tgaacgctta ccaagtattg atgccggatt tgggccaacc
cgccaaaagc cgtctccagc ttcactcggt ttagatgaca atgcacatac ttcggctcaa
accttatggc gagctcaagc caatgtttca tatgagctcg atttatttgg tcgtgtagca
agtagtgtca acgcagcaac agcggatcta cagcaacaag aggcactata tcagtcggca
cttttagctc tacaagcgga tgtagctcaa ggttattttc tgatacgtca acttgatacc
gaacaggcaa tttataaccg tacaatcaaa ttattaggtg aaacacgaga tttaatgcag
cttcgtttta aaaacggact ggtcagtgaa ttagatgttt ctcgtgcaca aaccgaactt
gctaccgcac aaaccactgc cctaaatatt gctcgtaaca gagccagtgc agaacatgcg
cttgcagtct tattaggaaa accaccagca gactttaact tggctgttca acctttaact
gcaaatagta tccgtctccc tgccggtttg ccgtcaactt tacttgaaag acgacccgat
attgcggctg cagagcgtgc aatggcagca gataatgcac gtattgggat tgctcgtgca
gcatttttcc caaaactcag tcttacagga gctttaggtt atgaatcttc aagtttaagc
gagttgggta aatggtcgag tcggactttt ttactaggac ctgtcgctgg tactattttg
tcgttacctt tatttgatgg tggacaacgt aaagcaggcg ttgctcaagc aagagcggct
tatgaggaaa gcgtcgccaa ctatagacaa actgtactaa acgcatttcg cgaagttgaa
aatggtttat ctgatcaaag aattctcgat cagcaaattc aggctcaaaa ccaagcactc
tcctcttctc gtcatgccaa tcaactttct catttacgtt atcgagaagg tgctattagc
tatcttgatg tcattgattc tgaccgcact attttgcaac aagaacaatt agcagctcag
ctgaaaggca gccaaatcat tgcaagcatc aatttaatcc gtgctttagg gggcggttgg
agtagttaa

>A1S_2735 (*adeI*) GenBank: CP000521.1

atgtcggcta agctttgggc accagccctt actgcttgcg cattagcaac aagtatcgcg
cttgttggtt gtagcaaagg ctccgatgag aaacagcaag ctgctgctgc tcagaaaatg
ccgcctgcag aagtaggtgt tattgttgct caaccacaaa gtgttgaaca aagcgttgag
ctttcaggcc gtacttcagc atatcaaatt tctgaagttc gtcctcagac aagtggcgtg
attttaaaac gcttatttgc tgaaggaagc tatgttcgtg aaggtcaggc gctttatgag
ctcgactcta gaacgaaccg tgcaacgtta gaaaatgcaa aagcatcact cctacaacaa
caggcaaatc tagcttcact acgtaccaag ttaaatcgtt ataaacaact tgtttctagt
aatgctgtgt ctaaacagga atatgatgac ttacttggtc aagtcaatgt tgcagaagca
caagttgcag cagctaaggc tcaagtaaca aatgcaaatg tagatcttgg ttattctaca
attcgctctc ctatttctgg ccaatctggt cgttcttcag taacggctgg tgctttggtt

actgcaaacc agactgaccc gttggtaacg attcaacagt tagatcctat ctatgttgat
attaatcagt ctagtgctga gttattgcgt ttacgtcaac aactaagcaa aggcagttta
aataacagta acaacacgaa agtaaaatta aagcttgaag atggttctac ctatccaatc
gaagggcaac ttgctttctc tgacgcttct gtaaaccaag atacaggaac aattacatta
cgtgccgtat tctctaaccc gaatcattta ttgcttccgg gtatgtatac cactgcgcaa
attgttcagg gcgttgttcc aaatgcttac ctgattcctc aagctgccat tactcgttta
cctacagggc aagctgtagc gatgcttgtt aatgctaaag gggttgttga gagccgtcct
gttgaaacct ctggtgttca aggacaaaat tggattgtga ctaacggctt aaaagccggc
gataaagtca ttgttgatgg tgttgccaaa gttaaagaag ggcaagaagt atcagcaaaa
ccttatcaag ctcaaccagc aaactctcaa ggtgcagcac caaatgctgc gaaaccggct
caatcaggta aacctcaagc agaacagaaa gcagcttcaa atgcataa

>A1S_2736 (*adeJ*) GenBank: CP000521.1

atggcacaat tttttattca tcgccccata tttgcgtggg tgattgcatt agtcattatg
ttggcgggta ttcttacgct aacaaaaatg cctattgcac aatatccaac gattgcacca
ccaaccgtaa cgattgctgc gacttatcct ggtgcatcgg ctgaaacagt tgaaaatact
gtaacccaga tcattgaaca acaaatgaat ggtcttgatg gcttacgtta tatttcatct
aacagtgctg gtaatggtca ggcatctatt caattaaact ttgaacaagg tgttgaccct
gatattgcac aggttcaagt tcaaaacaaa ttgcaatctg caactgcgct tttacctgaa
gatgtacaac gtcaaggtgt aacagttact aaatctggtg cgagcttctt gcaagttatt
gcattctatt caccagataa caacctgtca gactctgaca ttaaagacta cgtaaactcg
tcaattaaag aaccgcttag ccgtgttgcc ggtgttggtg aggtacaggt cttcggtggc
tcatacgcaa tgcgtatctg gcttgatcca gctaaattaa caagctacca acttactcct
agtgatattg caactgcctt acaagcgcag aactcgcaag ttgctgtagg tcagttaggt
ggtgctccgg ctgtacaagg tcaagttctt aacgcaacag taaatgcaca aagcttattg
cagactcctg aacagtttaa aaatatcttc ttaaagaaca cagcatcagg tgctgaggtt
cgattaaaag atgttgctcg cgtagaatta ggttcggata actatcaatt tgactcgaag
tttaacggta aaccggcagc tggtcttgca attaaaattg caacaggtgc taacgcactc
gacacagccg aagcagttga acaacgttta tctgaactac gtaagaacta tccaacaggt
cttgcagata aactggctta tgacacgact ccatttatcc gtctttcaat tgaaagtgta
gtacacacat taattgaagc cgtgattttg gtattcattg tcatgttcct attcttacaa
aactggcgtg caacgattat tccaacgctt gcagttccag tagttgtatt aggtacattt
gcggtcatta atatctttgg cttctcaatt aacaccttaa ccatgttcgc tatggtattg
gcaatcggtc ttctggtcga cgacgccatt gttgtagtcg aaaacgttga acgtgtgatg
agtgaagacc ataccgatcc ggttaccgcc acttctcgct caatgcagca gatttctggt
gcgttagtag gtattaccag cgtattgaca gcggtattcg taccaatggc tttctttggt
ggtacaacag gtgtaattta ccgccagttc tcgattaccc ttgtaactgc aatggttctg
tcgttaattg tagcgttgac gttcacaccg gcactttgtg caactatctt gaaacagcat
gatcctaata aagaaccaag caataatatc tttgcgcgtt tctttagaag ctttaacaat
ggttttgacc gcatgtcgca tagctaccaa aatggtgtta gccgcatgct taaaggcaaa
atcttctctg gcgtgctcta tgctgttgta gttgcccttt tagtcttctt gttccaaaaa
ctcccgtctt cattcttacc agaagaagat cagggtgtgg tcatgacact tgtacaatta
ccaccaaatg caacgcttga ccgtaccggt aaagtgattg acaccatgac taacttcttt
atgaatgaaa aagacaccgt ggaatctatt ttcactgttt ctggtttctc attcacaggt
gttggtcaaa acgctggtat tggcttcgtt aagttgaaag actggagcaa acgtacgaca
ccagaaactc aaattggttc attgattcag cgtggtatgg cattaaatat gatcattaaa
gatgcatcat atgttatgcc gttacagctt ccagcaatgc ctgaacttgg tgtaactgcc
ggatttaact tgcagcttaa agattcaagt ggtcaaggcc atgagaaact gatcgcagct
cgtaacacga ttttaggttt ggcatcacaa gataaacgtc ttgtaggtgt gcgtccaaat
ggtcaggaag atactcctca atatcaaatt aatgtagatc aggctcaagc tggtgctatg
ggcgttagta ttgccgaaat caacaataca atgcgtattg catggggtgg ctcatacatt
aacgatttcg ttgaccgtgg tcgtgtgaaa aaagtttatg ttcaaggtga tgcgggcagc
cgtatgatgc ctgaagactt aaacaaatgg tatgtacgta ataacaaagg tgagatggtt
ccattctcgg cgtttgctac aggcgaatgg acgtatggtt ctccacgtct cgaacgttat
aacggtgtgt catcagttaa cattcaaggt acacctgcac ctggcgtgag ctctggtgat
gccatgaaag caatggaaaa aattattggt aagttgcctt ctatgggctt acaaggtttc

gactatgaat ggacaggctt atcacttgaa gaacgtgagt ctggtgctca agcgccgttc
ttatacgcac tttcattgtt aatcgtattc ctttgcttgg ctgcactata tgaaagctgg
tcaattccgt tctcggtttt acttgtggta ccacttggtg tcattggtgc aatcgtattg
acctacttgg gcatgattat taaaggagat ccaaatctct caaataacat ttacttccaa
gtagcgatta ttgcggttat cggtctttct gcaaaaaatg cgatcttgat tgttgaattc
gcaaaagaat tgcaggaaaa aggtgaagat ctacttgatg caaccttaca tgctgcaaaa
atgcgtttac gtccaattat catgaccacc cttgccttcg gtttcggtgt acttccactt
gcactttcaa caggtgccgg tgcaggaagt cagcactctg taggctttgg tgtacttggt
ggcgtactca gcgcgacgtt cttaggtatc ttctttatcc ctgtattcta tgtgtggatt
cgtagtatct ttaagtacaa accaaaaacc ataaacactc aggagcataa atcgtga

>A1S_2737 (*adeK*) GenBank: CP000521.1

atgcaaaaag tatggtctat ttcaggtcgt agcattgcgg tatctgcact tgcgcttgct
ttggcagctt gtcaaagcat gcgcggccca gaaccagtcg tgaaaaccga tataccacaa
agctatgcat ataacagcgc ttctggtacg tctattgctg aacagggtta taaacagttc
tttgctgacc cgcgtttgct tgaagtgatt gatttggctc ttgccaataa ccgtgactta
cgtacagcaa cgctcaatat tgaacgtgct caacagcaat atcagattac acagaacaac
cagcttccaa caatcggagc aagtggtagt gcaattcgtc aggtttctca aagccgtgat
ccgaataatc cctactctac ttatcaagta ggtttgggtg taactgctta tgagctagat
ttctggggtc gtgttcgtag cctcaaagat gctgctttag atagttatct tgcaacacaa
agtgctcgtg attcgactca aatcagtctg attagccaag ttgctcaagc atggttaaat
tattcgtttg caacagcaaa cttaagactg gcagagcaaa cgcttaaagc acagttagat
tcttacaatc tcaacaaaaa acgttttgat gtaggtattg acagtgaagt tccattacgt
caagcacaga tttctgtaga aactgcgcgt aatgatgtag cgaactacaa aactcaaatt
gctcaagcac aaaacttgtt gaacttgctt gtaggccaac ctgttccaca aaacttgtta
cctacacaac ctgtaaaacg cattgctcaa caaaatgtgt ttactgccgg tttaccaagt
gacttgttaa ataaccgtcc ggatgtaaaa gctgctgaat acaacttaag cgctgcgggt
gcgaatatcg gtgctgcaaa agcacgttta ttcccaacca ttagcttaac gggttcggct
ggttatgcat caactgactt aagtgatcta tttaagtctg gtggttttgt atggtcagtt
ggtccaagct tagatttacc aatctttgac tggggtacac gccgtgccaa tgtaaaaatt
tctgaaactg atcagaaaat tgcattgtct gattatgaaa aatcagttca gtcggcgttc
cgtgaagtta atgacgcgct tgcaactcgt gccaacattg gtgagcgttt aacagcacaa
caacgtctag tagaagcgac taaccgcaac tacacacttt caaatgcccg cttccgtgct
ggtattgata gttacttgac tgttcttgat gcgcagcgtt cttcatatgc agctgaacaa
ggtttgttat tgcttcaaca agcaaactta aacaaccaaa tcgagttata caaaactcta
ggtggcggtt taaaagcaaa tacttcagat acagtggtac atcaaccatc tagtgctgaa
cttaaaaagc aataa

>ABUW_1949 (*amfA*) GenBank: CP008706.1

atggataacg tagctcagct agaaactgat actaatttcc aaagccgaaa gaaaataact
tggggtgttt ttagtgtcct gctgttattt ttagttgctg gcatcttata ttatttttt
gtataccgat tctatcaatc tactgataat gcttatgtac aagccgatgt cacttgggtg
atgccaaaga tttcaggcga agtgatggag ttattaatta acgataatca gtttgtaaaa
aaaggggaaa ctttagcggt attagaccat cgtgactacc aagctcgtta tgaccaagcc
cgttctgtgg tcagcttaaa agaagcagcg ctgggtgtac aacaacaaaa tgaaaagtct
gcacggtcgt caattattga agcaaatagt ggtgtagtgg cagcacaagc tgatttagcg
cgtttgaaaa aagagttcga gcgttatcaa gatttattaa aagatggcgt aattacccga
caaaattttg aaggaatcca gtctcaatat ttaacggctc aggcacagct cagcaaagcg
caagccgccg taaatgcagc agaagctcag ttggggagtt tacaagccag tcgagcgcag
cttttagcag atattcaaag tgccaatgca aacctaaacc tgtatcaggt cgatttggct
tcctcaaaag tggttagtcc tgtaagcggt aaaatcggta gtctggcaat tcaaaaaggc
tcacgtgttt ctccacaaac ccgcttaatg gcgatcattc ctgaaaatag tttgtatgta
caggcgaact tcaaagaaac ccaaattgaa aaaatgcata tcggtcagaa agttaaatta
aaacttgatg cttatccaag cctcaacttt accggaaaaa ttgagagttt ttctcccgct

tcaggcgcga ctttctcact tatgccacca gacaatgcca caggcaactt taacaaggtt
gtacagcgta ttcctgtacg tatcgccata gattcaagcc cacatattga tttgataaaa
cctggaatgt cggtgagcgc caccgttgac ctaagaactt aa

>A1S_1772 (*amfA*) GenBank: CP000521.1

tcatttcttc ccccgatcca taaatatggt taaaaaggcg gtcacaaaca taatgattgc
gagcatgcgt aataagtcat tgaaactcga tgtcagtgct tgaaagtgaa tgtcacgata
aatcacactc agtgcgattt gctgagcatt tgtaccaact tcttgatatt gcgccgtaag
ctggtcgagt ctttctgtaa atatccagtt ttgtggtgtc atcgactgat taatctgggt
aacatgcatg gcggttagcc aatctaagga cgagttaata agagccagtc caaccgcgcc
gccaatattg cgcatcaggt tataaatccc actggcatcg gcaactttac tgagtggcaa
tgtactcata gccaaatgcg agaccacaat caggcaaatc atgaggccga taccacggta
aatttgtggc caaaacataa agtcataatc actatgaatg ctcaaatgtg aattgagcca
gacaccaaag cccgccagaa tcattccgac aaatacggtt tttcgggtat caaaattagg
aatgagccac gcaagaaaag gcgcaaagca gaacatgaca atgcctgtca ccatcatgac
gtgaccaatt tggctactgt tcatttcacg gacttgccca agaaagacag gaatcatgta
acccaagcca tacagcgcca tgccaatcac aaatgttgtg atggcactta aagtaaagtt
tttatttta aataccgata aatcgagcaa aggcttaggc tgggtaaaac ttcgagagaa
gaaaatcata ccgcctacaa cacagaccat aaaagcaatc cgaacgcctg tgtctgcaag
ccagtcatgc cgtgcacctt catcaaggaa atattcaagc ccacccaaaa acatcgccat
acccaccaaa ctaaaccaat ccatgctttt gatgagtgaa tagttggcac ggtcaatatt
tggacctgag tagatgaccg tagcaatgat aatgcccgga ataatattga tcaggaacat
ccagtgccat gagaagttat tggtaagcca accgccaatg gttgggccaa ttgctggacc
taaagtactg atcatgccaa acatgaccaa aggtaatgag cgttttggtt ctggaaacag
taaatacaac gccgtcatgg aagtcggaat catcccgcca cccataaagc cttgaatgcc
acggaacacc agtaaacttt ccaagttcca tgacaaagca caaagtaaag aactgaccgt
aaaacctatt gcacacatgg tgtaatacac ccgtgttgaa agcactcgcg agacaatact
cgacattgga attgcaataa tttcggcaat taaataaacc gtttgtaccc aagtgacttc
ataacgactt gcactcatac cagcttgtac ttcgtttaaa gaactcgcca caatctgaat
atcaagaatc gccatgaagt tgccaaaaat catggcagca aaaattgccc atgcagtttt
tgcgggaaac ctccactcag cttcaacatg cttattcat

>ABUW_1950 (*amfB*) GenBank: CP008706.1

atgaataagc atgttgaagc cgagtggagg tttcccgcaa aaactgcatg ggcaattttt
gctgccatga tttttggcaa cttcatggcg attcttgata ttcagattgt ggcaagttct
ctaaacgaag ttcaagctgg tatgagtgca agtcgttatg aagtcacttg ggtacaaacg
gtttatttaa ttgccgaaat tattgcaatt ccaatgtcga gtattgtctc gcgagtgctt
tcaacacggg tgtattacac catgtgtgca atcggcttta cggtgagttc tttactttgt
gctttgtcat ggaacttaga aagtttactg gttttccgtg gcatacaagg gtttatgggc
ggcgggatga ttccgacttc catgacggcg ttgtacttac tttttccaga agcaaaacgc
tcattgcctt tggtcatgtt tggcatgatc agtacattag gcccagcgat tggccccacc
attggtggtt ggctcaccaa taatttctca tggcactgga tgttcctgat caatattatt
ccgggcatta tcattgctac ggtcatctac tcaggtccaa atattgaccg tgccaactat
tcactcatca aaagcatgga ttggtttagt ttggtgggta tggcgatgtt tttgggtggg
cttgaatatt tccttgatga aggtgcacgg catgactggc ttgcagacac aggcgttcgt
attgctttta tggtctgtgt tgtgggcggc atgattttct tctctagaag ttttactcag
cctaaacctt tgctcgattt gtccgtattt aaaaataaaa actttacctt aagtgccatt
acaacgtttg tgattggtat ggcgctgtat ggcttgggtt acatgattcc cgtgttcctt
gggcaagtcc gtgaaatgaa cagtagccaa attggtcacg tcatgatggt gacaggcatt
gtcatgttct gctttgcgcc gttcctggcg tggctcattc ctaattttga tacccgaaaa
accgtatttg tcggaatgat tctggcgggc tttggtgtct ggctcaattc acatttgagc
attcatagcg attatgactt tatgttttgg ccgcaaattt accgtggtat tggcctcatg
atttgcctga ttgtggtgtc acatttggct atgagtactt tgccactgag taaagttgcc
gatgccagcg gtatttataa cctgatgcgt aatattggcg gcgcggttgg actggctctt

attaactcat ccttagattg gctgaccgcc atgcatgtca cccagattaa tcagtcgatg
acaccgcaaa actggatatt tacagaacgg cttgatcagc ttacggcgca atatcaagaa
gtcggtgcaa atgcccagca aatcgcactc agcgtgatct atcgcgatat tcactttcaa
gcactgacat cgagtttcaa tgacttatta cgcatgctcg caatcatcat gtttgtgacc
gccttttttaa ccatatttat ggatcggggg aagaaaatga atatgtag

>A1S_1773 (*amfB*) GenBank: CP000521.1

ttaagttctt aggtcaacgg tggcgctcac cgacattcca ggttttacca aatcaatatg
tgggcttgaa tctatggcga tacgtacagg aatacgctgt acaaccttgt taaagttgcc
tgtggcattg tctggtggca taagtgagaa agtcgcacct gaagcgggag aaaagctctc
aatttttccg gtaaagttga ggctcggata ggcatcaagt tttaatttaa ctttctgacc
aatatgcatt ttttcaattt gagtttcttt gaagttcgcc tgtacataca aactattttc
aggaatgatc gccattaaac gggtttgtgg agaaacacgt gagccttttt gaattgccag
actaccgatt ttaccgctta caggactaac cacttttgat gaagccaaat cgacttgata
caggtttaaa tttgcatggg aactttgaat atctgctaaa agctgcgctc gactcgcttg
taaactcccc aactgagctt ctgctgcatt tacggcggct tgcgctttgc tgagctgtgc
ctgagccgtt aaatattgag actgaatccc ttcaaaattt tgtcgggtaa ttacgccatc
ttttaataga tcttgataac gctcgaactc ttttttcaaa cgcgctaggt ctgcttgcgc
tgccactaca ccactatttg cttcaataat tgacgaccgt gcagactttt cattttgttg
ttgtacaccc agtgcagctt cttttaggct gaccacagaa cgggcttggt cataacgagc
ttggtagtca cgatggtcta ataccgctaa agtttcccct ttttttacca cctgattatc
gttaattaat aactccatca cttcgcctga aatctttggc at

>ABUW_1930 (*amfC*) GenBank: CP008706.1

ttatttggtc gtatccacag aaaccacaac agatagacca ggacgcaaca atttaatatc
aggttggttc tcaaggagtt tgatgcgtaa aggtaaacgc tgaacaattt tagtaaagtt
acccgtcgca tttgttgctg aaattggcga gaagaatgca ccagtcgatg gtgaaaaact
atctaccaca ccttttaact caacgttata agcatcgaca taaacagtga caggctggcc
gattttaatt tgttttagct caatttcacg gaagtttgct tctacataca cttgatctaa
aggcacaact accatgagtg gattacctgc gccaacaaag ttgcccacat ttgcagactt
ctgcccaatc ataccatcaa taggcgctcg aatttctgta tagctcagat tcagttttgc
tttatcaagc gcagcttggg cttgtttcaa agccgcttgt ttagcttgaa cctgaatctt
atattggttg agctgatact gtgcatcaat gacttttttct ttactgctgt ccaagtcggc
atattgctcg gttagtgtgg tttttgactg ttgtgtaatc aatctagatt cagcgccaag
tgcctgtaat tgctcatagc gtgcggtatt atctttagtg agtttaatgc cggcttctac
ttttctaagc tgggcctctg tttctcgaat aacagttggt tgtctttcta ctgccagcat
tgcttcattt aagtcagctt gtgctttggc ataattagat tcagcttcag ctaaagccgc
ctgataatca cgtgcatcaa ttcgtgccaa aagctggcct ttttttacgg tctggtgatc
tttaatataa atttcttcaa tattacctga cacttttgga gcaatggttg agtactcgac
gtctacccgc gcatcgtcag ttttaacaat ggaagaaggt aaaaatataa cttttaaaat
ccataaaatg gaaactagaa cgataataaa tgcaataacc ataacccagt gtttcttaag
atattgcatc tttgttaact tgggtgactc ggtcatggag tgatcttggg cttcgagagt
actcat

>A1S_1799 (*amfC*) GenBank: CP000521.1

atgaatatac gaccactcat cggtttggca ggtgcaattt ttgcagccat gactgtcgaa
tttaataacc gaattagcag cattaccttg gtcgatattc gcggtgagat gggtattagt
gtcgactctg gttattgggt cagcagtatt tatgccagtg ccatgattat tgggatgatc
ctgtccacca gttgggcggt tatttttttct atgcgtcggg ttcttctttt tgcgatagga
ctttgcctct tctctagcgt tttaattcct tttagcccaa atatcgaaat attttattta
ttacggggct tacaaggact cgccaatggt ttaactattc ctttattaat ggcatgtgca
cttagattcc taggacctga aattcgtcta tggggcttgg cctgctatgc attgacagca

actttttcc caaacttaag cgctgcgctt gctgcctttt atttagatgt gattggttgg
aagatgatat ttttccaaac cattcctttt tgtgctttaa gtgctgcgtt agtttacttc
ggtattccgc aagatccgtt aaattactca agaataaaaa cttacgattg gactggcgcg
attctagcca ttattggttt ggcaagcctt agtaccatgc ttttgcatgg caatcatttg
gactggttcc attcaaaatt gatttgtgtt ttggctttaa taagtgccat taccctacct
ttatttttaa tacatgaatg gcgctatcca acaccattaa ttaaaccgca aatgctcgaa
atacgaaatt ttggttatgc tgttattgcg ttgttctgct ttgtggttat tggtatgtca
accagtacat taccccttaa ttacttaagc gctgtgcatg gttataagcc tactcaaacc
atgtggattg gcttacaaat tgccgcatta caatttatct atatcccgat tgttattaaa
gttttgaacc aagcttgggt tgatagccga tatgtacatg gatttggttt acttttggtt
atggttggct gcttaggtgc aagtcaactt gatacgactt ggaaccaaga ccaattctat
ttttggcatg caatctcatg tttaggacaa acctgtgtag tgctttcgct cctcatgatg
ggtacaaata gtgtccaccc aactatggca atctatgctt ctcctatgat taacaccccg
cgtgctatca gcggcgtact tggtgtgtgc cttttggact gggtcaatcg agtacgtggt
gaataccatt caacacggct gattgaaaat accgcacaac atgtttttca aaatattcaa
ggtcctgtta ttaatcctct taccccgcct gtgctgagtg cagatggtac cgaacgtgtt
tccggtggtt tatctgcctt aaattctgcg attcaggcac agcaatcggt gttagtcatt
agtgatcaat atctgatttt agcgggactt actgcaattt tatttatcgt tatgctgatt
ttgccagtta gaacttatcc accacgcatt gctctcatta agttaatgaa tagtcataac
tcaggaaaat ctttatga

>ABUW_1931 (*amfD*) GenBank: CP008706.1

tcataaagat tttcctgagt tatgactatt cattaactta atgagagcaa tgcgtggtgg
ataagttcta actggcaaaa tcagcataac gataaataaa attgcagtaa gtcccgctaa
aatcagatat tgatcactaa tgactaaaac tgattgctgt gcctgaatcg cagaatttaa
ggcagataaa ccaccggaaa cacgttcggt accatctgca ctcagcacag gcggggtaag
aggattaata acaggacctt gaatattttg aaaaacatgt tgtgcggtat tttcaatcag
ccgtgttgaa tggtattcac cacgtactcg attgacccag tccaaaaggc acacaccaag
tacgccacta atagcacgcg gggtgttaat cataggcgaa gcatagattg ccatagttgg
gtggacacta tttgtaccca tcatgaggag cgaaagcact acacaggttt gtcctaaaca
tgagattgca tgccaaaaat agaattggtc ttggttccaa gtcgtatcaa gttgacttgc
acctaagcag ccaaccataa ccaaaagcaa accaaaccca tgtacatatc ggctatcaac
ccaagcttgg ttcaaaactt taataacaat cgggatatag ataaattgta atgcggcaat
ttgtaagcca atccacatgg tttgagtagg cttataacca tgcacagcgc ttaagtaatt
aagaggtaat gtactggttg acataccaat aaccacaaag cagaacaatg caataacagc
ataaccaaaa tttcgtattt cgagcatttg cggtttaatt aatggtgttg gatagcgcca
ttcatgtatt aaaaataaag gtagggtaat ggcactcatt aaagccaaaa cacaaatcaa
ttttgaatgg aaccagtcca aatgattgcc atgcaaaagc atggtactaa ggcttgccaa
accaataatg gctagaatcg cgccagtcca atcgtaagtt tttattcttg agtaatttaa
cggatcttgc ggaataccga agtaaactaa cgcagcactt aaagcacaaa aaggaatggt
ttggaaaaat atcatcttcc aaccaatcac atctaaataa aaggcagcaa gcgcagcgct
taagtttggg aaaaaagttg ctgtcaatgc atagcaggcc aagccccata gacgaatttc
aggccctagg aatctaagtg cacatgccat taataaagga atagttaagc cattggcgag
tccttgtaag ccccgtaata aataaaatat ttcgatattt gggctaaaag gaattaaaac
gctagagaag aggcaaagtc ctatcgcaaa aagaagaacc cgacgcatag aaaaaataac
cgcccaactg gtggacagga tcatcccaat aatcatggca ctggcataaa tactgctgac
ccaataacca gagtcgacac taatacccat ctcaccgcga atatcgacca aggtaatgct
gctaattcgg ttattaaatt cgacagtcat ggctgcaaaa attgcacctg ccaaaccgat
gagtggtcgt atattcat

>A1S_1800 (*amfD*) GenBank: CP000521.1

atggttattg catttattat tgttctagtt tccattttat ggattttaaa agttatattt
ttaccttctt ccgttgttaa aactgacgat gcgcgggtag acgtcgagta ctcaaccatt
gctcccaaag tgtcaggtaa tatagaagaa atttatatta aagatcacca gaccgtaaaa

aaaggccagc ttttggcacg gattgatgca cgtgattatc aggcggcttt agctgaagct
gaatctaatt atgccaaagc acaagctgac ttaaatgaag caatgctggc agtagaaaga
caaccaactg ttattcgaga aacagaggcc cagcttagaa aagtagaagc cggcattaaa
ctcactaaag ataataccgc acgctatgag caattacagg cacttggtgc tgagtctaga
ttgattacac aacagtcaaa aaccacattg accgagcaat atgccgactt ggacagcagt
aaagaaaaag tcattgatgc gcagtatcag ctcaaccaat ataagattca ggttcaagct
aaacaagccg ctttaaaaca agcccaagct gcgcttgata aagcaaaact gaatctgagc
tatacagaaa ttcgagcacc tattgatggc atgattgggc aaaagtctgc aaatgtgggc
aactttgttg gcgcaggtaa tccactcatg gtggttgtgc ctttagatca agtgtatgta
gaagcaaact tccgtgaaat tgagctaaaa caaattaaaa tcggccagcc tgtcactgtt
tatgtcgacg cttacaatgt tgagttaaaa ggtgtggtag atagtttctc accatcgact
ggtgcattct tctcgccaaa tttcagcaac aaatgcgacg ggtaa